

Nanoparticle-mediated surface modification  
of hydrophobic polymeric films/scaffolds  
and their application towards  
tissue engineering

Thesis Submitted to AcSIR  
For the Award of the Degree of  
DOCTOR OF PHILOSOPHY  
In Chemical Sciences



By  
Poulomi Sengupta  
Enrollment number 10CC14J26006

Under the guidance of  
Dr. B. L. V. Prasad

CSIR National Chemical Laboratory

# Declaration

I, Poulomi Sengupta, hereby declare that the work described in this thesis titled ***“Nanoparticle-mediated surface modification of hydrophobic polymeric films/scaffolds and their application towards tissue engineering”*** was carried out by me for the degree of Doctor of Philosophy in Chemical Sciences under the guidance and supervision of Dr. B. L. V. Prasad, Physical and Materials Chemistry Division, CSIR-National Chemical Laboratory, Pune, India. I confirm that this work was done by me in a candidature for a research degree at this institute. This work is original and no part of this thesis has been submitted for a degree or diploma at this institution or any other institution. The interpretations put forth are based on my literature survey of the original articles and all the sources have been duly acknowledged in this thesis.

Date

Poulomi Sengupta

Place





# सीएसआयआर-राष्ट्रीय रासायनिक प्रयोगशाला

(वैज्ञानिक तथा औद्योगिक अनुसंधान परिषद)

डॉ. होमी भाभा मार्ग, पुणे - 411 008. भारत



## CSIR-NATIONAL CHEMICAL LABORATORY


(Council of Scientific & Industrial Research)

Dr. Homi Bhabha Road, Pune - 411008. India


### Certificate

This is to certify that the work incorporated in this Ph.D. thesis entitled *Nanoparticle-mediated surface modification of hydrophobic polymeric films/scaffolds and their application towards tissue engineering* submitted by *Ms. Poulomi Sengupta* to Academy of Scientific and Innovative Research (AcSIR) in fulfillment of the requirements for the award of the Degree of *Doctor of Philosophy*, embodies original research work under my supervision/guidance. I further certify that this work has not been submitted to any other University or Institution in part or full for the award of any degree or diploma. Research material obtained from other sources has been duly acknowledged in the thesis. Any text, illustration, table etc., used in the thesis from other sources, have been duly cited and acknowledged.

It is also certified that this work done by the student, under my supervision, is plagiarism free.

  
**Poulomi Sengupta**

(Student) 24-02-2019  
Pune

  
**Dr. B. L. V. Prasad**  
(Supervisor)

Communications  
Channels

NCL Level DID : 2590  
NCL Board No. : +91-20-25902000  
Four PRI Lines : +91-20-25902000



FAX

Director's Office : +91-20-25902601  
COA's Office : +91-20-25902660  
SPO's Office : +91 20 25902664

WEBSITE

[www.ncl-india.org](http://www.ncl-india.org)





# सीएसआयआर-राष्ट्रीय रासायनिक प्रयोगशाला

(वैज्ञानिक तथा औद्योगिक अनुसंधान परिषद)

डॉ. होमी भाभा मार्ग, पुणे - 411 008. भारत



## CSIR-NATIONAL CHEMICAL LABORATORY

(Council of Scientific & Industrial Research)

Dr. Homi Bhabha Road, Pune - 411008. India

### To Whom It May Concern

This is to certify that I have reviewed the doctoral research work carried out and subsequent thesis written by Ms. Poulomi Sengupta (AcSIR roll no. 10CC14J26006) and I am satisfied with the final product. I recommend Ms. Sengupta to proceed further with the submission of her thesis at the earliest.

*Poulomi Sengupta*

Poulomi Sengupta  
(Student)  
PMC division  
CSIR NCL

21-02-2019

Pune

*Dr. B. L. V. Prasad*

Dr. B. L. V. Prasad  
Ph.D. Supervisor  
PMC Division  
CSIR NCL



Communications  
Channels

NCL Level DID : 2590  
NCL Board No. : +91-20-25902000  
Four PRI Lines : +91-20-25902000

FAX

Director's Office : +91-20-25902601  
COA's Office : +91-20-25902660  
SPO's Office : +91 20 25902664

WEBSITE

[www.ncl-india.org](http://www.ncl-india.org)



# Acknowledgements

First and foremost, I am very much thankful to my Ph.D. supervisor Dr. B. L. V. Prasad for accommodating me in his group, and introducing me to the field of tissue engineering. Apart from excellent guidance, he has provided me flexibility, and independence, which a Ph. D. student of my stage can ask for. He was always approachable; open to discuss, and always provided room for independent thinking. I have seen his patience day in and day out and wish I could imbibe in some excellent qualities that he possesses.

My doctoral advisory committee members Dr. V. Premnath, Dr. S. Dhanasekaran, and chairperson Dr. S. K. Asha all spent valuable time understanding my work and providing important feedbacks. Beyond the regular DAC meetings all were approachable for discussion. They are truly perfectionist and great critics; this helped me extensively regarding re-thinking my work problems and re-designing the experiments.

I thank DST Wos-a scheme for consumable money and fellowship. I also thank AcSIR for Ph.D. registration, arranging for my thesis submission, and *viva*.

I sincerely thank Dr. Sourav Pal, and Dr. Ashwini Kumar Nangia, directors of CSIR-NCL for smooth running of all the facilities that I used in CSIR-NCL. My heartfelt thanks goes to Dr. Sivaram (ex-director, NCL) who introduced me to the lab. I thank Dr. Anil Kumar, and Dr. P. A. Joy (ex and current-HODs, PMC division) for their support.

My thanks go to several NCL scientists, facilities maintained by whom I have used extensively. They are: Dr. Thulasiram, Dr. Sayam Sen Gupta, Dr. Guruswamy Kumaraswamy, Dr. Anuya Nisal, Dr. Dheeman Sarkar, Dr. Mugdha Gadgil, Dr. S. Chinnathambi, Dr. M. V. Badiger, Dr. Janardan Kundu, Dr. Manjusha Shelke, Dr. Suresh Bhat. I thank our collaborator Dr. Vinay Agrawal from Clearvision, Mumbai for HDPE scaffolds, and Dr. Mathe from the Physics department, SPPU for plasma treatment. I have used common facilities like SEM, XPS, NMR in NCL. I thank all the operators and scientists in-charge. I thank SAC office, library, bill, accounts, purchase group admins for smooth functioning of errands.



On several occasions we have discussed our work with Dr. Ashutosh Ambade, Dr. Manohar Badigar from CSIR NCL, Dr. Anjali Shiras, Dr. Joman Joseph, Dr. Deepa of NCCS. Thank you all for your constructive feedback. Thank you Dr. Nirmalya Ballav (IISER Pune) for being a well-wisher.

I want to thank few students and NCL staff who have helped me during my Ph.D. journey. They are: Ms. Karthika, Mr. Shebeeb, Ms. Aarti Yadav, Mr. Abhishek, Dr. Trimukhe for helping me with various instruments. I also thank Ms. Sneha (IISER) and Ms. Supriya More (SPPU) for operating AFM and Plasma machines.

My labmates have seen me at each phase of Ph.D. I shared good times with them in discussing both science and non-science. Thank you Ravi, Anal, Vilas, Puspa, Prabhu, Jhumur, Bala, Pravin, Arun, Abhijit, Jayesh, Pooja, Mayur, Dr. Vijay, Shankar, Kaustav, Sachin, Hari, Akansha, Arivazhagan, Bhaskar, Ajay for all good memories. Masters students Karthika, Sabareesh, Yash, Aamir Khan had worked with me and helped me a lot. My bio-lab friends Nimisha, Vinita, Singham, Isha, Neha were very helpful and adjusting. Few IISER students Abhik, Sandeep, Aditi, Meenu, Sohan helped me at several situations. Thank you guys for being there.

I am very much indebted to my parents-in-law, parents, and my brother Aruni to come over to Pune several times during my difficult days and take care of the household. This helped me to focus more towards my thesis. My husband Dr. Sudipta Basu gave me the liberty to build my own career and shared all home-responsibilities in major part. A thank is never enough. My son Shubham compromised and cooperated during odd hours. I appreciate him to be an understanding little gentleman. Without their full-support I could never write a Ph.D. thesis.

Finally, I thank my parents and Mother Nature for this beautiful life.

---

Poulomi Sengupta



# Prologue

‘That’s one small step for a man, one giant leap for mankind’: these are the famous words spoken by Neil Armstrong upon landing on the moon’s surface back in 1969. This statement is not only true for a lunar expedition but also to any progress being achieved in research and technology. Truly, mankind is progressing at a rapid pace because of the advances in science and technology. This can bring about dramatic changes to all aspects of life in the coming days.

Like every other field, medical science also has received valuable inputs from the researchers and as a result evolved tremendously in past few decades. The breakthroughs are not necessarily limited to the discovery of a life saving elixir, but to the attention being put to improve a common person’s day-to-day life. Especially when they face a medical situation which has lead to a substantial increase in using human-made living aids, for example pacemakers, stents, catheters, joint replacements, prosthesis *etc.* For aesthetic reasons as well there has been a significant increase in affordable cosmetic corrections, which involve human-made materials. This has been possible because of rapid development in the fields of material synthesis and processing. Recently, numerous novel and simple (hence affordable) methods have been developed to synthesize a material (for example, polymer, ceramics, alloys) of desired mechanical properties. In addition to that, well-established processing techniques have made those materials usable as bio-implants. Some of these are surprisingly stable inside body, so for certain purposes they can be kept forever. Though rapid and giant strides have been made in this area of research, the process of placing a foreign material inside a human body is still not simple, straightforward and hassle free. At times there are necessities for multiple interventions, which can cause trauma and trouble to the patients. Many of the issues involved with these materials need serious attention towards research and development in the times to come.

In this thesis we have made a conscious effort to identify and address few of the important problems faced when a foreign object is placed inside human body.



Applying noble metal nanoparticles and surface modification techniques we have tried to provide methods to overcome some of them. We also have tried to explore their applicability as facile tissue integration, immune response, drug delivery and functional replacements. We strongly believe, by applying simple chemistry we can bring about major changes in the future of a functional material placed *in vivo*.

# Synopsis report

## Introduction

Day by day, as the life expectancy is increasing, mankind is getting more exposed to dysfunctional organs, cosmetic deformities etc. Other than natural degenerative diseases, there are unexpected accidents, and also aesthetic reasons, which persuade people to take advantage of an externally procured (man-made) implant made up of polymeric scaffolds. Contact lenses, catheters, joint prosthetics, pacemakers, and stents are to name a few. Unfortunately, after installation, these implants may result in adverse reactions involving slow integration with the live tissue, infection, fibrosis, immune rejection *etc.* In the literature it has been well documented that imparting the necessary functionalities to the surface of such implants (surface modification) may allow us to circumvent these issues. Here, in this thesis we have harnessed the 'surface modification techniques' to convert the readily available, widely-used, implant-making polymers into a tissue-friendly one, and also understand its applications towards easy tissue integration, immune response, drug delivery, functional replacement *etc.*

## Statement of the problem

Hydrophobic polymers, due to their favorable strength, ease of preparation, and bio-inertness are being used inside human body for various corrective purposes. It is understood that extreme hydrophobicity of mechanically strong polymers is the hindrance for easy integration with the live tissue<sup>1</sup>, which can be overcome by surface modification. Plasma treatment (in presence of gas like NH<sub>3</sub>, CO<sub>2</sub>, O<sub>2</sub>) is the best tool for polymeric surface modification. But it is associated with very fast surface reorganization, which restricts its shelf life. Dr. B. L. V. Prasad in his group has made a conscious effort to tackle the problem of bio-integration using layer-by-layer surface modification strategy<sup>2</sup>. Upon the intervention by plasma treatment, metallic nanoparticles coating and small molecules, they have shown that it is possible to arrest the surface reorganization to a considerable extent and modifying



the surfaces of polymers with lysine molecules leads to enhanced cell attachment and proliferation.

With this background we have tried to answer some questions:

- (i) Which surface modification will be cell friendly for faster integration with the active tissue?
- (ii) Can this strategy be used to make a dual-purpose scaffold/implant?
- (iii) Does change in the surface charge play a major role in terms of cellular attachment and proliferation?

The thesis is borne out of our efforts to answer the above questions and consists of three working chapters, which are:

- (i) **Working chapter 1** Arginine-mediated surface modification of polymers for tissue engineering applications.
- (ii) **Working chapter 2** Design and fabrication of a dual-purpose scaffold by a logical combination of drug-release and tissue engineering.
- (iii) **Working chapter 3** Response of Macrophages with respect to Surface Charge Alterations.

### **Methodology(s) used**

The polymeric films/scaffolds were surface modified following a sequence of steps, which involve plasma treatment, gold nanoparticle coating, dip coating in small molecules/proteins/polymers/cytotoxic drugs *etc.* For characterizations we have used solid state UV, FT-IR, contact angle, zeta potential, SEM, EDS, AFM and XPS. For application purpose we have used animal cell tissue culture facilities, cell counting, cell viability assay, flow cytometry assay, microscopy, collagen estimation assay, protein quantification assay *etc.*

### **Sample results with interpretation**

- (i) Working chapter 1: One of the main drawbacks of polymeric scaffolds inside body is their slow integration with the live tissue. Here we have used layer-by-layer

surface modification technique involving arginine as a small molecule to make the polymeric surface hydrophilic and cell loving. PEI films, after  $\text{NH}_3$  plasma treatment, citrate-stabilized AuNP coating, were dip-coated in arginine-water solution. In parallel, a fibronectin-coated film was also prepared as a positive control using the same strategy. Low contact angle on arginine-coated samples show extreme hydrophilicity, and these films adhered fibroblast at a very low time point when compared to untreated tissue culture plates. Proliferation of the adhered cells formed a healthy populated colony and produced collagen. In every case, the *in vitro* results with arginine-coated samples were at par with the fibronectin-coated ones. This chapter indicated, for tissue engineering purpose, a simple small molecule coating on a polymeric surface can be as good as a cell-adhering protein.

(ii) Working chapter 2: Some patients with solid tumor (especially in oral cancer), need to undergo a (tumor) surgery, chemotherapy (systemic chemotherapy involves extreme side effects), followed by an optional cosmetic surgery in a very short span of time. Motivated by their trauma we have designed a novel dual-purpose polymeric scaffold, which can serve the task of cytotoxic drug delivery (local release of drug can by-pass the toxic side effects) and with time, can act as a functional replacement.

Porous HDPE scaffolds were  $\text{N}_2 + \text{H}_2$  plasma treated, citrate-stabilized AuNP coated, followed by chemical conjugation with cisplatin molecules (cytotoxic drug). The scaffolds were seen to release almost all drug at 2 days time point in KB (human mouth cancer) cell lysate. Cell viability assay at 48 hours indicated that drug loaded scaffolds were cytotoxic with 40% cell death. Drug released scaffolds, when allowed to adhere and proliferate with fibroblasts (murine, L929) formed a colony at about 9 days. In this chapter we demonstrated that, preparation of dual-purpose scaffold was possible, which can release drug and can act as a functional replacement.

(iii) Working chapter 3: After the installation, many-a-times foreign implants are associated with inflammation, which can lead to bone resorption, osteolysis,



fibrosis, aseptic loosening *etc.* Immune cell's (macrophages) response dictates the future of an implant *in vivo*. In this chapter we modified polymeric surface and tried to understand macrophage's adhesion on the same.

Followed by N<sub>2</sub> + H<sub>2</sub> plasma treatment, PEI films were citrate-stabilized AuNP coated. Two polymers, PDADMAC (poly-diallyldimethylammonium chloride, positively charged) and PAA (poly-acrylic acid, negatively charged) were coated on the films. The films were probed for their cellular-adhesion capabilities at different time points. It was observed that at higher time point (2 hours) positively charged surfaces were favoring macrophages. While at lower time points (<2 hours), both positively charged and negatively charged surfaces were almost equivalent.

### **Citation of any publication resulting from thesis work**

1. *Surface Modification of Polymeric Scaffolds for Tissue Engineering Applications.* **Poulomi Sengupta**, Bhagavatula L. V. Prasad. *Regen. Eng. Transl. Med.* **2018** <https://doi.org/10.1007/s40883-018-0050-6>
2. *Surface modification of polymers for tissue engineering applications: Arginine acts as a sticky protein equivalent for viable cell accommodation.* **Poulomi Sengupta**, Bhagavatula L. V. Prasad. *ACS Omega*, **2018**, 3 (4), 4242-4251.
3. *Modification of porous polyethylene scaffolds for cell attachment and proliferation.* **Poulomi Sengupta**, Sachin S. Surwase, Bhagabatula L. V. Prasad. *International Journal of Nanomedicine*, **2018** Mar 15;13:87-90.

### **Bibliography**

---

<sup>1</sup> Fernandez-Bueno, I.; Di Lauro, S.; Alvarez, I.; Lopez, J. C.; Garcia-Gutierrez, M. T.; Fernandez, I.; Larra, E.; Pastor, J. C. Safety and Biocompatibility of a New High-Density Polyethylene-Based Spherical Integrated Porous Orbital Implant: An Experimental Study in Rabbits. *J. Ophthalmol.* 2015, No. 904096.

<sup>2</sup> D'Britto, V.; Tiwari, S.; Purohit, V.; Wadgaonkar, P. P.; Bhoraskar, S. V.; Bhonde, R. R.; Prasad, B. L. V. Composites of plasma treated poly(etherimide) films with gold nanoparticles and lysine through layer by layer assembly: a "friendly-rough" surface for cell adhesion and proliferation for tissue engineering applications. *J. Mater. Chem.* 2009, 19, 544–550.

# Table of contents

## Chapter 1 Introduction

S. No.	Description	Page
1.1	Introduction	23
1.1.1	Chemistry and material science	27
1.1.2.	Biology	27
1.1.3.	Medicine	27
1.1.4.	Engineering	27
1.2.	Cell-material interaction	28
1.2.1.	Role of cells	29
1.2.1.1.	Cellular adhesion and cell-ECM interaction	29
1.2.2.	Role of nutrients for tissue growth	31
1.2.3.	Role of scaffolds	31
1.3.	Materials developed for tissue engineering	32
1.4.	Role of hydrophobic polymers	35
1.5.	Surface modification techniques and their drawbacks	36
1.5.	Graft polymerization technique	43
1.5.2.	Nanoindentation method	44
1.5.3.	Surface modification by self-assembled monolayer formation	44
1.5.4.	Corona discharge	44
1.5.5.	Flame treatment	44
1.5.6.	UV irradiation	45
1.5.7.	Wet chemical treatment	45
1.5.8.	Plasma treatment	45
1.6.	Layer-by-layer surface modification technique-a possible way of arresting the surface re-organization	50
1.7.	Plan of this thesis	52
1.7.1.	Fast volume filling	53
1.7.2.	Sequential drug delivery and tissue engineering	53
1.7.3.	Understanding interaction of foreign bodies with the immune system	54
1.8.	Conclusion	55
1.9.	Bibliography	55



## Chapter 2

### Arginine Mediated Surface Modification of Polymers for Tissue Engineering Applications

S. No.	Description	Page
2.1.	Introduction	69
2.2.	Materials	72
2.3	Experimental section	72
2.3.1.	Preparation of arginine-coated PEI films	72
2.3.1.1.	Gold nanoparticles synthesis	72
2.3.1.2.	Casting of PEI films	73
2.3.1.3.	Plasma treatment	73
2.3.1.4.	AuNP-coating on PEI films	73
2.3.1.5.	Arginine-coating on gold-coated PEI films	73
2.3.1.6.	Fibronectin-coating on gold nanoparticle-coated PEI films	73
2.3.2.	Characterization of surface modified films	74
2.3.2.1.	UV-Vis spectrophotometry	74
2.3.2.2.	Surface hydrophilicity by contact angle measurement	74
2.3.2.3.	Water absorption study	74
2.3.2.4.	Surface atomic force microscopy	75
2.3.2.5.	IR spectroscopy	75
2.3.2.6.	Mechanical stability	75
2.3.3.	Cell culture experiments with modified films	75
2.3.3.1.	A common protocol for cell culture experiment	75
2.3.4.	Evaluation of cellular adhesion	76
2.3.4.1.	Cell adhesion assay by cell counting (Trypan blue assay)	76
2.3.5.	Cell viability and cytotoxicity	76
2.3.5.1.	Cell viability assay (by resazurin)	76
2.3.5.2.	Live-dead assay by fluorescence microscopy	77
2.3.6.	Effects on cellular proliferation	77
2.3.6.1.	Cell proliferation study by cell counting	77
2.3.6.2.	Cell populations on differently treated surfaces by fluorescence microscopy	77
2.3.6.3.	Cell morphology, and actin cytoskeleton staining	78
2.3.5.	Collagen production assay	78
2.4.	Result and discussion	79
2.4.1.	Preparation and characterization of films	79
2.4.2.	Cellular adhesion study	87
2.4.3.	Cell viability, and cytotoxicity	88
2.4.3.1.	Cell viability study by mitochondrial activity	88
2.4.3.2.	Cell viability by live-dead imaging	90

	2.4.4.	Cellular proliferation analysis	92
	2.4.4.1.	Cellular proliferation study by cell counting	92
	2.4.4.2.	Cellular population by fluorescence microscopy	92
	2.4.5.	Cellular morphology by actin cytoskeleton staining	94
	2.4.6.	Production of collagen	96
2.5.	Conclusion		98
2.6.	Bibliography		98

### Chapter 3

#### Design and Fabrication of a Dual Purpose Scaffold by a Logical Combination of Drug-release and Tissue engineering

S. No.	Description		Page
3.1.	Introduction		104
3.2.	Materials		106
3.3.	Experimental section		107
	3.3.1.	Preparation of scaffolds	107
	3.3.1.1.	Determination of cisplatin present on each scaffold	108
	3.3.2.	Characterization	110
	3.3.2.1.	UV-Vis spectrophotometry	110
	3.3.2.2.	Surface microstructure by SEM	110
	3.3.2.3.	Presence of platinum by XPS	110
	3.3.2.4.	Release kinetics experiment	110
	3.3.3.	Efficacy of drug conjugated scaffolds on KB cells	111
	3.3.3.1.	Cell viability (KB cells)	111
	3.3.3.2.	Estimation of cellular density by imaging	111
	3.3.3.3.	Live-dead imaging assay	112
	3.3.3.4.	Flow cytometry analysis	112
	3.3.3.5.	Expression of phosphatidylserine by Annexin V imaging	113
	3.3.4.	Regrowth experiment	114
	3.3.4.1.	Effect of fibroblasts on drug-released scaffolds	114
	3.3.4.2.	Imaging of re-grown cells	114
3.4.	Result and discussion		114
	3.4.1.	Preparation and characterization of surface modified films	114
	3.4.2.	Cell viability and apoptotic assay	118
	3.4.3.	Cellular regrowth experiment	128
3.5.	Conclusion		130
3.6.	Bibliography		131

## Chapter 4

### Response of Macrophages with respect to Surface Charge Alterations

S. No.	Description		Page
4.1.	Introduction		136
4.2.	Materials		138
4.3.	Experimental section		139
	4.3.1.	Preparation of surface-modified films	139
	4.3.1.1.	Casting PEI films, plasma treatment, gold nanoparticle preparation, and surface coating	139
	4.3.1.2.	PDADMAC-coating on PEI films	139
	4.3.1.3.	PAA-coating on PEI films	139
	4.3.2.	Characterization	140
	4.3.2.1.	UV-Vis spectrophotometry	140
	4.3.2.2.	Zeta potential measurement	141
	4.3.2.2.1.	Sample preparation for PDADMAC-coated citrate stabilized AuNPs	141
	4.3.2.2.2.	Sample preparation for PAA-coated citrate stabilized AuNPs	141
	4.3.2.3.	Contact angle measurement	141
	4.3.2.4.	FT-IR measurement (ATR mode)	142
	4.3.2.5.	Determination of the amount of polymer attached	142
	4.3.2.6.	Cellular adhesion assay	142
	4.3.2.7.	Live-dead assay	143
	4.3.2.8.	The population of cells on different surfaces	143
4.4.	Result and discussion		144
	4.4.1.	Synthesis and characterization of surface-modified films	144
	4.4.2.	Cellular adhesion assay	149
	4.4.3.	Fluorescent microscopy images for live-dead assay, and healthy cell quantification	152
4.5.	Conclusion		155
4.6.	Bibliography		156

## Chapter 5

### Conclusion

S. No.	Description		Page
5.1.	Introduction		159
5.2.	Conclusions drawn from different chapters		159
	5.2(a)	Fast volume filling application	159
	5.2(b)	Dual-purpose scaffolds	160
	5.2(c)	Understanding the immune reactions	161
5.3.	Bibliography		162

# List of schemes

## Chapter 2 Arginine Mediated Surface Modification of Polymers for Tissue Engineering Applications

S. No.	Description	Page
Scheme. 2.1	Schematic representation of surface modification for polyethyrimide films. 1. Plasma treatment on PEI films using 3:2 hydrogen, and nitrogen mixture. 2. Citrate stabilized gold nanoparticles incubation with plasma treated films. 3. Dip coating of films inside arginine water solution overnight. 4. Incubation of citrate gold coated films with a dilute solution of fibronectin.	71

## Chapter 3 Design and Fabrication of a Dual Purpose Scaffold by a Logical Combination of Drug-release and Tissue engineering

S. No.	Description	Page
Scheme. 3.1	Schematic representation of surface modification for HDPE scaffolds. 1. Plasma treatment polyethylene scaffolds using 3: 2 hydrogen, and nitrogen mixture. 2. Stirring of freshly plasma treated scaffolds with citrate stabilized gold nanoparticles (AuNPs). 3. Chemical conjugation between the scaffolds, and aqueated cisplatin.	107
Scheme. 3.2	Substitution of chloride with hydroxyl groups (in cisplatin) through precipitation of AgCl	108
Scheme. 3.3	Chemical conjugation of hydrated cisplatin to the HDPE scaffold via an ester bond formation	108

## Chapter 4 Response of macrophages with respect to surface charge alterations

S. No.	Description	Page
Scheme. 4.1	Schematic representation of surface modification of polyetherimide films. 1. Plasma treatment using 3: 2 hydrogen, and nitrogen mixture. 2. Incubation of plasma treated films in citrate stabilized AuNP sol. 3. Creation of positively charged surface using PDADMAC (overnight incubation) 4. Creation of negavely charged surface using PAA (3 h incubation)	140



## Chapter 5 Conclusion

S. No.	Description	Page
Scheme. 5.1	Outline of thesis: Surface modification of hydrophobic polymeric surface and different applications	160

# List of tables

## Chapter 1 Introduction

S. No.	Description	Page
Table. 1.1	Biomaterials for different purposes	25
Table. 1.2	Biomaterials for different systems	26
Table. 1.3	Biomaterials in different organs	26
Table. 1.4	The typical requirements of scaffolds and the characteristics of different materials	33
Table. 1.5	List of synthesized polymers and their applications	34
Table. 1.6	The summary of published literature on polyethylene, polypropylene surface modification	36

## Chapter 4

### Response of macrophages with respect to surface charge alterations

S. No.	Description	Page
Table. 4.1	Zeta potential measured with citrate-capped AuNP, AuNP-coated with polyionic polymers PDADMAC, and PAA.	146
Table. 4.2	Amount of polymers attached to per cm <sup>2</sup> of AuNP-coated PEI films.	149

# List of figures

## Chapter 1 Introduction

S. No.	Description	Page
Figure. 1.1	Location of different bioimplants in human body	24
Figure. 1.2	Schematic representation of a solid scaffold containing biological molecules and it's in vitro application in regeneration of tissues.	28
Figure. 1.3	Representation of various proteins responsible for cellular adhesion.	31
Figure. 1.4	Illustrations of the heart, liver, and bone at the level of organ (left), tissue, and cell/matrix interaction (center), followed by scanning electron micrographs of engineered scaffolds (right). The ECMs of various tissues have different composition, and spatial organization of molecules to maintain specific tissue morphologies.	32
Figure. 1.5	Kinetics of attachment of osteoblasts cultured on nonporous polylactide membranes treated with various plasmas (NM, nonmodified; O <sub>2</sub> , oxygen plasma; NH <sub>3</sub> , ammonia plasma; H <sub>2</sub> , Sand O <sub>2</sub> , sulfur dioxide-hydrogen plasma; *p<0.05).	47
Figure. 1.6	Transient hydrophilicity in plasma treatment as quantified by contact angle data.	47
Figure. 1.7	Measurement of water contact angle on two-dimensional HDPE surface.	49
Figure. 1.8	Extent of cellular (L929) adhesion on (N <sub>2</sub> +H <sub>2</sub> ) plasma treated surfaces.	49
Figure. 1.9	Layer-by-layer assembly of plasma treatment, nanomaterials, small molecules.	51
Figure. 1.10	Water contact angles obtained after different treatments of the PEI membrane.	51

**Chapter 2**  
**Arginine Mediated Surface Modification of Polymers for Tissue Engineering Applications**

S. No.	Description	Page
Figure. 2.1	Conversion of PEI beads to a film.	73
Figure. 2.2	Emitech plasma asher used for the work reported in this chapter	73
Figure. 2.3(a)	UV-Vis trace for citrate stabilized gold nanoparticles	80
Figure. 2.3(b)	TEM image of the same. Scale bar 20 nm	80
Figure. 2.4	Solid-state UV-Vis traces of arginine-coated (A), and fibronectin-coated (B) PEI films.	81
Figure. 2.5	Contact angle determination using 10 $\mu$ l water droplet on the treated film. Data represented $\pm$ SD of n=3.	82
Figure. 2.6	Water absorbed on each film is indicated by a plot of weight of water absorbed per unit weight of the film.	83
Figure. 2.7	Mechanical stability profiles of film (A), arginine-coated film (B), fibronectin-coated film (C)	84
Figure. 2.8	AFM images (contact mode) showing topography of surface coated films along with control untreated (A), gold coated (B), arginine dipped (C), and fibronectin dipped (D) films. Surface roughness parameters are provided with each individual images.	85
Figure. 2.9	Full-length IR spectrum of differently surface modified films under ATR mode. The relevant region is expanded in Figure 2.10.	86
Figure. 2.10	FT-IR spectrum taken in ATR mode for the characterization of signature peaks from PEI film (1), arginine-coated PEI film (2), and fibronectin-coated PEI film (3). (a) Broad peak at 1550-1600 $\text{cm}^{-1}$ corresponds to protonated, hydrated guanidium groups. (b) Amide I (from fibronectin) 1670 $\text{cm}^{-1}$ , and (c) Amide II 1560 $\text{cm}^{-1}$ .	87
Figure. 2.11	Cellular adhesion experiment by cell counting where not-adhered cells were estimated using Trypan blue. Data represented as a $\pm$ SD of n=3.	88
Figure. 2.12	Cell viability by mitochondrial activity using resazurin indicator at 48 h. Data represented as $\pm$ SD of n=3.	89
Figure. 2.13(a)	Live-dead assay by live cells imaging. Live, and dead cell stains are acridine orange (AO), and propidium iodide (PI). Scale bar 100 $\mu$ m.	91
Figure. 2.13(b)	Quantification of fluorescent tags from live-dead assay images. (A) Acridine orange (AO, green), and (B)	91

	Propidium iodide (PI, red) from figure 2.13.A. Data represented as a $\pm$ SD of n=7.	
Figure. 2.14	Cell proliferation study by cell counting using Trypan blue exclusion test. Data represented as the mean $\pm$ SD of n=3.	92
Figure. 2.15(a)	Visualization of L929 fibroblast cells (using DAPI, and CFSE) with the aid of a fluorescence microscope. Scale bar is 100 $\mu$ m.	93
Figure. 2.15(b)	Quantification of fluorescent tags from cells. CFSE and DAPI from figure 2.13.A. Data represented as a $\pm$ SD of n=7.	93
Figure. 2.16	Actin filament staining of L929 cells (using Alexafluor Phalloidin 488), and DAPI for nucleus counterstaining. Scale bar 20 $\mu$ m.	95
Figure. 2.16	Actin cytoskeleton staining of arginine-coated (A), and fibronectin-coated (B) films. Scale bar 5 $\mu$ m	95
Figure. 2.17	Expression of collagen on the surface of differently surface-modified films (A), in corresponding well's spent media (B). Data represented as $\pm$ SD of n=3.	96

### Chapter 3

#### Design and Fabrication of a Dual Purpose Scaffold by a Logical Combination of Drug-release and Tissue engineering

S. No.	Description	Page
Figure. 3.1	Determination of cisplatin concentration by colorimetric assay: Plot of the absorbance of cisplatin o-phenylenediamine complex (Y-axis) with amount of cisplatin (X-axis)	109
Figure. 3.2	UV-Vis profile of AuNP-coated HDPE, and cisplatin coated HDPE.	115
Figure. 3.3	Characterization of cisplatin coated HDPE scaffolds by XPS.	116
Figure. 3.4	Characterization using SEM: (A) HDPE scaffold, (B) AuNP-coated HDPE scaffold, (C) Cisplatin-conjugated HDPE scaffold, (D) EDX of sample cisplatin-conjugated HDPE scaffold.	118
Figure. 3.5	Release profile of hydrated cisplatin in different environments (pH 5.5 and pH 7.4). Optimal time for maximum drug release: 48 h.	119
Figure. 3.6	Cell viability assay by mitochondrial activity (using resazurin indicator) with KB (human mouth cancer) cells at 48 h. Data represented as the mean $\pm$ SD of n=3.	120

Figure. 3.7(a)	Cellular morphology analysis in cisplatin treated cells (using DAPI, and CFSE). Scale bar is 100 $\mu\text{m}$ .	121
Figure. 3.7(b)	High-resolution images of cisplatin affected KB cells, and controls. Scale bar is 50 $\mu\text{m}$ .	122
Figure. 3.7(c)	Quantification of fluorescence emission from microscopy images from Figure 3.7.A. DAPI (blue), and CFSE (green). Data represented as a $\pm\text{SD}$ of $n=7$ .	122
Figure. 3.8(a)	Live-dead assay by live cells imaging. Live and dead cell stains are acridine orange (AO), and propidium iodide (PI). Scale bar 100 $\mu\text{m}$ .	123
Figure. 3.8(b)	Quantification of fluorescent tags from live-dead assay images. (A) Acridine orange (AO, green), and (B) Propidium iodide (PI, red) from figure 2.13.A. Data represented as a $\pm\text{SD}$ of $n=7$ .	124
Figure. 3.9(a)	Analysis of cell-death mechanism (extent of apoptosis) on KB cells with the help of a flow cytometer. Annexin V-FITC: apoptosis marker, PI: dead cell marker.	125
Figure. 3.9(b)	Apoptosis assay plot (from Figure 3.9.A): Cells present in different quadrant for different treatments.	126
Figure. 3.10 Figure. 3.10	Expression of phosphatidyl serine in KB cells by imaging. Scale bar is 100 $\mu\text{m}$ .	127
Figure. 3.11	L929 regrowth on cisplatin scaffolds after drug release. Data represented as the mean $\pm\text{SD}$ of $n=3$ .	128
Figure. 3.12	Representative images on L929 regrowth on cisplatin scaffolds (stains: CFSE, and DAPI). Scale bar is 100 $\mu\text{m}$ .	129

## Chapter 4

### Response of macrophages with respect to surface charge alterations

S. No.	Description	Page
Figure. 4.1	Temporal sequence of events after biomaterial implantation.	137
Figure. 4.2	Solid-state UV-Vis trace of A. AuNP-coated PEI film, B. PDADMAC-coated PEI film, C. PAA-coated PEI film.	145
Figure. 4.3	Contact angle measurement using 10 $\mu\text{l}$ of water droplet on the surface modified film. Data represented $\pm\text{SD}$ of $n=3$ .	147
Figure. 4.4(a)	Full length FT-IR spectrum of PEI film (black), PDADMAC-coated PEI film (red), PAA-coated PEI film (blue).	148
Figure. 4.4(b)	Expanded 1400-2000 $\text{cm}^{-1}$ wavenumber range.	148



Figure. 4.5	Cellular adhesion experiment by resazurin assay: (a) RAW264.7, (b) HepG2, (c) L929 cells. Data represented as a $\pm$ SD of n=3.	150
Figure. 4.6(a)	Live-dead assay by live cells imaging. Live, and dead cell stains are acridine orange (AO), and propidium iodide (PI). Scale bar 100 $\mu$ m.	153
Figure. 4.6(b)	Quantification of fluorescent tags from live-dead assay images. (A) Acridine orange (AO, green), and (B) Propidium iodide (PI, red) from figure 2.13.A. Data represented as a $\pm$ SD of n=7.	154
Figure. 4.7	Visualization of different subtypes of cells (a) RAW264.7, (b) HepG2, (c) L929 on differently charged surfaces. Stains: CFSE, and DAPI. Scale bar 100 $\mu$ m.	155

## List of abbreviations

P-LbL: Plasma, layer by layer

AuNP: Gold nanoparticles

ECM: Extra cellular matrix

CAM: Cell adhesion molecules

RGD: Arginine-glycine-aspartic acid

GAG: Glycosamino glycan

FBR: Foreign body response

HDPE: High density polyethylene

UHMWPE: Ultra high molecular weight polyethylene

PEI: Polyetherimide

PAA: Polyacrylic acid

PDADMAC: poly diallyldimethylammonium chloride

BSA: Bovine serum albumin

PBS: Phosphate buffered saline

FBS: Fetal bovine serum

DMEM: Dulbecco's minimum essential medium

MEM: Minimum essential medium

AO: Acridine orange

PI: Propidium iodide

PFA: Paraformaldehyde

DNA: De-oxyribo nucleic acid

RNA: Ribo nucleic acid

DMA: Dynamic mechanical analyzer

SEM: Scanning electron microscope

NMR: Nuclear magnetic resonance

FT-IR: Fourier-transformed infrared

ATR: Attenuated total reflectance

AFM: Atomic force microscopy

# Chapter 1

## Introduction

**Parts of this chapter were published as:**

*Surface Modification of Polymeric Scaffolds for Tissue Engineering Applications.*

**Poulomi Sengupta**, Bhagavatula L. V. Prasad. *Regen. Eng. Transl. Med.* **2018**, 4, 75-91.

## 1.1. Introduction

Biomaterials are used to replace organs or parts of a body, when required, in a harmless, dependable and physiologically acceptable manner.<sup>1</sup> A diverse range of materials that include systems/devices as simple as sutures, needles, catheters, and tooth filling are being used in treating a disease or injury. Conversely, they could be more complex as a heart valve, hip or knee joint prosthesis, bone plates, intramedullary rod *etc.* Previously biomaterials were mainly being used for the superficial corrective surgery or only for the cosmetic purpose, but with time this notion has changed. With the introduction of 'tissue engineering'<sup>2</sup> the scope of biomaterials has increased and the concept is now not just limited to a superficial cosmetic correction; instead, it has risen the possibility of regenerating vital functional organs (e.g., heart, kidney, lung, and pancreas). Advanced research in the same line has yielded beating heart, ears, and bladders in laboratory starting from stem cells.<sup>3, 4, 5, 6</sup> For each of these purposes, biomaterials play an important role as they build the framework of the replaced tissue and mimic functions of the organ.

In 1982, the Clemson University Advisory Board for Biomaterials had formally defined the term biomaterial to be "*a systemically and pharmacologically inert substance designed for implantation within or incorporation with living systems*".<sup>7</sup> Within two decades, the reach of the field expanded and materials that can blend in with active tissue looks possible now. Thus a new definition for biomaterial was introduced as "*a nonviable material used in a medical device, intended to interact with biological systems*".<sup>8</sup> On the other hand, the word 'biomaterial' also created some misunderstanding when people confused it with the material of biological source. They defined biomaterial as "*a solid material, which occurs in and is made by living organisms, such as chitin, fibrin or bone*".<sup>9</sup> After a wise thought, Dr. D. F. Williams proposed a more logical and relevant definition. According to him, 'biomaterial' is a shorter form of 'biomedical material' (as a nanostructured material is commonly known as nanomaterial). Thus a '*biomedical material*' is defined as "*material which has an interface with tissues while performing its action*".<sup>14</sup> This is more appropriate as it considers the active performance of a foreign object (origin



may be biological) inside a human body.

In all, it may be summarized that biomaterials would include materials, that can replace a body part that has lost function due to disease or accident, support in recovery, improve functioning, and to correct few abnormalities. Bioimplants are a subset of biomaterials that are designed to interact with the body for a longer period; sometimes lifelong. Following three Tables (**Tables 1.1, 1.2, and 1.3**) list down biomaterials concerning purposes, location and system. **Figure 1.1** indicates the location of where biomaterials can be placed inside the human body.

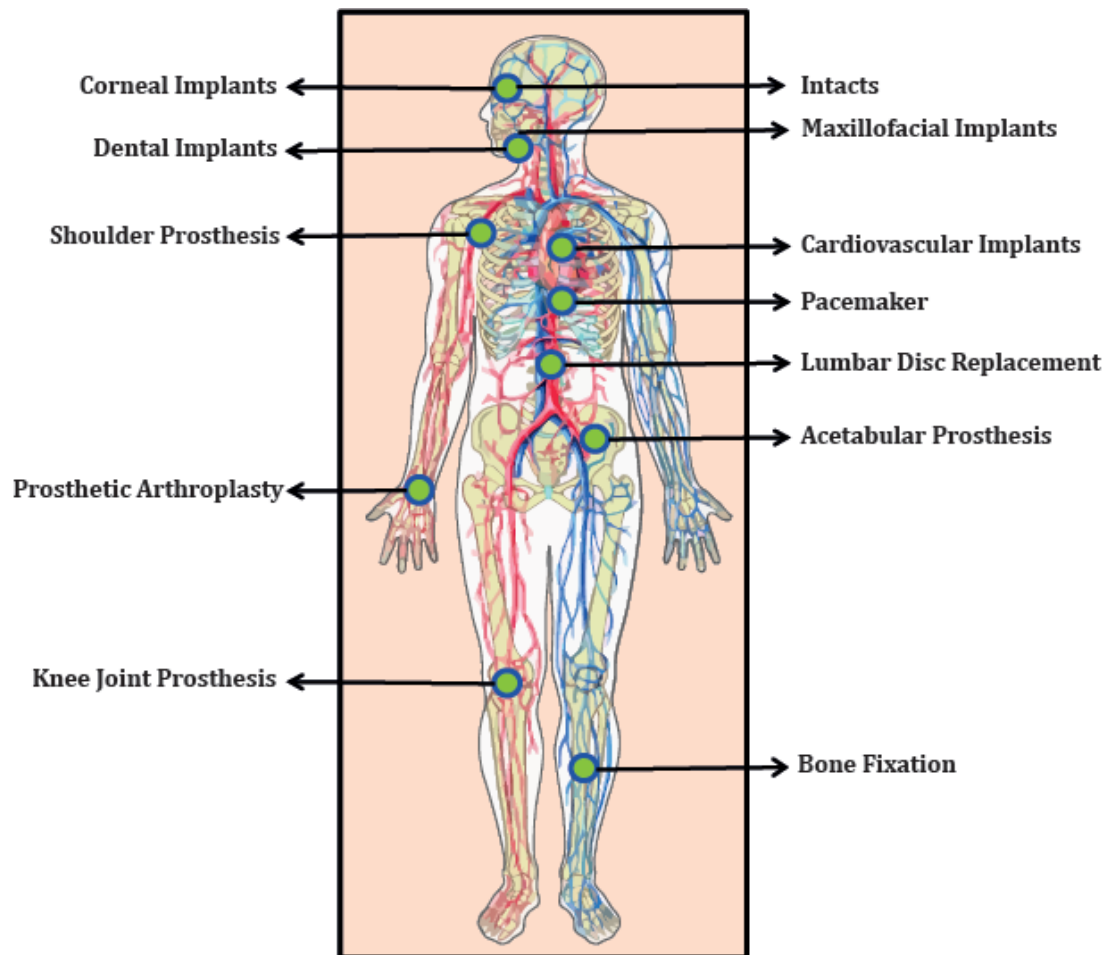


**Figure. 1.1:** Location of different bioimplants in human body. Image inspired from reference.<sup>10</sup>

<b>Purpose of biomaterials</b>	<b>Examples</b>
Replacement of diseased and damaged part	Artificial hip joints, knee joint, cardiac implants, artificial contour augmentation, dialysis set-up, blood vessel prosthesis, heart valve, blood prosthesis, biochips
Assist in healing	Sutures, meshes, bone pins, plates and screws, bone cement, surgical wires
Improve function	Cardiac pacemaker, intra-ocular lenses, corneal implants, vascular grafts, artificial stapes, cochlea implant
Correct functional abnormalities	Cardiac pacemaker
Correct cosmetic problems	Mastectomy augmentation, mammoplasty, chin, nose and lip augmentation, dental implants for tooth fixation, skin repair devices.
Aid to diagnosis	Probes to catheters
Aid to treatment	Catheters, drains, stents, antifouling coating material, bags

**Table. 1.1:** *Biomaterials for different purposes*

<b>Systems</b>	<b>Examples</b>
Skeletal	Bone plate, total joint replacements, craniofacial augmentation
Muscular	Sutures, muscle stimulator
Nervous	Hydrocephalus drain, cardiac pacemaker, nerve stimulator
Endocrine	Microencapsulated pancreatic islet cells
Reproductive	Augmentation mammoplasty, other cosmetic replacements

**Table. 1.2:** *Biomaterials for different systems*

<b>Organs</b>	<b>Examples</b>
Heart	Cardiac pacemaker, artificial heart valve, totally artificial heart, vascular stents, ventricular assist device
Lung	Oxy-generator machine
Eye	Contact lens, intraocular lens
Ear	Artificial stapes, cochlea implant
Bone	Bone plate, intra-medullary rod, bone cement, joint prosthesis
Kidney	Kidney dialysis machine, dialysis membrane
Bladder	Catheter and stent

**Table. 1.3:** *Biomaterials in different organs*

For the wide applications in healthcare, focused research on biomaterials/bioimplants is crucial and worthy of investing time, money as well as a human resource. Indeed, the past few decades have seen tremendous improvements in this field; some of them even ended up as *in vivo* prosthetics.<sup>11</sup> In the course of time, bioimplants required knowledge-based inputs of diverse fields like chemistry, material science, biology, medicine and engineering for the following reasons:

### **1.1.1. Chemistry and material science**

Metals, ceramics, polymers, and composites – these commonly used synthetic biomaterials require structure-property understanding and correlation with active tissues (blood and connective tissues). For any substantial change in functional properties of the implant, in-depth knowledge of chemistry and material science is necessary.

### **1.1.2. Biology**

For proper function/support of an implant, knowledge in cell and molecular biology (thorough understanding about extra cellular matrix or ECM), anatomy, animal and human physiology, histopathology, experimental surgery, immunology, *etc.* is very critical.

### **1.1.3. Medicine**

Understanding of all the clinical specialities, like dentistry, maxillofacial, neurosurgery, nephrology, obstetrics and gynaecology, ophthalmology, orthopaedics, plastic and reconstructive surgery, thoracic and cardiovascular surgery, veterinary medicine and surgery, *etc.* is required.

### **1.1.4. Engineering**

It is helpful in designing an implant with proper attributes that promote different functions. Engineering takes care of appropriate porosity, surface area, mechanical properties, movements, specialized functional properties (like joints, valves *etc.*).

Fields like chemical sciences and engineering have truly enriched the field as far as improvement in function of a material is considered. Active changes in the structure and design in order to promote different functions needed by the organs can be well understood from the knowledge of engineering. On the other hand changes in the surface properties (tuned chemical conjugation leading to presence/absence and release of different biomolecules) can aid in different functional behaviour of the bioimplants. Specifically, the presence of proper biomolecules on the surface of the material can very well dictate the future of new tissue generated through several means including stem cells differentiation.

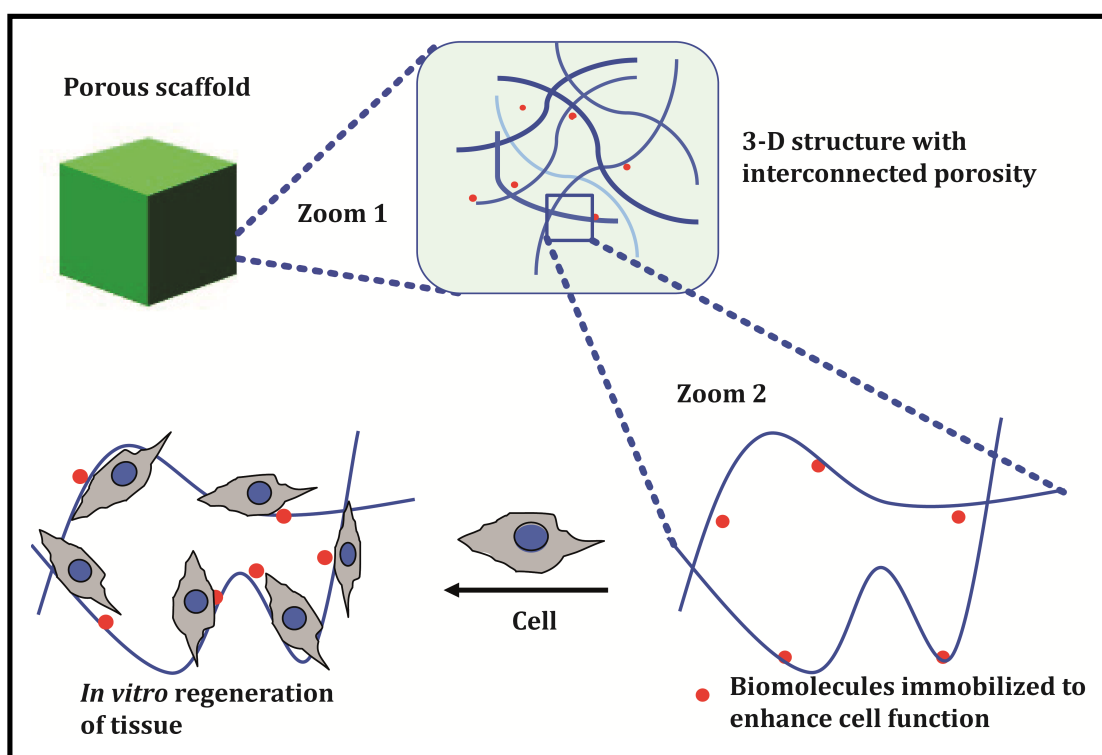


**Figure. 1.2:** Schematic representation of a solid scaffold containing biological molecules and its in vitro application in the regeneration of tissues.

Irrespective of the material source or the location of the implant in the body, all the materials listed in **Tables 1.1, 1.2** and **1.3** elicit biological responses to a certain extent. To understand what are these responses in detail, it is necessary to understand the mechanism of cell-material interaction.

## 1.2. Cell-material interaction

As depicted in **Figure 1.2**, cells bind to the three-dimensional scaffolds *in vitro*. Cellular adhesion depends not only on scaffold's intrinsic properties: like surface topography, charge, *etc.* but also on the nature of a biomolecule present on the surface that dictates the fate of an implant. The three most necessary elements for successful tissue growth are:

1. Cells and Cell-ECM interactions
2. Nutrients
3. Scaffolds

### 1.2.1. Role of cells

Cells are the building blocks of our body. The cells first structure into tissues and then develop into organs in a bottom-up approach. Proper development of an organ from cells is governed by the cell-ECM interaction. Cells do not interact with the naked material either *in vitro* or *in vivo* rather they continuously condition the surface/scaffold that they want to interact, with biological fluid components.<sup>12</sup> There are several factors involved in the cell-material interactions; such as pH, ionic composition/strength of the solution, temperature, and functional groups present on the matrix/scaffold as well as on the cellular proteins.

#### 1.2.1.1. Cellular adhesion and cell-ECM interaction

ECM<sup>13</sup> is a collection of molecules excreted by a living cell. It provides structure and support to the newly growing cell lines. ECM has three main components:<sup>14</sup> (i) proteoglycans: The main component is GAGs (glycosaminoglycans) with hyaluronic acids, which impart negative charges on themselves, and drags a lot of water molecules. This gives rise to a foamy viscous gel-like support, which helps cells to stay inside. The well-known proteoglycans are heparin sulfate, keratin sulfate and chondroitin sulfate *etc.*, (ii) insoluble collagen fibres: collagen is a trimer of glycoproteins, which provides support for strength and resistance to pulling forces, (iii) soluble extracellular proteins like fibronectin, laminin. Among these laminin is a cross-shaped protein, which sits on the collagen framework and crosslinks different sites adding strength and integrity to the basement membrane. It also helps in the

mobility of cells. Fibronectin is a repeating protein having multiple domains for interaction. It has a special cell-binding domain carrying RGD (arginine, aspartin, glycine) loops that is required to bind onto cells. This part is very essential for binding, movement and branching of the cells. Apart from these, there are cell adhesion molecules (CAMs) expressed in the cellular membranes. CAMs are cell membrane proteins expressed to promote cell adherence to the ECM or to each other. CAMs broadly consist of 4 subtypes. 1. Cadherins: there are 6 subtypes of cadherins. Mostly they help in adherence by hemophilic interaction at the cell-cell junction. 2. IgG or immunoglobulin superfamily: these also mediate cell-cell interaction at junctions. 3. Integrins: these are heterodimers facilitating cell-matrix interaction at focal adhesion point through their interaction with ECM protein fibronectin. 4. Selectins: primarily mediate heterotopic cell-cell adhesion. Thus ECM along with CAMs work as an excellent host for accommodating cells. But cellular proliferation starts with cellular adhesion.

The most crucial phase in tissue engineering is cell adhesion to ECM followed by differentiation and proliferation leading to its designated functions. The initial phase of the cell's interaction with ECM is governed by ionic forces and van der Waal interactions.<sup>15</sup> This is followed by a long adhesion phase involving ECM proteins, cell membrane proteins, integrins *etc.* The extracellular microenvironment plays a major role in cellular adhesion.<sup>16</sup> Therefore in the development of a synthetic scaffold, it is important to mimic the complexity of ECM both *in vitro* and *in vivo*.

After cellular adhesion, it is absolutely necessary to nurture the cells with nutrients, which will help in cellular maintenance, proliferation and differentiation.



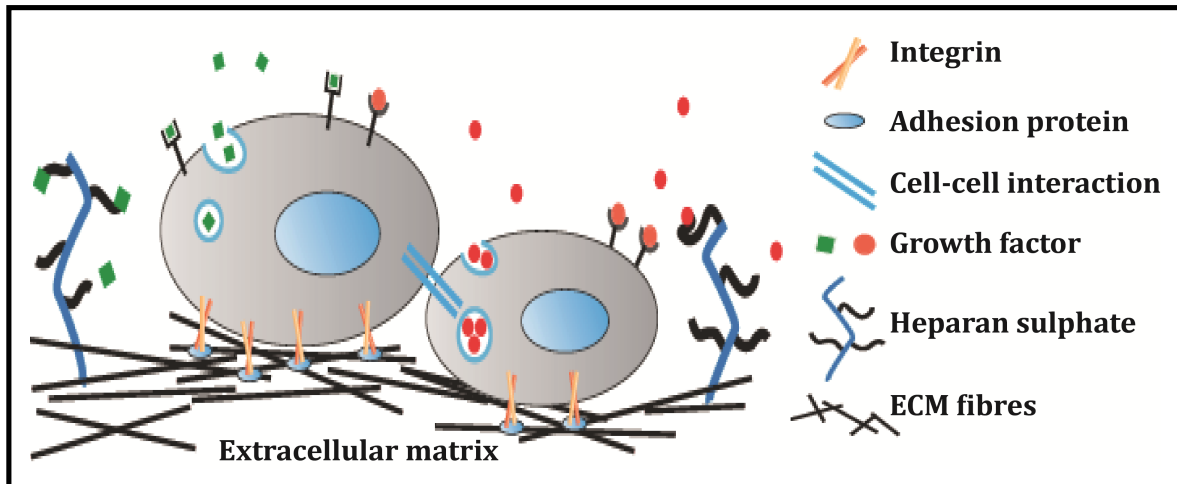


**Figure. 1.3:** Representation of various proteins responsible for cellular adhesion. Image adapted from reference.<sup>17</sup> The license agreement is in page 162

### 1.2.2. Role of nutrients for tissue growth

The nutrients can be (i) small molecules, (ii) polypeptides, proteins (especially growth factors), (iii) oligonucleotides (DNA, RNA to aid in gene transcription). Nutrients supplied to the cells with these aids are essential to initiate proliferation and differentiation so the cells can secrete the suitable extracellular components for the tissue development. Presence of pores in ECM help in the optimal exposure of already adhered cells to the nutrients it needs. High surface area and pore-connectivity also help in vascularization.

### 1.2.3. Role of scaffolds

Scaffolds are critical constituents of tissue engineering. They are the artificial analogue of ECM that cells comfortably adhere to during proliferation and differentiation. For tissue engineering purpose, scientists synthesize/modify solid supports that can help in cellular attachment and growth. The solid support in future can replace an organ (like a knee, hip joints), or if biodegradable, can help in the development of proper functional tissues and biodegrade with time (for example bioresorbable vascular scaffolds – coronary stents). Scaffolds can be of natural origin or artificial, but there has been a lot of research on modifying the surface properties of either type to make them biocompatible keeping in mind the

cell-ECM interactions. For example, cardiomyocytes take elongated shape as they nicely fit in the grooved array of ECM (**Figure 1.4**).<sup>18</sup> Similarly, for liver regeneration, the cells acquire polarization once they face the surface modifying molecules present on nanofibers (**Figure 1.4**, second row). Also, bone regeneration is favored only on hydroxyapatite nanostructure due to their specific shape, size and material property (**Figure 1.4** third row).

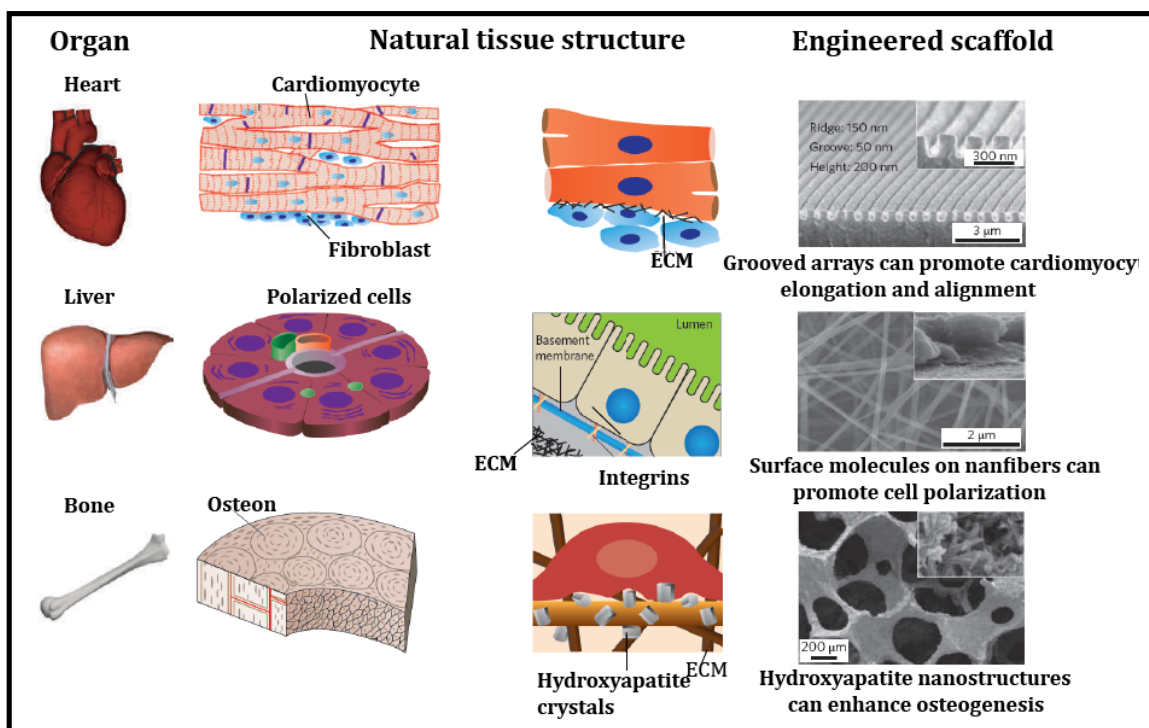


**Figure 1.4:** Illustrations of the heart, liver and bone at the level of the organ (left) and tissue and cell/matrix interaction (centre), followed by scanning electron micrographs of engineered scaffolds (right). The ECMs of various tissues have different composition and spatial organization of molecules to maintain specific tissue morphologies (Image adapted from.<sup>17</sup>) The license agreement is in page 162

### 1.3. Materials developed for tissue engineering

While metals<sup>19</sup> (inclusive of alloys, composites) and ceramics<sup>19</sup> are extensively being used as bioimplants even today, polymers are offering great hope as alternatives to these materials due to a broad range of material advantages. The comparison between these three has been summarized in **Table 1.4**.

	Ceramic	Material	Polymer
Hardness	++	-	--
Elastic modulus	++	+	-
High temperature strength	+	-	--
Thermal Expansion	-	+	+
Ductility	-	+	+
Corrosion resistance	+	-	-
Resistance to wear	+	-	-
Electrical conductivity	Neutral	+	-
Density	-	+	--
Thermal conductivity	Neutral	+	-

**Table. 1.4:** *The typical requirements of scaffolds and the characteristics of different materials.*<sup>20</sup>

Advancements in the field of polymer synthesis have brought up revolution in the modern world, including medical science. Prior to the advent of synthetic polymers, scaffolds based on natural animal protein-based biopolymers such as wool, silk fibroin, gelatin, and collagen were explored extensively.<sup>21</sup> The most important advantages of using biological polymer are that they may positively support cell adhesion and function and are expected to be less prone to immuno-rejection. Apart from proteins naturally occurring polycarbohydrates like chitin/chitosan, polysaccharides, cellulose, starch, alginate, hyaluronic acid *etc.* and their derivatives are also being extensively explored for tissue engineering/bioimplant applications. However, it is a challenging task to have control over the size, shape and desired functionalities in these natural polymers. Furthermore, isolating them from

naturally occurring ingredients turns out to be time consuming, low yielding hence costly most of the times. Nonetheless, collagen-based implants are widely being used in cardiac surgery (heart valve rings, separating septa of two heart chambers), pelvic floor surgery, treatment of osteoarthritis, lip augmentation, wound healing and facial rejuvenation<sup>22</sup> although they are expensive. Collagen along with gelatin, alginate, and silk has been found to blend well and widely researched in various applications.<sup>23</sup>

<b>Polymer</b>	<b>Applications</b>	<b>Areas</b>
Polyacrylates	Orthopaedics, dentistry, surgery, ophthalmology,	Cement, composites, bandages, contact lenses
Polyethylene	Orthopaedics, dentistry	Joint bearings, joint, floss
PET	Surgery	Sutures, patches, vascular grafts
Polyurethane	Orthopaedics, dentistry	Disk bearings, ligatures
Silicones	General	Soft tissues, leads, artificial skin, other space-filling implants, lung
Nylons	Surgery	Suture and patch materials
Polystyrene	Biochemistry	Assay dishes
Polypropylene	Surgery, Cardiovascular	Grafts, sutures
PTFE (Teflon)	Cardiovascular	Grafts
PVA	Burns	Wound dressing
Poly- $\alpha$ -OH acids	General	Suture, devices, drug delivery

**Table. 1.5:** List of synthesized polymers and their applications.

Besides these natural materials based ones, synthetic polymer-based composites have generated great hope as tissue engineering scaffolds.<sup>24</sup> **Table 1.5** lists major synthetic polymers that have been used in surgical or implant purposes.

It may be worth mentioning here that for a polymer scaffold to be accepted as a life-long replacement, it must possess few special criteria, which are listed below.

- (1) Presence of three dimensional and interconnected pores to encourage tissue integration and vascularization.
- (2) Bio-inertness and the ability to blend with the natural tissue inside body for permanent replacement.
- (3) Biodegradable and bioresorbable nature (if the bioimplant is meant to replace an organ).
- (4) Presence of proper surface functionalization so that it encourages cellular attachment, differentiation and proliferation.
- (5) Mechanical compatibility with the tissue/organs it is meant to replace.
- (6) The absence of any contamination, hence survival in sterilization condition.
- (7) Easy moldable nature into various shapes and sizes.

#### **1.4. Role of hydrophobic polymers**

Polymers like HDPE possess several advantageous special features that fulfill most of the above criteria such as: (i) the convenience in their manufacturing *via* easily controllable polymerization reactions (ii) the flexibility that is offered in terms of modulating their the molecular weight (iii) the ease with which porous scaffolds can be prepared (iv) the control that can be exercised on the porosity and surface area of these scaffolds. HDPE having tensile strength around 0.2-0.4 N/mm<sup>2</sup>, the density of 0.941-0.965 gm/cc, can produce material of enormous hardness. Most importantly, HDPE has an excellent track record for being used as bioimplant since decades. Several companies (Poriferous,<sup>25</sup> Medpore,<sup>26</sup> Biopore,<sup>27</sup> Porestar,<sup>28</sup> Synpor<sup>29</sup>) manufacture different HDPE and UHMWPE products intended to be used as bioimplants. It is a widely trusted material, due to its biocompatibility, resistance to microbial attack and tissue-friendly nature. Due to these favourable properties,

gamma treated ultra high molecular weight polyethylene (UHMWPE) is utilized in metal-on-plastic hip implants,<sup>30,31</sup> stents, catheters, and maxillofacial, cranial implants. It is noninfectious<sup>32</sup> and integrates with live tissue in the body in its due course of time. Hydrophobic polymers are inclined towards fibroblast attachment; also they are prone to migrate cells (migration rate of fibroblast on PE at contact angle 57° is 1111 cells/cm<sup>2</sup>.h).<sup>33</sup>

For reconstruction purpose, HDPE and UHMWHDPE are being used popularly, although some uses of Polypropylene, Styrene, LDPE are also reported.

### 1.5. Surface modification techniques and their drawbacks

Surface modification is essential for the successful implementation of tissue engineering.<sup>34</sup> Latest publications<sup>35</sup> indicate that with proper design biologically relevant surface modified functional materials can be constructed. There have been several approaches to modify the surfaces of hydrophobic polymers in order to make them more hydrophilic and cell-friendly. Below is a comprehensive list of saturated polymers attempted for surface modification.

Reference	Surface modification with	Polymer	Surface modification technique	Application
Richey <sup>36</sup> <i>et al.</i>	Acrylic acid and 2(dimethylamino) ethyl methacrylate	HDPE	UV method graft polymerization	Antithrombin drug delivery by balloon catheter
Gatenholm <sup>37</sup> <i>et al.</i>	Ozone	PP	Ozone induced grafting process (ozonation) of 2-hydroxyethylmethacrylate (HEMA)	
Liu <sup>38</sup> <i>et al.</i>	Phosphorycholine	PE	Acrylic acid graft copolymerized by UV. Choline hydroxide was	Platelet compatibility by <i>in vitro</i>

			chemically reacted on phosphorous oxychloride treated PE films	platelet compatibility tests
Lei <sup>39</sup> <i>et al.</i>	Acrylic acid	HDPE	Photografted using benzophenone	
Nakaoka <sup>40</sup> <i>et al.</i>	Collagen	PE	Immobilization of proteins on acrylic acid grafted polyethylene films	Inhibitory activity on polyethylene surfaces
Lavanant <sup>41</sup> <i>et al.</i>	Polyethylene Glycol	PE	Photobromination of the poly-ethylene substrate followed by surface-initiated ATRP of poly(ethylene glycol)	<i>In vitro</i> experiments to show integrin mediated cellular adhesion
Kidan <sup>42</sup> <i>et al.</i>	Antiplatelets and anticoagulants	PE, Glass, PTFE	Covalent immobilization by gamma-irradiation	Platelet deposition and fibrinogen adsorption
Yang <sup>43</sup> <i>et al.</i>	Glycopolymer	PP	UV-induced polymerization	BSA solution permeation and adherence of platelets
Tao <sup>44</sup> <i>et al.</i>	Acrylic acid	PP	Hyperbranched grafting with polyacrylic acid	Increase in adhesion
Rasmussen <sup>45</sup> <i>et al.</i>	Hydroxy groups	PE	Chromic acid and nitric acid	
Chanunpanich <sup>46</sup> <i>et al.</i>	Two types of C-Br bonds	LDPE	Gaseous bromination reaction	
Wang <sup>47</sup> <i>et al.</i>	Branches of PEG	LDPE	UV induced graft copolymerization	
Goddard <sup>48</sup> <i>et al.</i>	Lactose	PE	Covalent attachment of	Food packaging



<i>al.</i>			lactose <i>via</i> PEI	
Mamoo <sup>49</sup> <i>et al.</i>	Methacrylic acid, styrene	PE	Free radical graft polymerization	
Rubira <sup>50</sup> <i>et al.</i>	Hydroxy and carboxylic acid	PE, PP	Fe(CO) <sub>5</sub> sorption and oxidation	
Hoshi <sup>51</sup> <i>et al.</i>	Phospholipid	PE	Impregnation of CO <sub>2</sub> followed by <i>in situ</i> radical polymerization	Reduction of protein adsorption
Yao <sup>52</sup> <i>et al.</i>	Polyacrylic acid	PE	Graft copolymerization of acrylamide (AM) and acrylic acid (AA)	
Favaro <sup>53</sup> <i>et al.</i>	Hydroxy and carboxylic acid	HDPE, PP	Oxidation by KMnO <sub>4</sub> /HCl	
Qu <sup>54</sup> <i>et al.</i>	Chitosan and chitosan hydrogels	HDPE	Coating by chitosan or hydrogels after acrylic acid grafting on HDPE	
Gorbachev <sup>55</sup> <i>et al.</i>	Polyacrylic acid	PE, PP	Photoinduced graft polymerization of acrylic acid	
Moro <sup>56</sup> <i>et al.</i>	Phosphorylcholine	PE	Graft polymerization of MPC	Inhibition in bone osteolysis
Zand <sup>57</sup> <i>et al.</i>	Hydroxy groups	UHM WPE	Sodium hypochlorite reaction followed by acid treatment	Resistance in wear
Yamada <sup>58</sup> <i>et al.</i>	Glycidyl methacrylate	HDPE, LDPE	Photografting, then strengthening adhesive properties by amine or epoxy groups.	Optimization of autohesive and adhesive properties
Zhang <sup>59</sup> <i>et al.</i>	Glycidyl methacrylate	PE	Corona treatment followed by surface graft polymerization of	Surface wettability and hardening of

			glycidyl methacrylate	the surface
Lei <sup>60</sup> <i>et al.</i>	Poly acrylic acid	LLDPE	Grafting with acrylic acid <i>via</i> ultraviolet light	Hot melt adhesive
El Kholdi <sup>61</sup> <i>et al.</i>	Poly acrylic acid	LDPE	Graft polymerization with acrylic acid in presence of photoinitiators	
Wang <sup>62</sup> <i>et al.</i>	Glycidyl acrylate and acrylic acid	HDPE	Photografting glycidyl acrylate and acrylic acid	Mechanical adhesion
Amornsakchai <sup>63</sup> <i>et al.</i>	Methyl methacrylate	PE	Photoinitiated grafting technique using methyl methacrylate	
Deng <sup>64</sup> <i>et al.</i>	Vinyl acetate	LDPE	Photografting vinyl acetate	Effect of solvent compatibility
Irwan <sup>65</sup> <i>et al.</i>	N-Isopropylacrylamide (NIPAAm)	LLDPE	Photografting N-isopropylacrylamide	Extent of swelling and shrinking at two different temperatures
Irwan <sup>66</sup> <i>et al.</i>	Methacrylic acid	LLDPE	Photografting of methacrylic acid	Effect of solvent mixtures
Wang <sup>67</sup> <i>et al.</i>	poly(methacrylic acid)	PE	UV induced grafting of methacrylic acid	Effect of solvents of the location of grafting
Wang <sup>68</sup> <i>et al.</i>	Co-polymer of methacrylic acid and acrylic acid	PE	UV induced grafting of methacrylic and acrylic acid	Effect of solvent on the extent of grafting
Chen <sup>69</sup> <i>et al.</i>	Poly glycidyl methacrylate	PE	Ar plasma pretreatment and UV-induced graft polymerization of glycidyl methacrylate followed by immobilization of heparin	Enhance blood compatibility

Yang <sup>70</sup> <i>et al.</i>	Poly methyl methacrylate	LDPE	Photografting of methyl methacrylate without additional photoinitiator	Photoinitiator free grafting system
Tada <sup>71</sup> <i>et al.</i>	Sulfonation	PP	Exposure to hot concentrated sulfuric acid	Conformational changes on polypropylene backbone
Cross <sup>72</sup> <i>et al.</i>	Radical chlorination	LDPE	Heterogeneous gas-solid reaction of LDPE with chlorine gas	Depth and intensity of chlorination
Bergbreiter <sup>73</sup> <i>et al.</i>	Nitroxyl groups	PE	Entrapment functionalization of surface functionalized polyethylene in polyethylene powder	Control of surface functionalization
Bergbreiter <sup>74</sup> <i>et al.</i>	PEG	PE	Physically entrapping relatively short terminally functionalized ethylene oligomer	Control on surface grafted functional groups
Stoleru <sup>75</sup> <i>et al.</i>	Chitosan	PE	Chitosan grafting on corona treated PE surface by coupling reactions	Improved friction properties and tear resistance
Zheng <sup>76</sup> <i>et al.</i>	Ag nanoparticles and heparin	PE	PE exposure to O <sub>2</sub> plasma, followed by cysteamine conjugation, silver nanoparticle formation and heparin coating	Anticoagulant and antibacterial activity
Dhamodharan <sup>77</sup> <i>et al.</i>	Nitrogen and oxygen surface functionalities	LLDPE, PP	Mercury sensitized photochemical reaction in presence of aqueous ammonia (modified Mercat reaction)	
David E. Bergbreiter <sup>78</sup> <i>et al.</i>	Polyacrylic acid	PE	Grafting of t-butylacrylate after oxidizing polyethylene surface	Derivatization of hyperbranched surface

ZenonFoltynowicz <sup>79</sup> <i>et al.</i>	Long chain phosphocholines	LDPE	UV induced polymerization of long chain phosphocholines	
Chanunpanich <sup>80</sup> <i>et al.</i>	Aromatic thiolated compounds	PE	Reaction by bromination followed by reactions with aromatic thiolated molecules	
Moon Suk Kim <sup>81,82</sup> <i>et al.</i>	Streptavidin FITC	PE	Surface functionalization with corona discharge followed by biotin streptavidin-FITC recognition	Generation of a gradient PE surface
E.Ä. Kiss <sup>83</sup> <i>et al.</i>	Polyethylene oxide	PE	Surface halogenation followed by covalent attachment of polyethylene oxide	Surface wettability
Kavc <sup>84</sup> <i>et al.</i>	Sulfonic acid groups	PE	Photochemical interaction of polyethylene with SO <sub>2</sub> and H <sub>2</sub> O	Modification of membrane
Dahlia Fischer <sup>85</sup> <i>et al.</i>	Sulfonic acid groups	LDPE	32% SO <sub>3</sub> in H <sub>2</sub> SO <sub>4</sub> room temperature reaction	
S.B. Idage <sup>86</sup> <i>et al.</i>	Sulfate, keto and polyene	HDPE	Gas mixture of SO <sub>3</sub> and N <sub>2</sub> passed polyethylene	Surface groups present
Pandiyaraj <sup>87</sup> <i>et al.</i>	Chitosan	LDPE	Chitosan immobilization	Antithrombogenic nature
Theapsak <sup>88</sup> <i>et al.</i>	Chitosan	PE	Plasma followed by chitosan coating	Antibacterial packaging
Bergbreiter <sup>89</sup> <i>et al.</i>	Sulfonic acid groups	PE	Sulfuric acid treatment	Generation of hydrophilicity
Greene <sup>90</sup> <i>et al.</i>	Hydroxyl groups	PE	Oxygen glow discharge gas plasma	Generation of hydrophilicity
Bretagnol <sup>91</sup> <i>et al.</i>	Amine groups	PE	Low pressure low frequency NH <sub>3</sub> plasma	Comparison of physical properties

Santos <sup>92</sup> <i>et al.</i>	Charges	PE	Corona discharge	Surface engineering
Wang <sup>93</sup> <i>et al.</i>	polyacrylamide	PE	UV induced graft copolymerization with acrylamide	Making adhesive surface
Tahara <sup>94</sup> <i>et al.</i>	Peroxide groups	PE	Glow discharge plasma treatment	Enhancement of adhesive properties
Lehocky <sup>95</sup> <i>et al.</i>	Oxygenated groups	HDPE	Oxidative RF-plasma treatment	
Tajima <sup>96</sup> <i>et al.</i>	Oxygen containing functionalities	LDPE	Inductively coupled RF argon plasma	Surface wettability
Milani <sup>97</sup> <i>et al.</i>	Polar groups like C=O, COOR, OR, OH, etc.	HDPE	Plasma treatment, chlorinated phosphazenes, modification by trifluoroethanol and heptadecafluorononanol	Surface functionalization
Bismarck <sup>98</sup> <i>et al.</i>	Oxygen and nitrogen containing functional groups	LDPE, PC	Atmospheric pressure plasma treatment in presence of O <sub>2</sub> , N <sub>2</sub> , argon, air	Surface wettability
Farhat <sup>99</sup> <i>et al.</i>	same	UHM WPE	Atmospheric pressure air plasma treatment	Wear resistance
Drnovska <sup>100</sup> <i>et al.</i>	Hydroxyl and amine groups	HDPE	Reduced pressure plasma glow discharge treatment in presence of oxygen and ammonia	Examination of surface groups
Jung <sup>101</sup> <i>et al.</i>	Oxygenated groups	HDPE	Reduced pressure circulating fluidized bed reactor plasma in presence of oxygen	Examination of surface properties
Wang <sup>102</sup> <i>et al.</i>		PE	Atmospheric pressure dielectric barrier discharge plasma in presence of air	Surface wettability

Medard <sup>103</sup> <i>et al.</i>	-COOH groups	HDPE	CO <sub>2</sub> , H <sub>2</sub> O plasma	Surface degradation
Kong <sup>104</sup> <i>et al.</i>	Oxygenated groups	LDPE	K <sub>2</sub> Cr <sub>2</sub> O <sub>7</sub> /H <sub>2</sub> O/H <sub>2</sub> SO <sub>4</sub> (4.4/7.1/88.5)]/oxygen plasma.	Changes in the material properties of LDPE
Kolska <sup>105</sup> <i>et al.</i>	Amine groups	HDPE, LDPE	Cysteamine grafting	Cellular adhesion and proliferation
Reznickova <sup>106</sup> <i>et al.</i>	Polar groups	PE	Plasma	Cellular adhesion
Hengjun <sup>107</sup> <i>et al.</i>	Oxygenated functional groups	UHM WPE	oxygen plasma.	Changes in the mechanical properties

*MPC: methacryloyloxyethyl phosphorylcholine PET: Poly-Ethylene Terephthalate; PTFE: PolyTetraFluoroEthylene (Teflon); PVA: PolyVinylAlcohol; PCL: PolyCaproLactone; HDPE: High DensityPoly-Ethylene; PP: Poly-Propylene; PE: Poly-Ethylene; LDPE: Low Density PolyEthylene; UHMWPE: Ultra High Molecular Weight Poly-Ethylene*

**Table. 1.6:** *The summary of published literature on polyethylene, polypropylene surface modification.*

Furthermore, in the following we have tried to classify these surface modification techniques into different categories, highlighting their pros and cons.

### 1.5.1. Graft polymerization technique

In this method, polymerization reaction is carried out on the surface of any polymer. For example, HDPE has been used to initiate graft polymerization to induce hydrophilic properties.<sup>108, 109</sup> The covalently grafted polymer introduces new material properties (like modified surface) while maintaining the physical integrity (strength, elasticity, compressibility) of the substrate. Polymer grafting and graft polymerization have been achieved by chemical, photochemical, plasma-induced, and enzymatic grafting methods.<sup>110</sup> The disadvantages of this type of surface modification include the fact that the chemical, photochemical, and radiation-based

techniques generally are time-consuming. Surface modifications using radiations generate free radicals that may elicit cytotoxicity when used inside the body. Additionally, graft polymerization or polymer grafting on HDPE surfaces many times becomes inhomogeneous due to the limited availability of accessible functional groups.

### **1.5.2. Nanoindentation method**

Traditionally nanoindentation has been/being used to measure the hardness of a solid. But recently it is being used to increase roughness, micropatterning that has been shown to promote cellular adherence. Unfortunately, this method requires great precision for achieving optimal roughness and hence would be difficult to implement on a large scale.

### **1.5.3. Surface modification by self-assembled monolayer formation**

In this method, the metal surface is modified by ligands through metal-ligand bond formation. This introduces surface roughness and may increase hydrophilicity, which attracts cells.<sup>111,112</sup> But this method is not generic and is also not applicable for polymers in general.

### **1.5.4. Corona discharge**

It is a simple, low cost, continuous process where an electrically induced stream of ionized air bombards the polymeric surface with the result of various oxygen-containing functional groups. It does not operate in a vacuum. So contamination, local moisture and humidity are the drawbacks of this method.

### **1.5.5. Flame treatment**

In this technique, the polymer surface is bombarded with ionized air with the result of surface functionalization of the top several layers of the polymer. It imparts hydroxyl, aldehyde, and carboxylic acid functional groups on polyethylene, which has been utilized to increase printability, wettability and adhesion.<sup>113</sup> However, it suffers from the drawbacks such as reduction in the optical clarity of the polymer



and the necessity to optimize several parameters like flame temperature, contact time, composition thus resulting in inconsistent surface functionalization.

#### **1.5.6. UV irradiation**

Reactive sites generated on polymers upon UV irradiation can initiate graft polymerization of bioactive molecules like N-vinyl pyrrolidinone.<sup>114</sup> But the non-uniform and low density of functionalization is a drawback of this method.

#### **1.5.7. Wet chemical treatment**

In this method concentrated acid is used to treat polyethylene and polypropylene surfaces.<sup>115,116</sup> Chromic acid in the presence of potassium permanganate and concentrated sulfuric acid produces reactive oxygen, which can convert polyethylene and polypropylene surfaces. Chromium oxide when mixed with water and concentrated sulfuric acid at 72 °C, initiates surface functionalization of polyethylene in one minute.<sup>117</sup> The problem with wet chemical techniques is the introduction of a range of oxygen-containing functional groups that are non-specific. Further with wet chemical techniques, hazardous chemical waste gets created and the surface etching irregular. Thus this method, although suited for lab experiments, is difficult to scale it up for an industrial process.

#### **1.5.8. Plasma treatment**

Plasma is a high-energy state of matter in which a gas (or a mixture) is partially ionized into charged particles, electrons and neutral molecules. In the high-energy state when the ions are bombarded with present polymer surface, the molecules in contact get functionalized. This technique does not require the use of solvents, hence does not involve the production of any chemical waste.

Plasma treatment has gained its popularity because of several reasons:

1. Uniformity: Reaches all surface area in a very short time, most plasma treatment machines operate under pressure followed by a vacuum application.
2. Reliable, reproducible relatively inexpensive.

3. Applicable to various materials of different geometries (metals, polymers).
4. Can be scaled up to meet industrial needs.
5. Operator friendly, dry and environmentally friendly.

In plasma treatment, the types of functionalization can be varied using different gas (argon, nitrogen, oxygen, water vapour, carbon dioxide, ammonia) and operating parameters like pressure, temperature, power, time, and gas flow rate *etc.* Oxygen plasma has been used on polyethylene to functionalize the surface molecules with hydroxyl groups.<sup>118</sup> CO<sub>2</sub> plasma introduces -COOH groups on polypropylene, polyethylene.<sup>119, 120, 121</sup> Plasma can also be used as a pretreatment for graft polymerization. For example, argon plasma pretreatment on polyethylene introduces grafts of poly(ethylene glycol) monomethacrylated 4-vinylpyridine on polyethylene.<sup>122</sup> Gugala *et al.*, have used various plasmas (O<sub>2</sub>, CO<sub>2</sub>, N<sub>2</sub>, NO<sub>2</sub>, SO<sub>2</sub> + H<sub>2</sub>, NH<sub>3</sub>) to study the attachment characteristics of osteoblasts on nonporous and porous membranes of poly(L/DL-lactide) 80/20%. The number of attached cells was evidently highest in case of membranes treated with ammonia plasma, thus making it a better choice for surface functionalization.<sup>123</sup>

However, despite a huge number of publications and patents on this topic, only very few plasma treated materials have found commercial acceptability. This primarily is due to surface reorganization of polymer molecules, which regenerates hydrophobicity on long-standing (sometimes overnight). A recent report<sup>124</sup> has shown the significant change in water contact angle on plasma-treated super hydrophobic surfaces over time. Even upon storage at low temperature and low humidity, the plasma treated surfaces developed hydrophobicity to a definite extent. A comparatively older report<sup>125</sup> also has claimed storage of plasma treated silicone rubber in the air affects the surface hydrophilicity. So, irrespective of the chemical composition of the material, the effects of plasma treatment are transient. Since surface hydrophilicity or wettability is one of the key requirements for cellular adhesion, such a reorganization of the surface renders the polymeric scaffold incompetent for integration. For example, Gugala<sup>40</sup> *et al.* (**Figure 1.5**) have shown

the decrease in osteoblast adherence when the plasma-treated PLLA membranes are stored for a longer time.

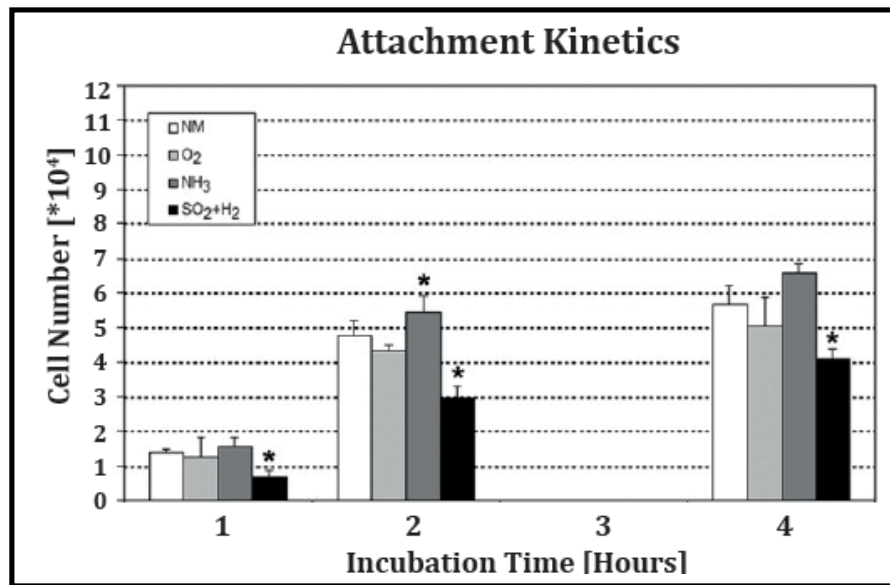


**Figure. 1.5:** Kinetics of attachment of osteoblasts cultured on nonporous polylactide membranes treated with various plasmas (NM, nonmodified; O<sub>2</sub>, oxygen plasma; NH<sub>3</sub>, ammonia plasma; H<sub>2</sub>, Sand O<sub>2</sub>, sulfur dioxide–hydrogen plasma; \* $p < 0.05$ ) Image adopted from reference.<sup>40</sup>

In order to crosscheck this observation, we very closely inspected the change in water contact angle on plasma treated HDPE scaffolds with respect to time (in days). Our results indicate (**Figure 1.6**) in case of plasma treated polyethylene scaffolds within 7 days the hydrophobicity gets regenerated.

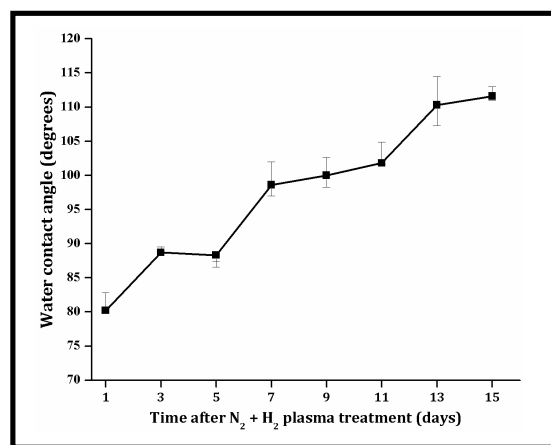


**Figure. 1.6:** Transient hydrophilicity in plasma treatment as quantified by contact angle data.

This (change in contact angle with time) is attributed to polymer chain dynamics and related surface reconstructions. Thus this surface reorganization and the regeneration of hydrophobicity after a certain time poses a huge problem in so far as 'storing' the potential tissue replacement scaffolds.

It has been observed<sup>126</sup> that with the decrease of water contact angle (as the hydrophilicity decreases) the cellular adhesion also decreases. To confirm this statement in our system we planned an experiment to check the relationship in between contact angle and cellular adhesion. 4 sets (4×4) of HDPE sheets (two-dimensional) were plasma treated (N<sub>2</sub> + H<sub>2</sub>) in a gap of one week for consecutive 4 weeks and stored under ambient conditions. The contact angle of the plasma-treated sheets were measured using a Kruss drop shape analyser (version 1.41-02). On the 5<sup>th</sup> week, mouse fibroblast L929 cells (40,000) were seeded on each polymeric sample. All setups with cells were incubated for 90 minutes (time optimized from a screening experiment). The supernatant was aspirated and the sheets were washed with sterile PBS. The attached cells on the sheets were estimated by their mitochondrial activity using resazurin assay (**Figure 1.8**). From both **Figure 1.7** and **Figure 1.8** it can be concluded that with time the changed surface arrangement can be a key reason for cellular adhesion. Changing, as well preserving a surface is, therefore, a crucial step for the excellent performance of the implants inside the human body.

However, the contact angle measurement results from **Figures 1.6** and **1.7** are not to be compared since the microstructures of the two materials are different. One is HDPE scaffold (**Figure 1.6**) while the other one is two-dimensional HDPE-sheets (**Figure 1.7**). The plasma ashers, as well as the contact angle meters, are also different in these two cases.

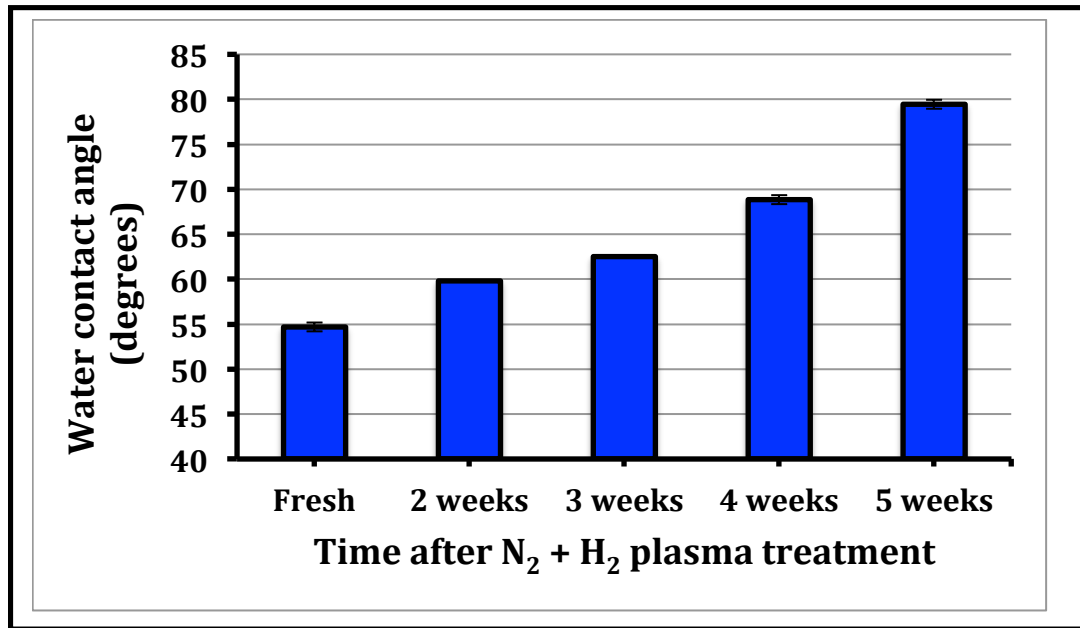


**Figure. 1.7:** Measurement of water contact angle on the two-dimensional HDPE surface. Data represented  $\pm SD$  of  $n=3$ .

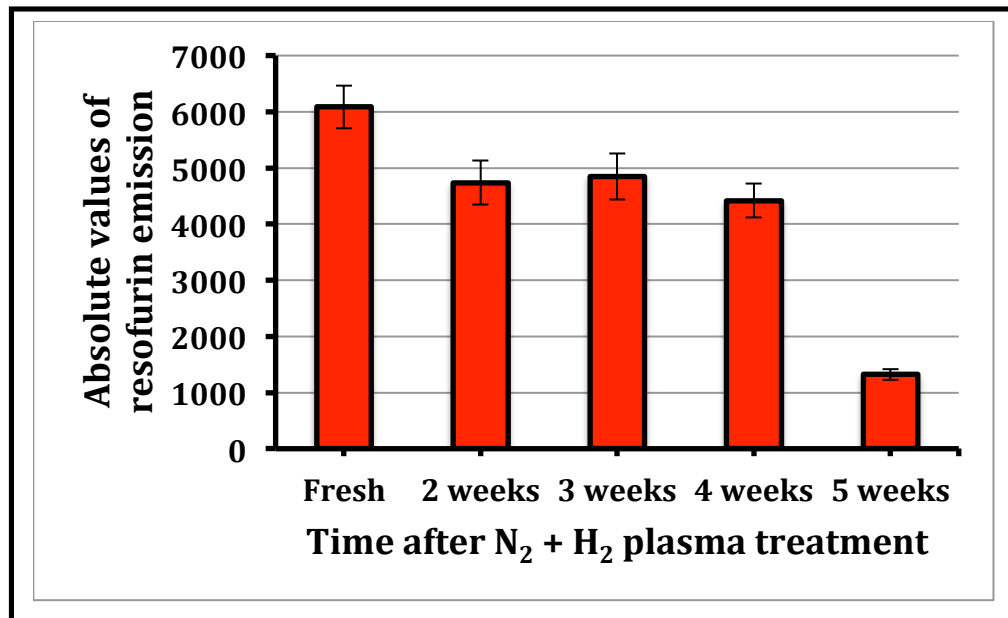


**Figure. 1.8:** Extent of cellular (L929) adhesion on ( $N_2+H_2$ ) plasma treated surfaces measured by resazurin reduction. Data represented  $\pm SD$  of  $n=3$ .

### **1.6. Layer-by-layer surface modification technique-a possible way of arresting the surface re-organization**

We envisaged that anchoring of metallic nanoparticles on plasma-treated polymeric surface could provide a solution to this problem. It can offer several advantages: (i) the anchoring of nanoparticles to the surface functionalized groups prevents the surface reorganization and the regeneration of hydrophobicity thus retaining the hydrophilicity or wettability of polymeric surface for a long time, (ii) the presence of nanoparticles provides greater surface area and (iii) increases the surface roughness enables enhanced cell attachment and (iv) nanomaterials have a broad spectrum of ligand acceptability, making any further surface modification very convenient. Few recent publications<sup>127, 128</sup> have shown that with metallic nanoparticle intervention it is possible to attract and attach mammalian cells or convert a polymeric surface into antibacterial one. Also, few layer-by-layer assembly (**Figure 1.9**) approaches were reported<sup>129</sup> which are very attractive. In these approaches hydrophobic PEI films were plasma treated with nitrogen and hydrogen gas plasma ( $N_2:H_2 = 2:3$ ) for 20 minutes under 60 watts power. This treatment generated transient amine groups on the polymeric surface. These films then were immediately dipped into citrate stabilized negatively charged gold sol for overnight. This allowed gold nanoparticle deposition on the polyetherimide films. It was followed by dip-coating in 0.1 mM lysine solution in water for overnight and dried. Films modified in this manner were found to be permanently hydrophilic. Furthermore, they were found to attract and stabilize CHO-K1 epithelial cells. Layer-by-layer assembly not only improved (**Figure 1.10**) the hydrophilicity of hydrophobic polymers, it even prolonged it for a very long period (at least up to 6 months upon storage at room temperature, data not shown), which allows longtime storage of hydrophobic polymers. In this way, the storage issue with tissue engineering materials can be solved and the relevant polymers can be used commercially.

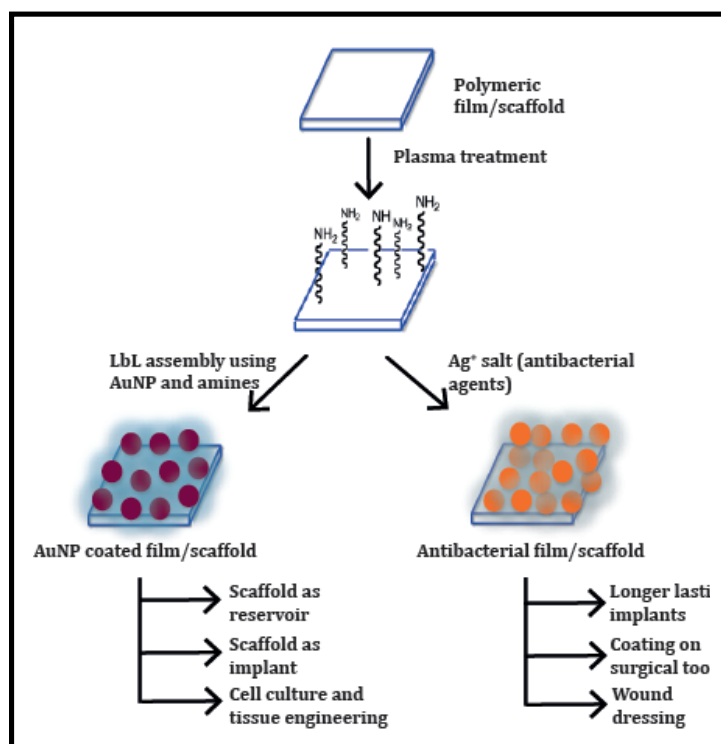


**Figure. 1.9:** Layer-by-layer assembly of plasma treatment, nanomaterials, small molecules.

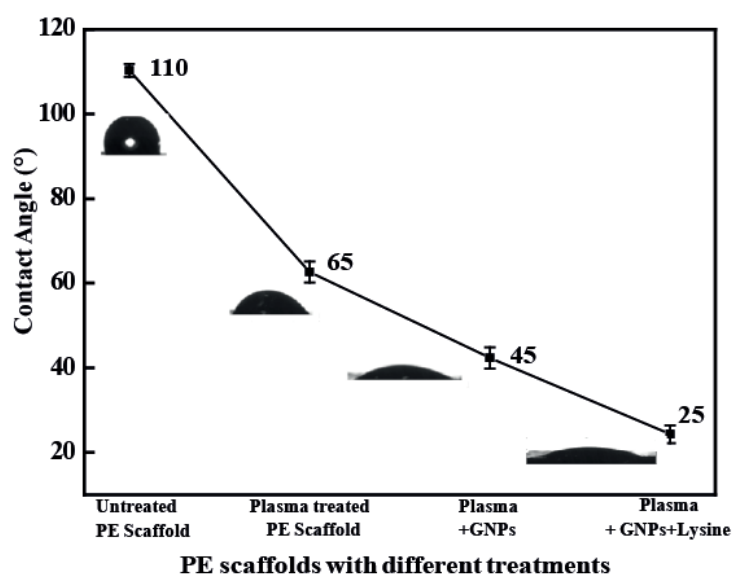


**Figure. 1.10:** Water contact angles obtained after different treatments of the PEI membrane Image adopted from reference.<sup>129</sup>

*Surface modification with silver nanoparticles and their antibactericidal properties:* Expanding the applicability of the procedure developed so far, polyethylene scaffolds were modified similarly by layer-by-layer assembly resulting in antibacterial surface.<sup>130</sup> First, the scaffolds were modified by  $N_2 + H_2$  plasma, which generated primary amine groups *in situ*. These groups were chemically coupled to the carboxylic acid units present in sophorolipids (a class of glycolipids). After decorating the polymer surface with these sophorolipids, they were incubated with Ag(I) solution. Sophorose sugar units *in situ* reduced Ag(I) to Ag(0) and caused silver nanoparticle deposition on the polyethylene scaffolds. Such Ag nanoparticle containing scaffolds acted as antibacterial surface, which discouraged *Bacillus Subtilis* growth. Quite interestingly, although it acted as an antibacterial surface, they strongly encouraged the adherence of CHO-K1 epithelial cells, which proves the silver concentration level present of the surface of the scaffolds is safe to be used *in vivo*.

Therefore, plasma treatment followed by layer-by-layer assembly based surface modification of HDPE scaffolds opens up a broad horizon for tissue engineering. Citrate stabilized gold has varying surface chemistry, which allows facile attachment of a very broad spectrum of small molecules, nucleic acids, proteins, polymers *etc.* Gold(III) and gold(I) make a strong bond (bond strength 126 kJ/mole) with thiol and the reaction is very irreversible. Thus, it is an excellent tool to decorate the surface of gold nanoparticles, hence the hydrophobic base polymer as well. Gold nanoparticles, covered with citrate groups impart negative zeta potential. A large spectrum of proteins can very well be electrostatically attached to gold nanoparticles, which may express several activities.

### **1.7. Plan of this thesis**

Surface modification of sturdy polymers (especially HDPE and UMWHDPE, which are extensively used as implants) has been a challenge for long because of the shortcomings of the available methods. Layer-by-layer surface modification after plasma treatment opens a big horizon of several bright future directions. With this background, we started our work to take the plasma treatment+layer-by-layer



assembly strategy further to meet several unmet needs in the area of tissue engineering.

### **1.7.1. Fast volume filling**

Conversion of hydrophobic surface to permanently hydrophilic one is the basic advantage of the plasma treatment+layer-by-layer assembly (P-LbL) strategy for surface modification. It can lead to tissue regeneration and volume filling applications. But, there are situations where one needs very fast volume filling in order to achieve a faster recovery. For this purpose, scaffolds need to be modified in such a way that ideally they would welcome, accommodate, and help in faster proliferation. Generally, scaffolds are surface modified with cell penetrating peptides like RGD, R9, K9 because they have the ability to internalize to the animal cell membrane more efficiently. Arginine, an amino acid containing guanidium group is present in most of these peptides. So we started our work in this thesis by asking a question whether the small molecule amino acid 'arginine' could perform as a promoter of cell attachment followed by cellular proliferation? Our contention is supported by literature reports where it was shown that arginine-coated nanoparticles interact well with living cells, where nanoparticles are readily engulfed by cellular macropinocytosis.<sup>131</sup> This is probably due to the guanidium groups present on the side chain of arginine, which make arginine to get electrostatically attracted to the phospholipid bilayer of a cell membrane, which in turn will aid in cell attachment. Faster attachment can be followed by faster proliferation of cells with the effect of fast volume filling. Accordingly, in Chapter 2 entitled "*Arginine Mediated Surface Modification of Polymers for Tissue Engineering Applications*" of this thesis we have depicted the work performed in this direction and discussed the results.

### **1.7.2. Sequential drug delivery and tissue engineering**

Drug delivery is always a challenge in cancer chemotherapy due to its cytotoxic outbursts. In a typical treatment of solid tumour surgery is followed by radiations and chemo sessions depending on the severity of the tumour. Series of radiations

and chemo therapy can lead to trauma and side effects (like vomiting, hair fall *etc.*). To prevent that, cytotoxic drugs can be chemically conjugated on the scaffolds that will slowly release locally. Due to its local release, it will reduce the negative side effects in other healthy organs. For some special cases (for example oral cancer), the treatment regime requires chemotherapy followed by a cosmetic correction. Back to back exposure to two surgeries in combination with chemotherapy is quite traumatic to a cancer patient. In order to bypass these two consecutive surgeries, we have designed a smart 'dual purpose scaffold' based on the P-LbL strategy. Here cytotoxic drug cisplatin is chemically conjugated to porous polyethylene scaffold *via* chemical conjugation. When the drug-containing scaffold is placed *in vivo*, the drug releases in the ambient condition. To an added advantage, the scaffolds retain its hydrophilicity after leaching out of the drug – a healthy tissue can very well form here. In this way, hydrophobic HDPE can have diverse applications, which have immediate use. Developing this idea in Chapter 3 we present our work on "*Design and Fabrication of a Dual Purpose Scaffold by a Logical Combination of Drug-release and Tissue engineering*".

### **1.7.3. Understanding the interaction of foreign bodies with the immune system**

Inflammation is a common problem for any foreign body (e.g., implants, scaffolds, stents) placed inside living organisms. This originates from the very first interaction of a foreign body with the immune system, which decides the long-term fate of an implant inside the body. The mechanism of immune cells attack is not totally known. In literature so far there is no significant planned research that has been carried out to understand the response of immune cells towards a scaffold inside living systems, especially with respect to the presence of negative or positive charges on the surface of the scaffold. On the contrary, there has been a good amount of trial to evade the immune system.<sup>132</sup> It is essential to understand the response of immune cells towards a scaffold to design the new generation implants.

Surface modification as described before in this chapter (section 1.6) is a very strong tool to change the surface properties of a solid scaffold. Above all, gold

nanoparticles possessing diverse surface chemistry can certainly adhere to different ligands imposing surface negative or positive charges. In Chapter 4 we have modified gold nanoparticle coated polymeric surfaces with charged linear polymers and imposed opposite charges (positive and negative) on the scaffolds. We have exposed immune cells towards these surface modified polymeric scaffold surfaces and tried to follow up their attachment and morphology using colourimetric assays and microscopy. This research included in the chapter “*The response of macrophages with respect to surface charge alterations*” will shed some light on the behaviour of immune cells in presence of opposite charges and help in designing next-generation implants.

### 1.8. Conclusion

Through the literature, we got convinced about the tremendous potential of the surface modification technique. The chapters mentioned above will depict how we have exploited the P-LbL method in order to solve several implant-related problems.

### 1.9. Bibliography

---

<sup>1</sup>Bronzino, J. D. The Biomedical Engineering Handbook. 2nd edition. Taylor and Francis; **2000**.

<sup>2</sup>Langer, R.; Vacanti, J. P. Tissue engineering. *Science*, **1993**, *260*(5110), 920-926.

<sup>3</sup>Murphy S. V.; Atala, A. Organ engineering--combining stem cells, biomaterials, and bioreactors to produce bioengineered organs for transplantation. *Bioessays*. **2013**, *35*(3), 163-72.

<sup>4</sup>Körbling, M.; Estrov, Z. Adult stem cells for tissue repair—a new therapeutic concept? *N. Engl. J. Med.* **2003**, *349*(6), 570-582.

<sup>5</sup>Chai, C.; Leong, K. W. Biomaterials approach to expand and direct differentiation of stem cells. *Mol. Ther.* **2007**, *15*(3), 467-480.

<sup>6</sup>Bianco, P.; Robey, P. G. Stem cells in tissue engineering. *Nature*. **2001**, *414*(6859), 118-121.

<sup>7</sup>Black, J. The education of the biomaterialist: Report of a survey. *J. Biomed. Mater. Res.* **1982**, *16*(2), 159-167.

---

<sup>8</sup>Ratner, B. D.; Hoffman, A. S.; Schoen, F. J.; Lemons, J. E. *Biomaterials science: an introduction to materials in medicine*. 2<sup>nd</sup> edition. Academic press. **2004**.

<sup>9</sup>Walker, P. M. B. *Larousse dictionary of science and technology*. Larousse Press. **2006**.

<sup>10</sup>Manivasagam, G.; Dhinasekaran, D. and Rajamanickam, A. *Biomedical Implants: Corrosion and its Prevention - A Review, Recent Patents on Corrosion Science*. **2010**, *2*, 40-54.

<sup>11</sup>Repairing Knee Joints by Growing New Cartilage Using an Injectable Hydrogel <http://www.datlof.com/8axamal/docs/marketing/jhu/je/index.htm> Accessed January 2019

<sup>12</sup>Boyan, B. D.; Hummert, T. W.; Dean, D. D.; Schwartz Z. Role of material surfaces in regulating bone and cartilage cell response. *Biomaterials*. **1996**, *17*(2), 137-146.

<sup>13</sup> Frantz, C.; Stewart, K. M.; Weaver, V. M. The extracellular matrix at a glance. *J. Cell Sci*. **2010**, *123*(24), 4195–4200.

<sup>14</sup>Horwitz, A. R. The origins of the molecular era of adhesion research. *Nat. Rev. Mol. Cell Biol*. **2012**, *13*(12), 805–811.

<sup>15</sup>Williams, D. F.; On the nature of biomaterials. *Biomaterials*. **2009**, *30*, 5897–5909.

<sup>16</sup> Lutolf, M. P.; Hubbell, J. A. Synthetic biomaterials as instructive extracellular microenvironments for morphogenesis in tissue engineering. *Nature Biotechnology*. **2005**, *23*, 47-55.

<sup>17</sup> Dvir, T.; Timko, B. P.; Kohane, D. S.; Langer, R. Nanotechnological strategies for engineering complex tissues, *Nature Nanotechnology*, **2011**, *6*, 13-22

<sup>18</sup>Boyan, B. D.; Hummert, T.W.; Dean, D. D.; Schwartz, Z. Role of material surfaces in regulating bone and cartilage cell response, *Biomaterials*, **1996**, *17*(2), 137-146.

<sup>19</sup>Prakasam, M.; Locs, J.; Salma-Ancane, K.; Loca, D.; Largeteau, A.; Cimdina, L. B. Biodegradable Materials and Metallic Implants—A Review. *J. Funct. Biomater*. **2017**, *8*, 44.

<sup>20</sup>[http://www.keramverband.de/brevier\\_engl/5/5\\_1.htm](http://www.keramverband.de/brevier_engl/5/5_1.htm) Accessed January, 2019

<sup>21</sup>Ha, T. L. B.; Quan, T. M.; Vu, D. N.; Si, D. M. Naturally Derived Biomaterials: Preparation and Application. Chapter 11. *Regenerative Medicine and Tissue Engineering*, Jose A. Andrades (Ed.), InTech, **2013**

<sup>22</sup>Glowacki, J.; Mizuno, S. Collagen scaffolds for tissue engineering. *Biopolymers*. **2008**, *89*(5), 338-44.

---

<sup>23</sup>Sun, K.; Li, H.; Li, R.; Nian, Z.; Li, D.; Xu C. Silk fibroin/collagen and silk fibroin/chitosan blended three-dimensional scaffolds for tissue engineering. *Eur. J. Orthop. Surg. Traumatol.* **2015**, *25*, 243–249.

<sup>24</sup>Quirk, R. A.; France, R. M.; Shakesheff, K. M.; Howdle, S. M. Supercritical fluid technologies and tissue engineering scaffolds. *Curr. Opin. Solid State Mater. Sci.* **2004**, *8*, 313-821.

<sup>25</sup>Noble APoriferous: Provides design, development, manufacture and distribution of sterile craniomaxillofacial polyethylene implants for reconstructive surgery. <http://www.poriferous.com> Accessed on January 2019

<sup>26</sup> Orthopaedics Driven to be your ortho service line leader <https://www.stryker.com/us/en/portfolios/orthopaedics.html> Accessed on January 2019

<sup>27</sup>Biopore lightweight material. <http://www.biopore.in/> Accessed on January 2019

<sup>28</sup> A new class of implant material with bone-like architecture <http://www.anatomics.com/applications/cranio-maxillo-facial/facial-implants/> Accessed January 2019

<sup>29</sup> <https://www.depuysynthes.com/hcp/cm/Products/qs/synpor> Accessed January 2019

<sup>30</sup>Farhat, S.; Gilliam, M.; Rabago-Smith, M.; Baran, C.; Walter, N.; Zand, A. Polymer coatings for biomedical applications using atmospheric pressure plasma. *Surf. Coat. Technol.* **2014**, *241*, 123–9.

<sup>31</sup>James, S. P.; Oldinski, R.; Zhang, M.; Schwartz, H. UHMWPE Biomaterials Handbook. *Elsevier.* **2009**

<sup>32</sup> Tsuchii, A.; Suzuki, T.; Fukuoka, S. Microbial degradation of polyethylene oligomers. *Rep. Ferment. Res. Inst.* **1980**, *55*, 35–40.

<sup>33</sup>Choe, J. H.; Lee, S. J.; Lee, Y. M.; Rhee, J. M.; Lee, H. B.; Khang G. Proliferation rate of fibroblast cells on polyethylene surfaces with wettability gradient, *J. Appl. Polym. Sci.* **2004**, *92*(1), 599-606.

<sup>34</sup>(a) Yamaguchi, M.; Shinbo, T.; Kanamori, T.; Wang, P.; Niwa, M.; Kawakami, H.; Nagaoka, S.; Hirakawa, K.; Kamiya, M. Surface modification of poly (L-lactic acid) affects initial cell attachment, cell morphology, and cell growth. *J. Artif. Organ.* **2004**, *7*, 187-193. (b) Mathieu, H. J.; Gao, X.; Chevolot, Y. D.; Balazs, J. Surface Functionalization for Biomedical Applications in Surface Chemistry in Biomedical and Environmental Science. *Springer Netherlands.* **2006**.

- 
- <sup>35</sup>(a) Alexander, C.; Theme issue Biomedical Materials. *J. Mater. Chem.* **2007**, *17*, 3963. (b) Hoffmann, B.; Volkmer, E.; Kokott, A.; Weber, M.; Hamisch, S.; Schieker, M.; Mutschler, W.; Ziegler, G. A new biodegradable bone wax substitute with the potential to be used as a bone filling material. *J. Mater. Chem.* **2007**, *17*, 4028-4033. (c) Chen, R.; Hunt, J. A. Biomimetic materials processing for tissue-engineering processes. *J. Mater. Chem.* **2007**, *17*, 3974-3979.
- <sup>36</sup>Richey, T.; Iwata, H.; Oowaki, H.; Uchida, E.; Matsuda, S.; Ikada, Y. Surface modification of polyethylene balloon catheters for local drug delivery. *Biomaterials.* **2000**, *21*(10), 1057-1065.
- <sup>37</sup>Gatenholm, P.; Ashida, T.; Hoffman, A. S. Hybrid biomaterials prepared by ozone-induced polymerization. I. Ozonation of microporous polypropylene. *J. Polym. Sci. Polym. Chem. Part A.* **1997**, *35*(8), 1461-1467.
- <sup>38</sup>Liu, J. H.; Jen, H. L.; Chung, Y. C. Surface modification of polyethylene membranes using phosphorylcholine derivatives and their platelet compatibility. *J. App. Polym. Sci.* **1999**, *74*(12), 2947-2954.
- <sup>39</sup>Lei, J.; Gao, J.; Zhou, R.; Zhang, B.; Wang, J. Photografting of acrylic acid on high density polyethylene powder in vapour phase. *Polym. Inter.* **2000**, *49*, 1492-1495.
- <sup>40</sup>Nakaoka, R.; Tsuchiya, T.; Kato, K.; Ikada, Y.; Nakamura, A. Studies on tumorpromoting activity of polyethylene: Inhibitory activity of metabolic cooperation on polyethylene surfaces is markedly decreased by surface modification with collagen but not with RGDS peptide. *J. Biomed. Mater. Res.* **1997**, *35*, 391-397.
- <sup>41</sup>Lavanant, L.; Pullin, B.; Hubbell, J. A.; and Klok, H. A. A Facile Strategy for the Modification of Polyethylene Substrates with Non-Fouling, Bioactive Poly (poly (ethylene glycol) methacrylate) Brushes. *Macromol. Biosci.* **2010**, *10*, 101-108.
- <sup>42</sup>Kidane, A.; Lantz, G. C.; Jo, S.; Park, K. Surface modification with PEO-containing triblock copolymer for improved biocompatibility: in vitro and ex vivo studies, *J. Biomater. Sci. Polym. Ed.* **1999**, *10*, 1089-1105.
- <sup>43</sup>Yang, Q.; Xu, Z. K.; Dai, Z. W.; Wang, J. L.; Ulbricht, M. Surface modification of polypropylene microporous membranes with a novel glycopolymer. *Chem. Mater.* **2005**, *17*, 3050-3058.
- <sup>44</sup>Tao, G.; Gong, A.; Lu, J.; Sue, H. J.; Bergbreiter, D. E. Surface functionalized polypropylene: synthesis, characterization, and adhesion properties. *Macromolecules.* **2001**, *34*, 7672-7679.

---

<sup>45</sup>Rasmussen, J. R.; Stedronsky, E. R.; Whitesides, G. M. Introduction, modification, and characterization of functional groups on the surface of low-density polyethylene film. *J. Am. Chem. Soc.* **1977**, *99*, 4736-4745.

<sup>46</sup>Chanunpanich, N.; Ulman, A.; Strzhemechny, Y. M.; Schwarz, S. A.; Janke, A.; Braun, H. G.; Kraztmuller, T. Surface modification of polyethylene through bromination. *Langmuir*. **1999**, *15*, 2089-2094.

<sup>47</sup>Wang, P.; Tan, K. L.; Kang, E. T.; Neoh, K. G. Surface functionalization of low density polyethylene films with grafted poly (ethylene glycol) derivatives. *J. Mater. Chem.* **2001**, *11*(12), 2951-2957.

<sup>48</sup>Goddard, J. M.; Talbert, J. N.; Hotchkiss, J. H. Covalent Attachment of Lactase to LowDensity Polyethylene Films. *J. Food Sci.* **2007**, *72*, E036-E041.

<sup>49</sup>Mamoor, G. M.; Qamar, N.; Farooq M. Free radical graft modification of polyethylene with methacrylic acid and styrene monomer. *Chemical Engineering Research Bulletin*, **2011**, *15*, 34-38

<sup>50</sup>Rubira, A. F.; Da Costa, A. C.; Galembeck, F.; Escobar, N. F. L.; Da Silva, E.C.; Vargas, H. Polyethylene and polypropylene surface modification by impregnation with manganese (IV) oxide. *Colloids and surfaces*, **1985**, *15*, 63-73.

<sup>51</sup>Hoshi, T.; Sawaguchi, T.; Matsuno, R.; Konno, T.; Takai, M.; Ishihara, K. Control of surface modification uniformity inside small-diameter polyethylene/poly (vinyl acetate) composite tubing prepared with supercritical carbon dioxide. *Journal of Materials Chemistry*, **2010**, *20*(23), 4897-4904.

<sup>52</sup>Yao, Z. P.; RÅnby, B. Surface modification by continuous graft copolymerization. I. Photoinitiated graft copolymerization onto polyethylene tape film surface. *Journal of Applied Polymer Science*, **1990**, *40*(9-10), 1647-1661.

<sup>53</sup>Fávaro, S. L.; Rubira, A. F.; Muniz, E. C. Radovanovic, E. Surface modification of HDPE, PP, and PET films with KMnO<sub>4</sub>/HCl solutions. *Polymer Degradation and Stability*. **2007**, *9*, 1219-1226.

<sup>54</sup>Qu, X.; Wirsén, A.; Olander, B.; Albertsson, A. C. Surface modification of high density polyethylene tubes by coating chitosan, chitosan hydrogel and heparin. *Polym. Bull.* **2001**. *46*(2-3), 223-229.

<sup>55</sup>Gorbachev, A. A.; Tretinnikov, O. N.; Shkrabatovskaya, L. V.; Prikhodchenko, L. K. Photoinduced Graft-Polymerization of Acrylic Acid on Polyethylene and Polypropylene Surfaces: Comparative Study Using IR-ATR Spectroscopy. *J. Appl. Spectrosc.* **2014**, *81*, 754-757.

<sup>56</sup>Moro, T.; Takatori, Y.; Ishihara, K.; Konno, T.; Takigawa, Y.; Matsushita, T.; Chung,

---

U.; Nakamura, K. Kawaguchi, H. Surface grafting of artificial joints with a biocompatible polymer for preventing periprosthetic osteolysis. *Nature Materials*, **2004**, *3*, 829-836.

<sup>57</sup>Zand, A.; Walter, N.; Bahu, M.; Ketterer, S.; Sanders, M.; Sikorski, Y.; Beholz, L. Preparation of hydroxylated polyethylene surfaces. *J. Biomater. Sci. Polymer Edn*, **2008**, *19*, 467-477

<sup>58</sup>Yamada, K.; Takeda, S.; Hirata, M. Improvement of autohesive and adhesive properties of polyethylene plates by photografting with glycidyl methacrylate. *J. Appl. Polym. Sci.* **2007**, *103*, 493-500.

<sup>59</sup>Zhang, J.; Kato, K.; Uyama, Y.; Ikada, Y. Surface graft polymerization of glycidyl methacrylate onto polyethylene and the adhesion with epoxy resin. *Journal of Polymer Science: Part A Polymer Chemistry*, **1995**, *33*, 2629-2638

<sup>60</sup>Lei, J.; Gao, J.; Jiang, L. Structure and adhesion properties of linear low-density polyethylene powders grafted with acrylic acid via ultraviolet light. *J. Appl. Polym. Sci.* **2006**, *100*, 2549-2553.

<sup>61</sup>El Kholdi, O.; Lecamp, L.; Lebaudy, P.; Bunel, C.; Alexandre, S. Modification of adhesive properties of a polyethylene film by photografting. *J. Appl. Polym. Sci.* **2004**, *92*, 2803-2811.

<sup>62</sup>Wang, H.; Brown, H. R. Lamination of high-density polyethylene by bulk photografting and the mechanism of adhesion. *J. Appl. Polym. Sci.* **2005**, *97*, 1097-1106.

<sup>63</sup>Amornsakchai, T.; Kubota, H. Photoinitiated grafting of methyl methacrylate on highly oriented polyethylene: Effect of draw ratio on grafting. *J. Appl. Polym. Sci.* **1998**, *70*, 465-470.

<sup>64</sup>Deng, J. P.; Yang, W. T.; Rånby, B. Surface Photograft Polymerization of Vinyl Acetate on Low Density Polyethylene Film: Effects of Solvent. *Polym. J.* **2000**, *32*, 834-837.

<sup>65</sup>Irwan, G. S.; Kuroda, S. I.; Kubota, H.; Kondo, T. Photografting of N-isopropylacrylamide on polyethylene film in mixed solvents composed of water and organic solvent. *J. Appl. Polym. Sci.* **2003**, *87*, 458-463.

<sup>66</sup>Irwan, G. S.; Kuroda, S. I.; Kubota, H.; Kondo, T. Photografting of methacrylic acid on polyethylene film: Effect of mixed solvents consisting of water and organic solvent. *J. Appl. Polym. Sci.* **2002**, *83*, 2454-2461.

<sup>67</sup>Wang, H.; Brown, H. R. UV grafting of methacrylic acid and acrylic acid on high-density polyethylene in different solvents and the wettability of grafted



---

high-density polyethylene. II. Wettability. *J. Polym. Sci., Part A: Polym. Chem.* **2004**, *42*, 263-270.

<sup>68</sup>Wang, H.; Brown, H. R. Ultraviolet grafting of methacrylic acid and acrylic acid on high-density polyethylene in different solvents and the wettability of grafted high-density polyethylene. I. Grafting. *J. Polym. Sci., Part A: Polym. Chem.* **2004**, *42*, 253-262.

<sup>69</sup>Chen, Y.; Liu, P. Surface modification of polyethylene by plasma pretreatment and UV-induced graft polymerization for improvement of antithrombogenicity. *J. Appl. Polym. Sci.* **2004**, *93*, 2014-2018.

<sup>70</sup>Yang, P.; Deng, J.; Yang, W. Surface Photografting Polymerization of Methyl Methacrylate in N, N-dimethylformamide on Low Density Polyethylene Film. *Macromol. Chem. Phys.* **2004**, *205*, 1096-1102.

<sup>71</sup>Tada, H.; Ito, S. Conformational change restricted selectivity in the surface sulfonation of polypropylene with sulfuric acid. *Langmuir.* **1997**, *13*, 3982-3989.

<sup>72</sup>Cross, E. M.; McCarthy, T. J. Radical chlorination of polyethylene film: control of surface selectivity. *Macromolecules.* **1992**, *25*(10), 2603-2607.

<sup>73</sup>Bergbreiter, D. E.; Hu, H. P.; Hein, M. D. Control of surface functionalization of polyethylene powders prepared by coprecipitation of functionalized ethylene oligomers and polyethylene. *Macromolecules.* **1989**, *22*(2), 654-662.

<sup>74</sup>Bergbreiter, D. E.; Srinivas, B.; Gray, H. N. Surface graft polymerization on polyethylene using macroinitiators. *Macromolecules.* **1993**, *26*(12), 3245-3246.

<sup>75</sup>Stoleru, E.; Munteanu, S. B.; Dumitriu, R. P.; Coroaba, A.; Drobotă, M.; Zemljic, L. F.; Vasile, C. Polyethylene materials with multifunctional surface properties by electrospraying chitosan/vitamin E formulation destined to biomedical and food packaging applications. *Iranian Polymer Journal.* **2016**, *25*(4), 295-307.

<sup>76</sup>Zheng, Y.; Miao, J.; Zhang, F.; Cai, C.; Koh, A.; Simmons, T. J.; Mousa, S. A.; Linhardt, R. J. Surface modification of a polyethylene film for anticoagulant and anti-microbial catheter, *React. Funct. Polym.* **2016**, *100*, 142-150

<sup>77</sup>Dhamodharan, R.; Nisha, A.; Pushkala, K.; McCarthy, T. J. Investigation of the mercat reaction as a tool for the introduction of nitrogen surface functionality on linear low-density polyethylene (LLDPE) and polypropylene (PP). *Langmuir.* **2001**, *17*, 3368-3374.

<sup>78</sup>Bergbreiter, D. E.; Franchina, J. G.; Kabza, K. Hyperbranched grafting on oxidized polyethylene surfaces, *Macromolecules.* **1999**, *32*, 4993-4998.

---

<sup>79</sup>Foltynowicz, Z.; Yamaguchi, K.; Czajka, B.; Regen, S. L. Modification of low-density polyethylene film using polymerizable surfactants. *Macromolecules*. **1985**, *18*, 1394-1401.

<sup>80</sup>Chanunpanich, N.; Ulman, A.; Malagon, A.; Strzhemechny, Y. M.; Schwarz, S. A.; Janke, A.; Kratzmueller, T.; Braun, H. G. Surface modification of polyethylene films via bromination: Reactions of brominated polyethylene with aromatic thiolate compounds. *Langmuir*. **2000**, *16*, 3557-3560.

<sup>81</sup>Kim, M. S.; Seo, K. S.; Khang, G.; Lee, H. B. Preparation of a gradient biotinylated polyethylene surface to bind streptavidin-FITC. *Bioconjugate Chem*. **2005**, *16*, 245-249.

<sup>82</sup>Kim, M. S.; Seo, K. S.; Khang, G.; Lee, H. B. First preparation of biotinylated gradient polyethylene surface to bind photoactive caged streptavidin. *Langmuir*. **2005**, *21*, 4066-4070.

<sup>83</sup>Kiss, E.; Samu, J.; Toth, A.; Bertoti, I. Novel ways of covalent attachment of poly (ethylene oxide) onto polyethylene: surface modification and characterization by XPS and contact angle measurements. *Langmuir*. **1996**, *12*, 1651-1657.

<sup>84</sup>Kavc, T.; Kern, W.; Ebel, M. F.; Svagera, R.; Pölt, P. Surface modification of polyethylene by photochemical introduction of sulfonic acid groups. *Chem. Mater*. **2000**, *12*(4), 1053-1059.

<sup>85</sup>Fischer, D.; Eysel, H. H. Analysis of polyethylene surface sulfonation. *J. Appl. Polym. Sci.*, **1994**, *52*, 545-548.

<sup>86</sup>Idage, S. B.; Badrinarayanan, S.; Vernekar, S. P.; Sivaram, S. X-ray photoelectron spectroscopy study of sulfonated polyethylene. *Langmuir*. **1996**, *12*, 1018-1022.

<sup>87</sup>Pandiyaraj, K. N.; Ferraria, A. M.; do Rego, A. M. B.; Deshmukh, R. R.; Su, P. G.; Halleluyah, J. M.; Halim, A. S. Low-pressure plasma enhanced immobilization of chitosan on low-density polyethylene for bio-medical applications. *Appl. Surf. Sci*. **2015**, *328*, 1-12.

<sup>88</sup>Theapsak, S.; Watthanaphanit, A.; Rujiravanit, R. Preparation of chitosan-coated polyethylene packaging films by DBD plasma treatment, *ACS Appl. Mater. Interfaces*. **2012**, *4*, 2474-2482.

<sup>89</sup>Bergbreiter, D. E.; Kabza, K. Annealing and reorganization of sulfonated polyethylene films to produce surface-modified films of varying hydrophilicity. *J. Am. Chem. Soc*. **1991**, *113*, 1447-1448.

<sup>90</sup>Greene, G.; Yao, G.; Tannenbaum, R. Wetting characteristics of plasma-modified porous polyethylene. *Langmuir*. **2003**, *19*, 5869-5874.

---

<sup>91</sup>Bretagnol, F.; Tatouliau, M.; Arefi-Khonsari, F.; Lorang, G.; Amouroux, J. Surface modification of polyethylene powder by nitrogen and ammonia low pressure plasma in a fluidized bed reactor. *Reactive and functional polymers*. **2004**, *61*(2), 221-232.

<sup>92</sup>Santos, L. P.; Bernardes, J. S.; Galembeck, F. Corona-treated polyethylene films are macroscopic charge bilayers. *Langmuir*. **2013**, *29*, 892-901.

<sup>93</sup>Wang, T.; Kang, E. T.; Neoh, K. G.; Tan, K. L.; Liaw, D. J. Surface modification of low-density polyethylene films by UV-induced graft copolymerization and its relevance to photolamination. *Langmuir*. **1998**, *14*, 921-927.

<sup>94</sup>Tahara, M.; Cuong, N. K.; Nakashima, Y. Improvement in adhesion of polyethylene by glow-discharge plasma. *Surf. Coat. Technol.* **2003**, *174*, 826-830.

<sup>95</sup>Lehocký, M.; Drnovská, H.; Lapčíková, B.; Barros-Timmons, A. M.; Trindade, T.; Zembala, M. and Lapčík, L. Plasma surface modification of polyethylene. *Colloids and Surf. A*. **2003**, *1*, 125-131.

<sup>96</sup>Tajima, S.; Komvopoulos, K. Surface modification of low-density polyethylene by inductively coupled argon plasma. *J. Phys. Chem. B*. **2005**, *109*, 17623-17629.

<sup>97</sup>Milani, R.; Gleria, M.; Sassi, A.; De Jaeger, R.; Mazzah, A.; Gengembre, L.; Frere, M.; Jama, C. Surface functionalization with phosphazenes, Part 3: Surface modification of plasma-treated polyethylene with fluorinated alcohols using chlorinated phosphazenes as coupling agents. *Chem. Mater.* **2007**, *19*, 4975-4981.

<sup>98</sup>Bismarck, A.; Brostow, W.; Chiu, R.; Hagg Lobland, H. E.; Ho, K. K. Effects of surface plasma treatment on tribology of thermoplastic polymers. *Polym. Engg. Sci.* **2008**, *48*, 1971-1976.

<sup>99</sup>Farhat, S.; Gilliam, M.; Rabago-Smith, M.; Baran, C.; Walter, N.; Zand, A. Polymer coatings for biomedical applications using atmospheric pressure plasma. *Surface Surf. Coat. Technol.* **2014**, *241*, 123-129.

<sup>100</sup>Drnovská, H.; Lapčík, L.; Buršíková, V.; Zemek, J.; Barros-Timmons, A. M. Surface properties of polyethylene after low-temperature plasma treatment. *Colloid. Polym. Sci.* **2003**, *281*, 1025-1033.

<sup>101</sup>Jung, S. H.; Park, S. H.; Lee, D. H.; Kim, S. D. Surface modification of HDPE powders by oxygen plasma in a circulating fluidized bed reactor. *Polym. Bull.* **2001**, *47*, 199-205.

<sup>102</sup>Šimor, M.; Rahel, J. J.; Vojtek, P.; Brablec, M. A. C. Atmospheric-pressure diffuse coplanar surface discharge for surface treatments. *Appl. Phys. Lett.* **2002**, *81*, 2716-

---

2718.

<sup>103</sup>Médard, N.; Soutif, J. C.; Poncin-Epaillard, F. CO<sub>2</sub>, H<sub>2</sub>O, and CO<sub>2</sub>/H<sub>2</sub>O plasma chemistry for polyethylene surface modification. *Langmuir*. **2002**;18:2246-2253.

<sup>104</sup>Kong, J. S.; Lee, D. J.; Kim, H. D. Surface modification of low-density polyethylene (LDPE) film and improvement of adhesion between evaporated copper metal film and LDPE. *J. Appl. Polym. Sci.* **2001**, 82, 1677-1690.

<sup>105</sup> Kolska, Z.; Reznickova, A.; Nagyova, M.; Slepickova, N.; Sajdi, P.; Slepicka, P. Svorcik, V. Plasma activated polymers grafted with cysteamine improving surfaces cytocompatibility. *Polymer Degradation and Stability* **2014**, 101, Pages 1-9

<sup>106</sup> Reznickova, A.; Novotna, Z.; Kolska, Z.; Kasalkova, N. S.; Rimpelova, S.; Svorcik, V. Enhanced adherence of mouse fibroblast and vascular cells to plasma modified polyethylene. *Materials Science and Engineering: C*, **2015**, 52, Pages 259-266

<sup>107</sup> Liu, H.; Xie, D.; Qian, L.; Deng, X.; Leng, Y. X.; Huang, N. The mechanical properties of the ultrahigh molecular weight polyethylene (UHMWPE) modified by oxygen plasma, *Surface and Coatings Technology*, **2011**, 205(8-9), 2697-2701

<sup>108</sup>Yamamoto, K.; Miwa, Y.; Tanaka, H.; Sakaguchi, M.; Shimada, S. Living radical graft polymerization of methyl methacrylate to polyethylene film with typical and reverse atom transfer radical polymerization. *Journal of Polymer Science, Part A. Polymer Chemistry*. **2002**, 40(20), 3350-3359.

<sup>109</sup>Matyjaszewski, K.; Teodorescu, M.; Miller, P. J.; Peterson, M. L. Graft copolymers of polyethylene by atom transfer radical polymerization. *Journal of Polymer Science, Part A. Polymer Chemistry*. **2000**, 38(13), 2440-2448.

<sup>110</sup>Tendero, C.; Tixier, C.; Tristant, P.; Desmanson, J.; Leprince, P. Atmospheric pressure plasmas: A review. *Spectrochim. Acta B*. **2006**, 61(1), 2-30.

<sup>111</sup>(a) Wilbur, J. L.; Whitesides, G. M. Self-Assembly and Self-Assembled Monolayers in Micro- and Nanofabrication. Springer-Verlag AIP Press: New York, 1999. Chapter 8 331-369. (b) Bain, C. D.; Whitesides, G. M. Molecular-level control over surface order in self-assembled monolayer films of thiols on gold. *Science*. **1988**, 240(4848), 62-63.

<sup>112</sup>Chang, C. H.; Liao, J. D.; Chen, J. J.; Ju, M. S.; Lin, C. C. K. Cell adhesion and related phenomena on the surface-modified Au-deposited nerve microelectrode examined by total impedance measurement and cell detachment tests. *Nanotechnology*. **2006**, 17, 2449-57.

---

<sup>113</sup>Briggs, D.; Brewis, D.M.; Dahm, R. H.; Fletcher, I. W. Analysis of the surface chemistry of oxidized polyethylene: comparison of XPS and ToF-SIMS. *Surface and Interface Analysis*. **2003**, *35*, 156-7.

<sup>114</sup>Xing, C. M.; Deng, J. P.; Yang, W. T. Synthesis of antibacterial polypropylene film with surface immobilized polyvinylpyrrolidoneiodine complex. *J. Appl. Polym. Sci*. **2005**, *97*, 2026-31.

<sup>115</sup>Zand, A.; Walter, N.; Bahu, M.; Ketterer, S.; Sanders, M.; Sikorski, Y. Preparation of hydroxylated polyethylene surfaces. *J. Biomater. Sci. Polym. Ed*. **2018**, *19*, 467-477.

<sup>116</sup>Mutimer, J.; Devane, P. A.; Adams, K.; Horne, J. G. Highly crosslinked polyethylene reduces wear in total hip arthroplasty at 5 years. *Clin. Orthop. Relat. Res*. **2010**, *468*, 3228-3233.

<sup>117</sup>Rasmussen, J. R.; Stedronsky, E. R.; Whitesides, G. M. Introduction, modification, and characterization of functional- groups on surface of low-density polyethylene film. *Journal of American Chemical Society*. **1977**, *99*, 4736-4745.

<sup>118</sup>Kong, J. S. Surface Modification of Low-Density Polyethylene (LDPE) Film and Improvement of Adhesion Between Evaporated Copper Metal Film and LDPE. *J. App. Polym. Sci*. **2001**, *82*, 1677-90.

<sup>119</sup>Aouiniti, M.; Bertrand, P. Characterization of polypropylene surface treated in a CO<sub>2</sub> plasma. *Plasmas and Polymers*, **2003**, *8*, 225-236.

<sup>120</sup>Terlingen, J. G. A.; Gerritsen, H. F. C.; Hoffman, A. S.; Feijen J. Introduction of functional groups on polyethylene surfaces by a carbon dioxide plasma treatment. *App. Polym. Sci*. **1995**, *57*, 969-982.

<sup>121</sup>Medard, N. Characterization of CO<sub>2</sub> plasma-treated polyethylene surface bearing carboxylic groups. *Surf. Coat. Technol*. **2002**, *160*, 197-205.

<sup>122</sup>Wang, P.; Tan, K. L.; Kang, E. T.; Neoh, K. G. Surface functionalization of low-density polyethylene films with grafted poly (ethylene glycol) derivatives. *J. Mater. Chem*. **2001**, *11*(12), 2951-2957.

<sup>123</sup>Gugala, Z.; Gogolewski, S. Attachment, growth and activity of rat osteoblasts on polylactide membranes treated with various low-temperature radiofrequency plasmas. *J. Biomed. Mater. Res. A*. **2006**, *76*, 288-299.

<sup>124</sup>Chen, F.; Liu, J.; Cui, Y.; Huang, S.; Song, J.; Sun, J.; Xu, W.; Liu, X. Stability of plasma treated superhydrophobic surfaces under different ambient conditions. *J. Colloid Interface Sci*. **2016**, *470*, 221-228.

---

<sup>125</sup>Williams, R. L.; Wilson, D. J.; Rhodes, N. P. Attachment, growth, and activity of rat osteoblasts on polylactide membranes treated with various low-temperature radiofrequency plasmas. *J. Biomed. Mater. Res. A* **2004**, *76*(2), 288-99.

<sup>126</sup> Takahiro, Ishizaki.; Nagahiro, Saito.; Osamu, Takai. Correlation of Cell Adhesive Behaviors on Superhydrophobic, Superhydrophilic, and Micropatterned Superhydrophobic/Superhydrophilic Surfaces to Their Surface Chemistry. *Langmuir*, **2010**, *26*(11), 8147–8154.

<sup>127</sup>Kasálková, N. S.; Slepíčka, P.; Kolská, Z.; Sajdl, P.; Bačáková, L.; Rimpelová, S.; Švorčík, V. Cell adhesion and proliferation on polyethylene grafted with Au nanoparticles. *Nucl. Instr. Meth. Phys. Res.* **2012**, *272*, 391-395.

<sup>128</sup>De Rancourt, Y.; Couturaud, B.; Mas, A.; Robin, J. J. Synthesis of antibacterial surfaces by plasma grafting of zinc oxide based nanocomposites onto polypropylene. *J. Colloid Interface Sci.* **2013**, *402*, 320-326.

<sup>129</sup>D'Britto, V.; Tiwari, S.; Purohit, V.; Wadgaonkar, P. P.; Bhoraskar, S. V.; Bhonde, R. R.; Prasad, B. L. V. Composites of plasma treated poly (etherimide) films with gold nanoparticles and lysine through layer by layer assembly: a “friendly-rough” surface for cell adhesion and proliferation for tissue engineering applications *J. Mater. Chem.* **2009**, *19*(4), 544-550.

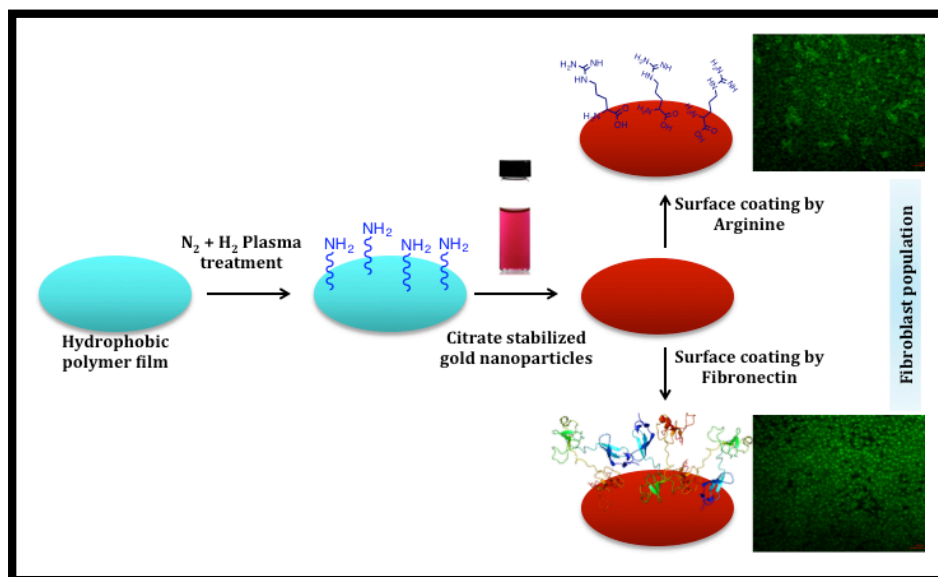
<sup>130</sup>D'Britto, V.; Kapse, H.; Babrekar, H.; Prabhune, A. A.; Bhoraskar, S. V.; Premnath, V.; Prasad, B. L. V. Silver nanoparticle studded porous polyethylene scaffolds: bacteria struggle to grow on them while mammalian cells thrive. *Nanoscale*, **2011**, *3*(7), 2957-2963.

<sup>131</sup> Hu. Y.; Winn, S. R.; Krajbich, I.; Hollinger, J.O. Porous polymer scaffolds surface-modified with arginine-glycine-aspartic acid enhance bone cell attachment and differentiation in vitro. *Journal of Biomedical Materials Research Part A*. **2003**, *64*(3), 583-590.

<sup>132</sup> Lee, S. K. C.; Woods, E. C.; Acharya, A. P.; Gardener, A. B. Biomaterials-Based Modulation of the Immune System. *BioMed Research International*. **2013**, *2013*, Article ID 732182, 7 pages.

# Chapter 2

## Arginine Mediated Surface Modification of Polymers for Tissue Engineering Applications



Parts of this chapter were published as

*Surface modification of polymers for tissue engineering applications: Arginine acts as a sticky protein equivalent for viable cell accommodation.* **Poulomi Sengupta**, Bhagavatula L. V. Prasad. *ACS Omega*, **2018**, 3(4), 4242-4251.

*Modification of porous polyethylene scaffolds for cell attachment and proliferation.* **Poulomi Sengupta**, Sachin S. Surwase, Bhagabatula L. V. Prasad. *International Journal of Nanomedicine*, **2018**, 13, 87-90.

### **Abstract**

Hydrophobic polymers are immensely popular choice as permanent bio-implants because of their material properties. These materials are absolutely bio-inert for years, but throw up challenges when it comes to fast integration with healthy tissue. In this chapter, we present a surface modification technique of converting the surface of hydrophobic polymeric films into hydrophilic ones using a layer-by-layer assembly process (P-LbL) involving gold nanoparticles, and small molecules like amino acids. These films showed much-improved animal cell (murine fibroblast) adherence properties compared to the commercially available tissue culture plates. Moreover, arginine-modified films exhibited nearly equivalent cell viability compared to the films modified with the natural ECM component fibronectin. Surface hydrophilicity, and roughness of the modified film were characterized by contact angle measurement, and atomic force microscopy (AFM). Cell counting, fluorescence microscopy, cell viability, and collagen estimation assays were employed to demonstrate that the modified film favoured much-improved cell adherence, and was capable of maintaining a healthy cell population in comparison to commercially available tissue culture plates.



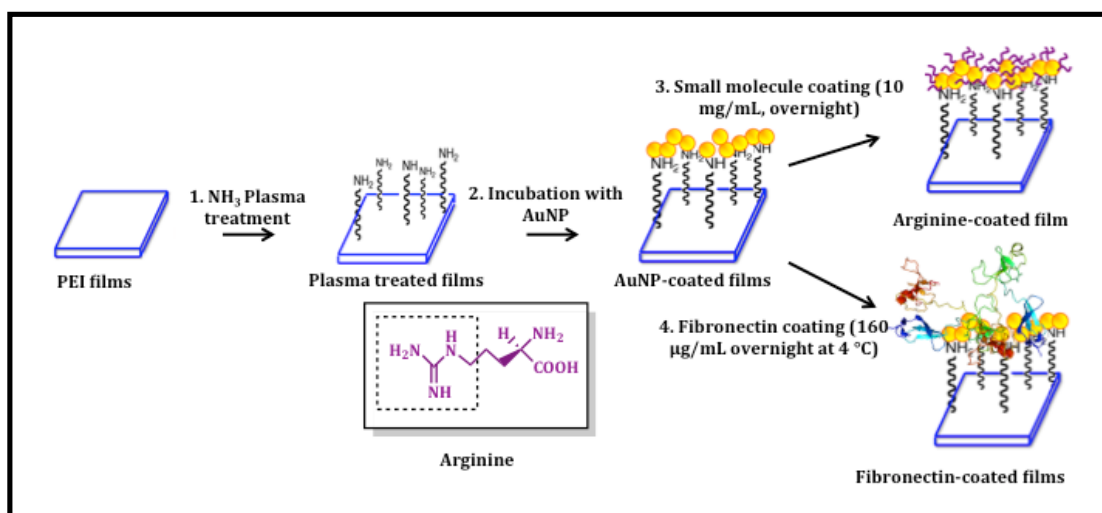
### 1.1. Introduction

Synthetic polymeric scaffolds are being extensively used as tissue replacements inside the human body.<sup>1</sup> In addition to providing strength, and durability, synthetic polymers can be molded into different shape/size porosity. For these reasons, polymers like polyethylene have a very long history of being 'the material of choice' as an implant.<sup>2,3</sup> Conversely, inherent hydrophobicity restricts them towards tissue integration, which may lead to dislocation, and fibrosis followed by multiple corrective surgeries.<sup>4,5,6</sup> Surface modification, can change this situation and this drawback can be circumvented where the bulk properties (mechanical strength, elasticity) of a material remain unaltered, whereas small modifications to the surface impart necessary characteristics allowing a faster integration of the implant with the tissue. In this context, surface modification of the polymers with proteins (fibronectin, vitronectin, laminin) present in the extracellular matrix (ECM) is a regularly practised strategy.<sup>7,8</sup> These proteins include a specific tri-peptide sequence RGD (arginine-glycine-aspartic acid) that is very specifically recognised by the cell surface receptor protein integrin. It has been widely reported in the literature that fibronectin-coated polymeric scaffolds portray enhanced cellular adherence leading to a drastically improved cellular proliferation.<sup>9,10</sup> To avail the benefits of both polymer (as material), and fibronectin/vitronectin (as surface modifying agents), an even coating of ECM protein on polymer will be ideal. But the polymer of choice being hydrophobic, uniform surface modification with protein is impossible exclusive of multistep chemical interventions (in order to achieve permanent chemical bond formation). In this context, the layer-by-layer<sup>11,12,13,14</sup> the assembly can produce ubiquitously uniform surface modification. Previous reports from our group have already established that plasma treatment of hydrophobic polymeric films followed by layer-by-layer assembly of gold nanoparticle, and lysine can 'lock' the hydrophilic characteristics of the surface, and increase the cell friendliness of the surface and promote cell growth.<sup>15,16</sup> This method is unquestionably superior to sole  $N_2 + H_2$  plasma treatment due to the prolonged retention of hydrophilicity. Moreover, such a modified surface works as an excellent

support for cell attachment, and proliferation. At room temperature, films that were modified following the above strategy were found to retain hydrophilic characteristics for more than 6 months (data not shown). In contrast, with only plasma treated films the hydrophobic character got regenerated within a week.<sup>17</sup>

In this chapter, with the aim of creating a cell-friendly surface out of the readily available materials by a simple, and convenient technique, we have surface modified plasma-treated PEI (polyetherimide) films *via* layer-by-layer assembly of gold nanoparticles, and arginine (P-LbL). We continued using PEI (instead of HDPE scaffolds) films because PEI is similar to HDPE in many respects. However, PEI is available as films unlike HDPE, which was available to us as scaffolds, obtained by fusing together micron size HDPE granules. This makes the use of PEI films easier compared to HDPE, as it was challenging to perform a cellular adhesion assay on HDPE scaffolds (because of the porous nature, most of the media along with cell suspension drained out rendering less contact time). On the other hand, with PEI films (2-dimensional, and no pores) there was no chance of drainage. It may also be noted that, after  $N_2 + H_2$  plasma treatment, AuNP favours covering the PEI films upon overnight incubation (**Scheme. 2.1**) equally well as witnessed in case of HDPE scaffolds. Thus, we can safely conclude that after P-LbL steps, both HDPE, and PEI polymers behaved in similar fashion as both are similarly decorated with AuNPs. As an added advantage, PEI films are transparent, which helped in characterization, and microscopy experiments. It may be noted that in the last step of the P-LbL procedure we used 'arginine' instead of lysine, which was different from the work done previously by others in our group.<sup>15</sup> Arginine is a component in 'RGD sequence', which is responsible for  $\beta$  integrin recognition. Moreover, arginine, because of its cell-penetrating nature has been commercialized in all transfection agents (like R9), and is expected to show favourable cell membrane recognition property. The guanidium groups present in the side chains of arginine make it more hydrophilic, and water adsorbing. All these properties should constructively help in recognizing a cellular membrane, and help with the easy stretching, and adherence of cells on a material surface. We even compared the arginine, and lysine-coated surfaces with respect to healthy cell accommodation. While, both were way better

than bare film, arginine was the best (data not shown here). Accordingly, we evaluated the adherence, and proliferation of L929 (murine fibroblasts) cells on PEI films surface modified by the P-LbL strategy using arginine. As a positive control, we have taken fibronectin-coated (on gold-coated films) films (**Scheme 2.1**) and compared several properties like cellular adhesion, and proliferation, the quantification of live cells, the expression of F-actin, and the quantification of collagen.



**Scheme. 2.1:** Schematic representation of surface modification for polyetherimide films. 1. Plasma treatment on PEI films using 3:2 hydrogen, and nitrogen mixture. 2. Citrate-stabilized gold nanoparticles incubation with plasma treated films. 3. Dip coating of films inside arginine water solution overnight. 4. Incubation of citrate gold coated films with a dilute solution of fibronectin.

To our surprise, we have found nearly comparable results in both the treatments, which led to the conclusion that small molecule arginine can be considered to be a sticky protein equivalent when it comes to viable cell population on a surface modified polymeric film. To rationalize our observation, we also have shown that L929 cells grown on both arginine, and fibronectin-coated films produce an equivalent amount of collagen on prolonged culture indicating that the cellular accommodation mechanism with both these molecules is probably the same.

## 2.2. Materials

PEI (polyetherimide) sold under the trade name Ultem 1000®, was obtained from General Electrical Co., Schenectady, NY, USA. Chloroauric acid was obtained from the Seisco Research Laboratory, India. Arginine, fibronectin (tissue culture grade), carboxyfluoresceinsuccinimidyl ester (CFSE), 4', 6-diamidino-2-phenylindole (DAPI), phosphate-buffered saline (PBS) powder, resazurin, and propidium iodide (PI) were purchased from Sigma Aldrich. Murine originated fibroblast cell line L929 was procured from the cell line repository of NCCS Pune, India. DMEM, and FBS were purchased from Invitrogen. Collagen estimation kit (K218) was purchased from Biovision. Trypan blue was purchased from Himedia. F-actin marker Alexafluor 488 phalloidin conjugate was bought from Thermo Fischer Scientific.

## 2.3. Experimental section

### 2.3.1. Preparation of arginine-coated PEI films

#### 2.3.1.1. Gold nanoparticles synthesis

Gold nanoparticles were synthesized by the Turkevich method<sup>18</sup> where 0.1 mM chloroauric acid was reduced by 10 mg/mL citric acid under boiling water conditions. The particles were characterized by UV-Vis [**Figure 2.3(a)**], and TEM [**Figure 2.3(b)**].

#### 2.3.1.2. Casting of PEI films

PEI (available as solid polymer beads) was weighed, and made into a solution of 0.0675 gm/mL in dry chloroform. It was carefully poured into 150 mm clean dry grease free flat glass Petri dish, and was covered with aluminium foil. The overnight setting at room temperature yielded a transparent light yellow coloured film (**Figure 2.1**).



**Figure. 2.1:** Conversion of PEI beads to a film.

### 2.3.1.3. Plasma treatment

The plasma treatment was carried out using  $N_2 + H_2$  plasma at 60 watts power for 20 minutes. The flow ratio was maintained at 3:2  $H_2$  to  $N_2$ . The instrument employed was Emitech Plasma Asher K1050X (**Figure 2.2**).



**Figure. 2.2:** Emitech plasma asher used for the work reported in this chapter.

### 2.3.1.4. AuNP-coating on PEI films

Freshly plasma ( $N_2 + H_2$ ) treated PEI films were dipped in citrate stabilized gold nanoparticle sol at room temperature, and stirred overnight. After some time the gold sol was found to lose its wine red colour following which it was replenished until a uniform gold layer formed on the films.

### 2.3.1.5. Arginine-coating on gold-coated PEI films

The gold-coated films obtained from the above step were immersed overnight in a solution of arginine (4g/L) in milli-q water. After incubation, the films were washed with PBS, and carried forward for characterization or applications.

### 2.3.1.6. Fibronectin-coating on gold nanoparticle-coated PEI films

Gold nanoparticle-coated films were soaked in 40 µg/mL of fibronectin in PBS overnight at 4 °C. All the films were washed with PBS, and air-dried before characterization or application.

### 2.3.2. Characterization of surface modified films

#### 2.3.2.1. UV-Vis spectrophotometry

In this experiment, PEI films were cut into 1 cm × 4 cm rectangular strips. After plasma treatment followed by AuNP-coating, dry films were placed in UV cuvettes facing the 1 cm width across the incident beams. CARY 300 Conc UV-Vis spectrophotometer was used for the collection of the UV-Vis spectrum. After following proper protocols for coating arginine, and fibronectin (following 2.3.1.5., and 2.3.1.6.) the films were washed in PBS, and dried. They were put inside UV cuvettes for the collection of the UV spectrum.

#### 2.3.2.2. Surface hydrophilicity by the contact angle measurement

Surface hydrophilicity was measured by dropping 10 µL water droplets on the modified polymer surface at room temperature, and atmospheric pressure. Data were collected from a minimum of ~5 locations and the average contact angle values were determined. Kruss Drop Shape Analyser Version 1.41-02 was used for this purpose.

#### 2.3.2.3. Water absorption study

The hydrophilicity generated on the arginine-coated films can be well expressed by a water absorption study. In this experiment, films were prepared after dipping them in arginine, and fibronectin solutions (as per the protocol followed in sections 2.3.1.5., and 2.3.1.6.). The modified films were air-dried followed by high vacuum exposure for 2 h. Each film was weighed using a microbalance. Each film was separately dipped into water, taken out, wicked off using a tissue paper and again weighed in the microbalance. The weight difference is the amount of water adsorbed on the film. The amount of water absorbed per unit weight of the film has been expressed in **Figure 2.9**.

#### *2.3.2.4. Surface atomic force microscopy*

Surface-modified films (AuNP-coated film, arginine-, and fibronectin-coated films), and control (pristine films) were placed on glass slides and scanned using Nano Wizard Atomic Force Microscopy by the contact method.

#### *2.3.2.5. IR spectroscopy*

Surface-modified films were subjected to characterization using solid-state IR spectroscopy. In this method, Perkin Elmer Spectrum 2 spectrophotometer was used in ATR (Attenuated Total Reflectance) mode to collect data using 40 scans in the wavenumber range 500-4000  $\text{cm}^{-1}$ . For both of these surface modified films background with only PEI was also taken.

#### *2.3.2.6. Mechanical stability*

Tensile testing was performed on a TA Instruments dynamic mechanical analyzer (DMA, RSA- III). Stretching experiments were performed using the rectangular tension geometry for the PEI sheets (control, arginine-coated, fibronectin-coated). Samples were cut into dog bone shapes for tensile testing. They were then clamped vertically in the rectangular geometry and stretched at a constant rate of 0.01 mm/s. Young's modulus was determined from these experiments.

### **2.3.3. Cell culture experiments with modified films**

#### *2.3.3.1. Common protocol for cell culture experiment*

In all the tissue culture experiments non-treated sterile 24 well plates were used. Films (modified as well as controls) were cut into 15 mm diameter circles and sterilized under UV inside tissue culture hood for 30 minutes on each side. They were aseptically put into an untreated 24 well plate. 10,000 murine fibroblast L929 cells were suspended in 50  $\mu\text{L}$  complete medium and seeded on each film. After 2 h incubation, the medium was aspirated and washed with 100  $\mu\text{L}$  of complete medium. Following this, all the films were allowed to incubate with 500  $\mu\text{L}$  complete DMEM medium under tissue culture conditions for the mentioned period of time. Results from each experiment were plotted as a mean including  $\pm$  SE for  $n=3$ .

Sample preparation for imaging: For imaging experiments, films were washed twice with PBS, fixed with 4% PFA for 15 minutes, followed by washing with PBS. Cells were incubated in 0.1% Triton X-100 in PBS for 5 minutes followed by washing (PBS). They were further incubated in 5% BSA for 20 minutes to avoid non-specific binding. Further, they were incubated with appropriate dyes. Images pertaining to a single experiment were taken using equal exposure time.

### **2.3.4. Evaluation of cellular adhesion**

#### *2.3.4.1. Cell adhesion assay by cell counting (Trypan blue assay)*

In this experiment, arginine-coated PEI films were aseptically put into an untreated 24 well plate. 10,000 healthy L929 fibroblast cells dispersed in 50  $\mu$ L complete DMEM medium were seeded on each film. At each predetermined time point, media was aspirated and collected. Followed by this, the films were also washed with 50  $\mu$ L PBS ( $\times 3$ ). This step was performed to exclude gravitationally precipitated but non-adhered cells. All these aliquots were consolidated ( $\sim 200$   $\mu$ L along with washing liquid) and mixed with Trypan blue. Cell number present in the aliquot was counted with the help of an inverted microscope. In this way the cellular density of 'unattached' cells was determined. The data was compared with the same number of cells seeded into each well of an untreated 24 well tissue culture plate, and normalized with the number of cells used for seeding.

### **2.3.5. Cell viability, and cytotoxicity**

#### *2.3.5.1. Cell viability assay (by resazurin)*

Cell seeding, and incubation were performed as per the common protocol mentioned (section 2.3.3.1). At 48 h, the cells were incubated with 100  $\mu$ M resazurin (in complete DMEM), and allowed to incubate for 6 h under cell culture condition. The relative amount of viable cells was estimated by reading the emission at 590 nm (excitation 530-560 nm). The readings of cells grown on surface modified films were normalized with the reading from control cells grown on the adhering plate, and plotted in per cent cell viability.



### *2.3.5.2. Live-dead assay by fluorescence microscopy*

50,000 healthy L929 cells in 50  $\mu$ L complete DMEM media were seeded on each surface modified films, and controls. After 2 h, the media was aspirated and replenished with 500  $\mu$ L complete DMEM media. At 2 days time point, cells were washed with PBS, incubated in 0.1% TritonX-100 for 5 minutes in the dark, and 5% BSA in PBS. The films were washed twice with PBS. Subsequently, they were incubated with the live-dead assay stain of 10  $\mu$ L 7.5 mM propidium iodide, 1  $\mu$ L 0.67 mM acridine orange in 1 mL complete DMEM media (for each well) under cell culture conditions for 1 h. The wells were washed with PBS, and directly viewed under Axio Observer Z1 Carl Zeiss microscope using green, and red channels. Emission of both the colours representing live, and dead cells was quantified, normalized with respect to area and plotted.

## **2.3.6. Effects on cellular proliferation**

### *2.3.6.1. Cell proliferation study by cell counting*

Cell seeding and incubation were done according to the common protocol discussed. After 1, and 2 days of incubation under cell culture conditions, the media was aspirated. The wells (containing films) were washed twice with PBS, and the films were trypsinized with 100  $\mu$ L Trypsin EDTA (for each film). After proper dilutions of the aliquots, the cell numbers were counted with the help of Trypan blue stain, and inverted microscope. The plotted data was normalized with respect to the number of cells seeded.

### *2.3.6.2. Cell populations on differently treated surfaces by fluorescence microscopy*

Cell seeding was performed according to the common protocol discussed. At 48 h time point, the cells were fixed, and blocked. They were treated with CFSE in PBS (5  $\mu$ M) for 15 minutes at room temperature in the dark followed by washing with PBS. The films were incubated with 300 nM DAPI at room temperature in the dark for 4 minutes followed by another brief PBS wash. They were mounted on clean glass slides with mounting media, sealed, and observed using Axio Observer Z1 Carl Zeiss

microscope using green, and cyan filters. Emission of fluorescein, and DAPI from adhered cells were quantified, normalized with respect to area and plotted.

### *2.3.6.3. Cell morphology, and actin cytoskeleton staining*

The cells were seeded according to the protocol discussed. They were incubated for 24 h in complete DMEM media. After 2 times PBS wash films were fixed, and blocked. Actin filaments were stained by 100 times diluted alexafluor 488 phalloidin (in PBS) incubated in the dark for 30 minutes at room temperature. Cell nuclei were counter stained with DAPI at 300 nM concentration for 4 minutes at room temperature (in the dark) followed by two times wash in PBS. Films were directly placed on a coverslip slide cells facing down (light source from bottom), and the images were captured using green, and cyan filters by epi-fluorescence microscopy using Axio Observer Z1 Carl Zeiss microscope.

### **2.3.5. Collagen production assay**

$1 \times 10^6$  L929 cells were suspended in 200  $\mu$ L complete media and seeded on surface modified (arginine-coated, and fibronectin-coated) UV-sterilized films (diameter 35 mm) kept in 6 well plates. Media was aspirated after 2 h, and 2 mL of fresh complete media was added to each well. At 24 h, the media was changed. The aspirated media was saved. At 2 days time point media was aspirated, and 1 mL spent media (from the combination of both days media) of each well were stored. After washing the films two times with sterile PBS cells were scraped off using a cell scraper, and 400  $\mu$ L PBS. From cells, collagen was estimated by lysing followed by oxidation. From spent media, protein was precipitated, oxidized, and estimated according to the protocol mentioned in collagen estimation kit K218 from Biovision. The amount of collagen generated in each sample was estimated by a calibration curve. The data plotted was normalized with the amount of collagen present on bare film, and presented in percent. From the data points (**Figure 2.17**) it may seem that fibronectin-coated films have higher amount of collagen formed. Genuinely, the difference (**Figure 2.17**, 3<sup>rd</sup>, and 4<sup>th</sup> columns) is not significant as proved by a ttest using Microsoft Excel.

## 2.4. Results and discussion

### 2.4.1. Preparation and characterization of films

Our strategy involved the preparation of arginine-, and fibronectin-coated PEI films by P-LbL followed by dip-coating. This became possible as gold nanoparticles have versatile surface chemistry, which allows easy association with most proteins, polymers, and polar (small) molecules. The resulting films were characterized using UV-Vis, IR, AFM, and Dynamic Mechanical Analyzer (DMA). Our strategy to surface modify the polymeric films (which could be easily extended to porous scaffolds) was initiated with the plasma treatment of a hydrophobic polymeric film. For the plasma treatment, we used a mixture of  $H_2 + N_2$  gases inside a plasma asher chamber (**Figure 2.2**), which was expected to generate ammonia plasma<sup>18,19</sup> *in situ*. This reactive ammonia plasma interacts with the surface of the polymers generating hydrophilic functional groups<sup>20</sup> (mostly  $-NH_2$  groups) (**Scheme 2.1**). These films were then dipped in a gold nanoparticle hydrosol. These gold nanoparticles were in turn prepared by the well-established Turkevich method.<sup>21</sup> The as-prepared gold nanoparticle sol has a characteristic wine-red colour displaying an absorbance peak at  $\sim 530$  nm in the UV-Vis spectrum [**Figure 2.3(a)**]. The absorbance is attributed to the localized surface plasmon resonance. The TEM analysis indicated that the particles are around 20 nm [**Figure 2.3(b)**].

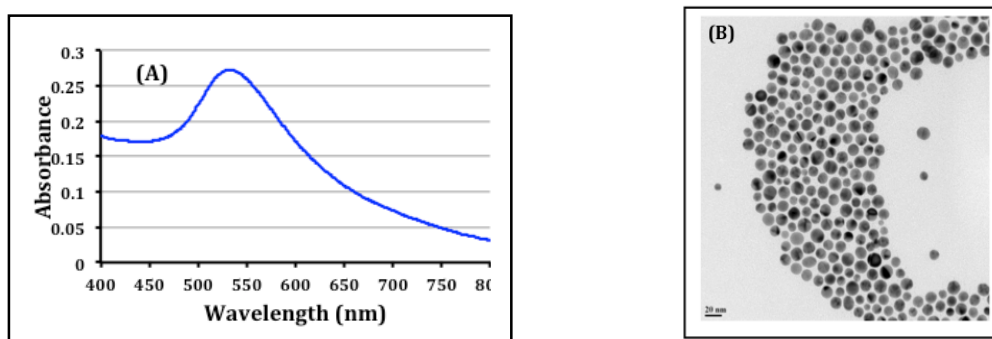


**Figure. 2.3(a):** UV-Vis trace for citrate stabilized gold nanoparticles. **2.3(b):** TEM image of the same. Scale bar 20 nm.

As expected, a simple dipping of the plasma-treated PEI films in the above described gold nanoparticle hydrosol led to a quick, and firm attachment of the nanoparticles to the plasma treated film surface due to the electrostatic attraction between the positive, and negative charges of amine generated on the PEI films due to plasma treatment, and citrate groups present on the AuNP surfaces. This contention was supported by the UV-Vis spectrum of the gold nanoparticle adhered film, which shows a peak at 580 nm (**Figure 2.4.A, B**, red lines) that is significantly different from the peak observed for as-prepared gold sol [**Figure 2.3(a)**]. This shift in surface plasmon resonance is expected and is ascribed to the aggregated nature of gold nanoparticles on the film. To check how strongly these AuNPs adhere to the PEI film, we immersed the gold decorated PEI films in water at 90 °C under stirring conditions. We did not notice any leaching of AuNP into the hot water as judged by the absence of the surface plasmon peak of gold nanoparticles in water (data not shown). Thinking that small quantity of gold nanoparticles if present in the supernatant could go unnoticed, we evaporated water from the supernatant to dryness, and added aqua-regia to it. This would oxidize any gold nanoparticles if present into Au<sup>+3</sup> and can be detected by UV-vis spectrophotometry. Here again, we did not visualize any peak corresponding to Au<sup>+3</sup> (data not shown).

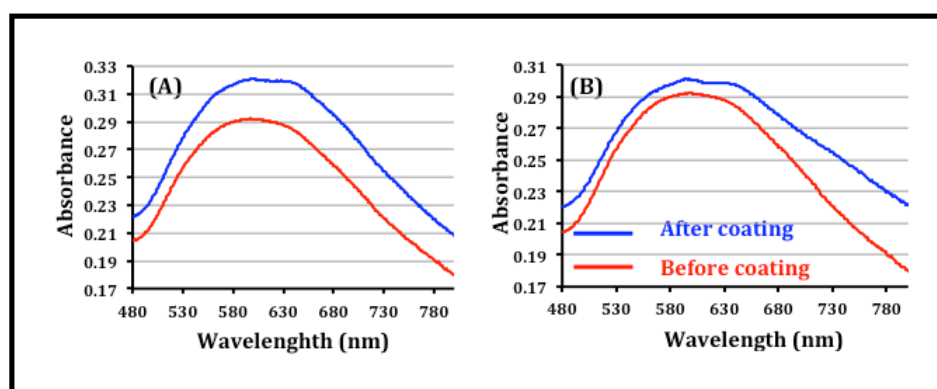


**Figure. 2.4:** Solid-state UV-Vis traces of arginine-coated (A), and fibronectin-coated (B) PEI films.

**Figure 2.4** displays the solid-state UV-Vis trace of arginine-, and fibronectin-coated PEI films (red curves in **Figure 2.4.A**, and **2.4.B**), which were previously modified with AuNPs. Both of them (blue lines) indicate the retention of the LSPR peak from

AuNPs. This observation strongly stresses on the fact that after coating in arginine, and fibronectin solutions, gold-coating was strong, and stable on the PEI films.

The 'contact angle measurement' is a strong tool for the determination of hydrophilicity and accordingly, we measured the contact angles after different surface modification procedures, which are presented in **Figure 2.5**. As it can be noticed, the pristine PEI films exhibited a contact angle value of 83 ° with 10 μL of water at the air-water interface. This observation clearly indicates that the pristine PEI films are considerably hydrophobic. Upon N<sub>2</sub> + H<sub>2</sub> plasma treatment, and citrate stabilized gold nanoparticle coating, the contact angle decreased to ~ 75 ° indicating a lowering in the hydrophobic character of the film. The attachment of the citrate-stabilized gold nanoparticle coating on the plasma treated PEI films changed the contact angle only slightly (76 °). Overnight incubation of AuNP-coated films in arginine solutions followed by aerial drying produced the extremely hydrophilic arginine-coated film, having a contact angle in the low range around ~ 19 °.

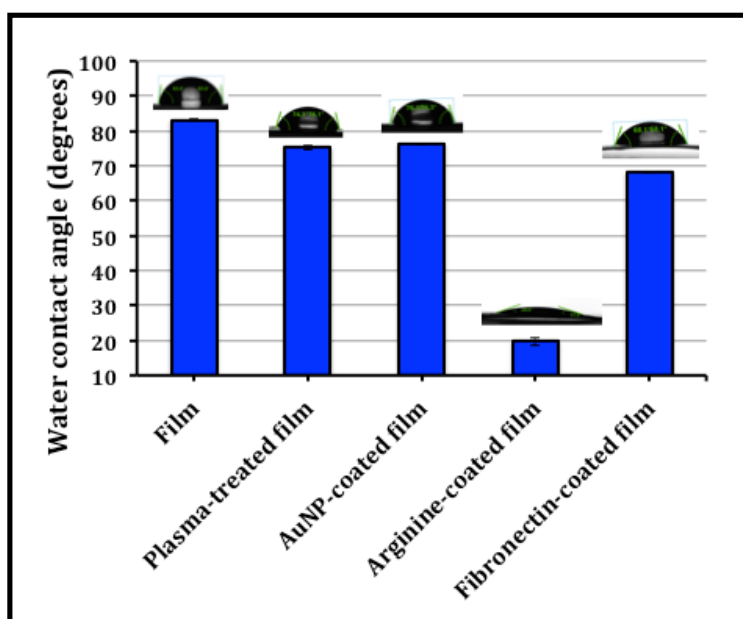


**Figure. 2.5:** Contact angle determination using 10 μl water droplet on the treated film. Data represented ±SD of n=3.

This is attributed to the guanidium group present in the side chain of arginine molecule (see **Scheme 2.1**), which is extremely hydrophilic. Once guanidium or any

amine group from arginine anchors on the gold nanoparticle surface, the other amine or carboxylic acid groups (present in arginine) will be exposed outwards and will preferentially interact with water thus explaining the enhanced hydrophilicity.

On the other hand, fibronectin-coated films did not show a great change in the contact angle (changed from 76 ° in AuNP-coated film to 68 °) value. This could be rationalized by considering the composition of fibronectin, which is a combination of both hydrophilic, and hydrophobic amino acids.

A set of water absorption studies were carried out, which have revealed that arginine coated film can retain significantly more amount of water on the surface in comparison to fibronectin-coated film or the bare film. The results are presented in **Figure 2.6**. Bare PEI films, having no surface functionalization, is unable to hold water in a large amount, while fibronectin-coated films exhibit a moderate amount of water retention.

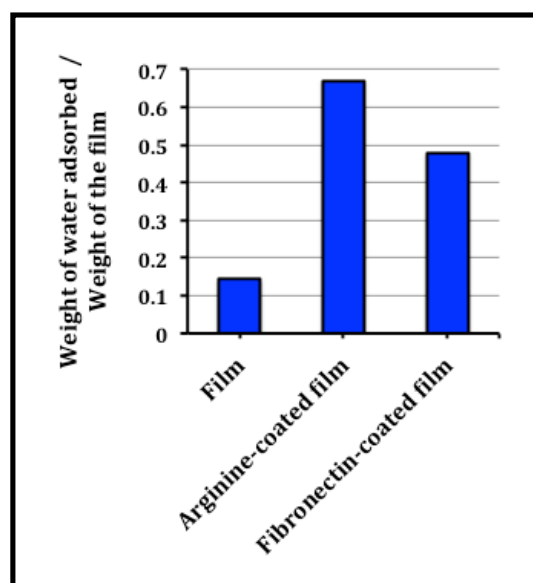


**Figure. 2.6:** Water absorbed on each film is indicated by a plot of weight of water absorbed per unit weight of the film.

We also checked the tensile strength of the films after different surface modifications using DMA (**Figure 2.7**). It may be noticed that in all cases (the bare PEI, arginine-coated, and fibronectin-coated films) there was no significant change

in Young's modulus value (value lies in the range of 1000-2000 MPa) of the bulk polymeric film. In spite of several surface modifications, until the application of 30 MPa pulling force, no breaking of the film was experienced. This observation hints towards the high mechanical robustness of the film, which remained unaltered withstanding several surface treatments.

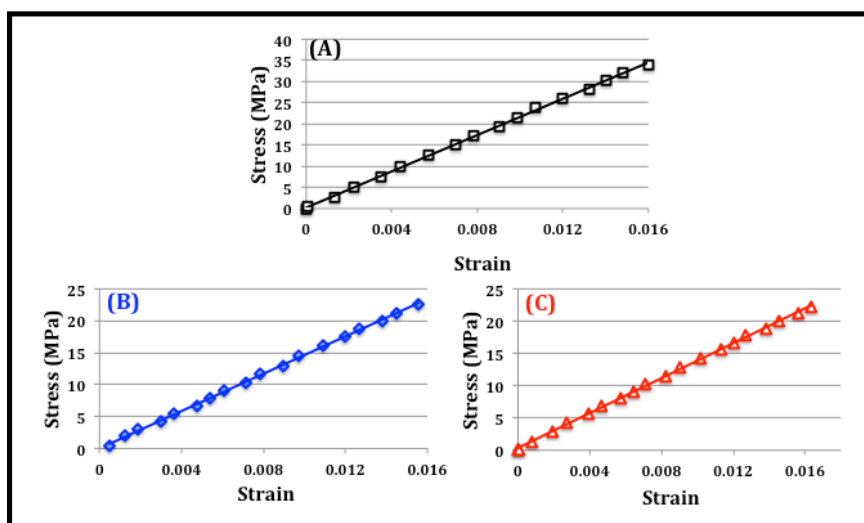


**Figure. 2.7:** Mechanical stability profiles of the film (A), arginine-coated film (B), fibronectin-coated film (C).

The trends in contact angle changes and water absorption data are reflected in the surface roughness characteristics determined from the AFM as well (**Figure 2.8**). In case of the pristine PEI film, the surface roughness parameter was estimated to be  $R_a=9.85$  nm (**Figure 2.8.A**). For gold-coated films, the roughness value increased to  $\sim 50$  nm (**Figure 2.8.B**). Interestingly, when the same films were surface modified with arginine (**Figure 2.8.C**) the surface roughness parameter increased drastically ( $R_a=107$  nm) which may be attributed to the restructuring of nanoparticles on the polymeric film surface in the presence of arginine (**Figure 2.8.C**). On the other hand, fibronectin coating on gold-coated PEI surface did not change the surface roughness parameter (**Figure 2.8.D**) very much although a little elevation in its value ( $R_a=66.1$  nm), when compared to only gold-coated films was observed. This may be attributed to a higher molecular entanglement present in protein in comparison to small molecules.

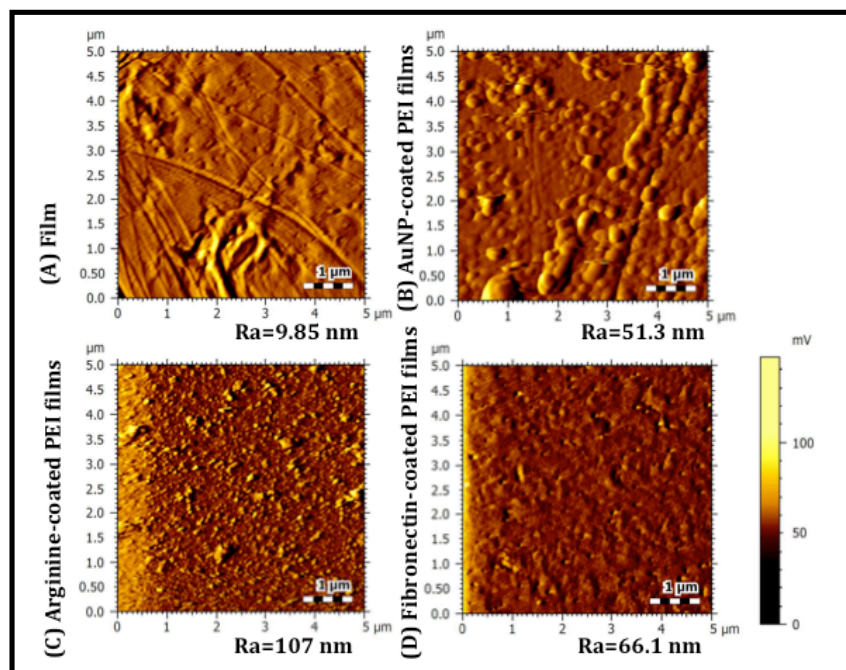


**Figure. 2.8:** AFM images (contact mode) showing the topography of surface coated films along with control untreated (A), gold coated (B), arginine dipped (C), and fibronectin dipped (D) films. Surface roughness parameters are provided with each images.

While the changes in UV-Vis spectra, contact angle, water absorption, and surface roughness values do provide indication of the changes in the surface characteristics of the films due to the sequential layer-by-layer assembly of gold nanoparticles, and the coating of arginine or fibronectin onto them, characterization by IR provides conclusive evidence of the presence of arginine, and fibronectin on the films. Solid state FT-IR (ATR mode) is a robust technique for determining the signatures in surface modified films. It has to be kept in mind that PEI itself (**Figure 2.9** curve 1, black line) is a chemically complex molecule, which has several signature peaks representing either aromatic C-H units or phthalimide groups *etc.* The FT-IR spectrum of PEI alone displayed a sharp peak at  $1720\text{ cm}^{-1}$  corresponding to the lactam carbonyl group present in it (Curve 1 in **Figure 2.9**). Therefore, in all surface modified films, a baseline with only PEI was performed. In **Figure 2.10** the IR spectra in between  $1300\text{ cm}^{-1}$  and  $1800\text{ cm}^{-1}$  was expanded. Accordingly, from FT-IR analysis it can be very clearly seen that in arginine-coated films, a broad peak of



protonated, hydrated guanidium group appears in the range  $1500\text{-}1600\text{ cm}^{-1}$  [peak (a), curve 2, blue, **Figure 2.10**]. The stretching motion of the CO group at  $1630\text{ cm}^{-1}$  (**Figure 2.10**) could be seen. The band at  $1520\text{ cm}^{-1}$  was assigned to the bending vibration of  $\text{-OH}$  (indicated as peak a, **Figure 2.10**). Further, the sharp peak at  $1410\text{ cm}^{-1}$  corresponds to symmetric in-plane bending, and the asymmetric bending of  $\text{CH}_3$  groups could be seen around  $1450\text{ cm}^{-1}$ . Also, when fibronectin-coated films were probed with FT-IR, a strong  $\gamma_{\text{N-H}}$  [peak 3(b) amide I  $1670\text{ cm}^{-1}$  and peak 3(c) amide II  $1560\text{ cm}^{-1}$  in **Figure 2.10**] stretching frequencies were observed, confirming protein attachment to the AuNP-coated films.

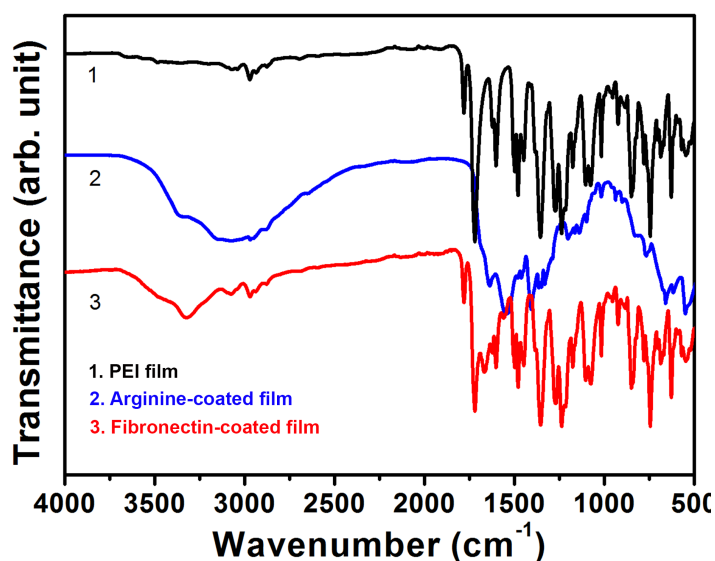


**Figure. 2.9:** Full-length IR spectrum of differently surface modified films under ATR mode. The relevant region is expanded in Figure 2.10.

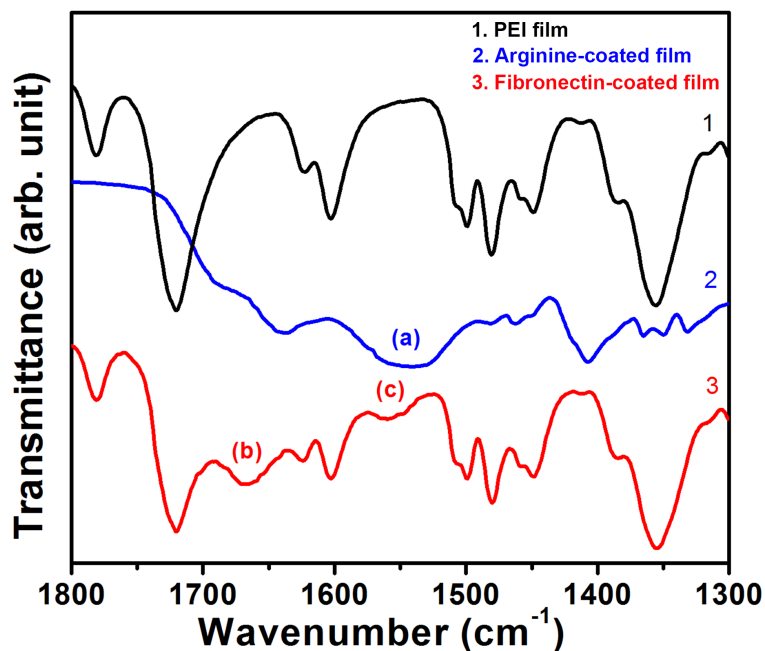


**Figure. 2.10:** FT-IR spectrum took in ATR mode for the characterization of signature peaks from PEI film (1), arginine-coated PEI film (2), and fibronectin-coated PEI film (3). (a) The broad peak at 1550-1600  $\text{cm}^{-1}$  corresponds to protonated, hydrated guanidium groups. (b) Amide I (from fibronectin) 1670  $\text{cm}^{-1}$  and (c) Amide II 1560  $\text{cm}^{-1}$ .

#### 2.4.2. Cellular adhesion study

After establishing that the layer-by-layer assembly of AuNPs, and fibronectin or arginine can be achieved by simply dipping the PEI films in the respective solutions, we proceeded to evaluate the cellular adhesion capability of PEI films surface modified by arginine. In this experiment, the cell attaching properties of arginine-coated films were evaluated in comparison to non-treated polystyrene plates. From the cell count experiment using optical microscopy (**Figure 2.11**) it can be clearly seen that with the increase in time, more and more number of murine fibroblast cells get adhered to the arginine-coated film. The number of cells present in the supernatant decreased with time, indicating that more than 40% of the cells adhered to the arginine-coated films within 1 min, while in control non-treated plate, less than 20% cells adhered. Similarly, within one hour almost 60% of cells adhered to the arginine-coated films, while for the bare plate, the extent remained

around 30%. At 2 h the change was drastic, where almost 85% of cells adhered to arginine-coated films and only around 35% cells adhered to the control plate. In summary, we observed that almost all the cells were found adhered to the arginine-coated films at  $\leq 2$  h.

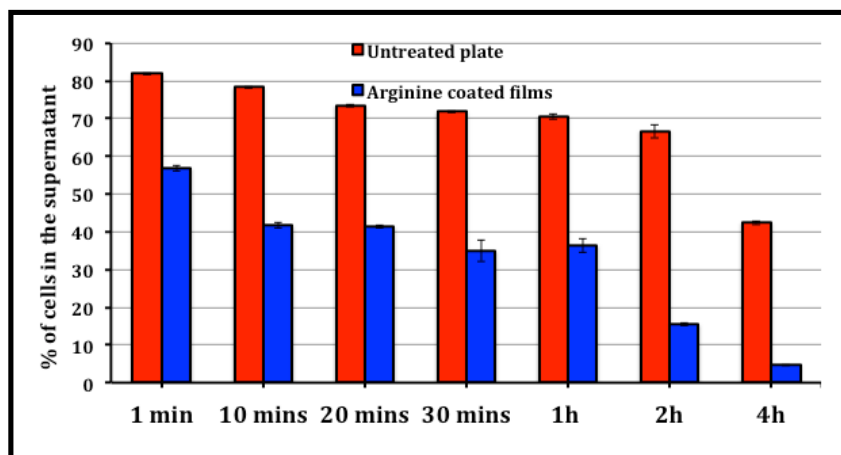


**Figure. 2.11:** Cellular adhesion experiment by cell counting where not-adhered cells were estimated using Trypan blue. Data represented as a  $\pm$ SD of  $n=3$ .

We attribute this to the hydrophilic character of the arginine-coated films (evident from contact angle, water absorption measurements **Figures 2.5**, and **2.6**), roughness (evident from AFM measurements **Figure 2.8**), and the presence of positive charges (from the guanidium side chain present in arginine). The ultimate goal of these surface modified films is to accommodate healthy cells. So, after establishing that arginine-coated films support strong cell adherence, we wanted to check their cell proliferation capability over time. Thus from this point onwards, we chose to compare the cell viability properties with a strong positive control: the fibronectin-coated films.

### 2.4.3. Cell viability and cytotoxicity

#### 2.4.3.1. Cell viability study by mitochondrial activity

In this experiment, viable cells were estimated by mitochondrial activity (**Figure 2.12**), as indicated by the reduction of resazurin to resofurin (emission at 590 nm), which is a standard chemical for this purpose. The data presented here were

normalized with respect to the quantity of resofurin signal obtained from the untreated plate. In accordance with the cell counting experiment, it was observed that both fibronectin-, and arginine-coated films allowed cell proliferation from 122% to 125% at the end of 2 days. The two values are almost equivalent indicating an equal amount of viable cells in both arginine-, and fibronectin-coated films (**Figure 2.12**). Plasma treated films also showed a high amount of viable cells. This can be attributed to the hydrophilic nature imparted to polymer surface due to plasma treatment (for better comparison we did these experiments on PEI films immediately after plasma treatment as it provides only transient surface modification). As expected, untreated and gold-coated surfaces showed less number of cells. In the case of untreated films, this could be due to their hydrophobic character, which did not allow facile cellular adhesion in the first place, whereas in case of gold nanoparticle-coated films the negative charge of the citrate molecules present on their surface may be implicated for the cell unfriendliness. We wish to emphasize here that all data from different films showed considerably higher cellular proliferation in comparison to the non-treated tissue culture plate, which supports the fact that the PEI films per se are not at all cytotoxic.

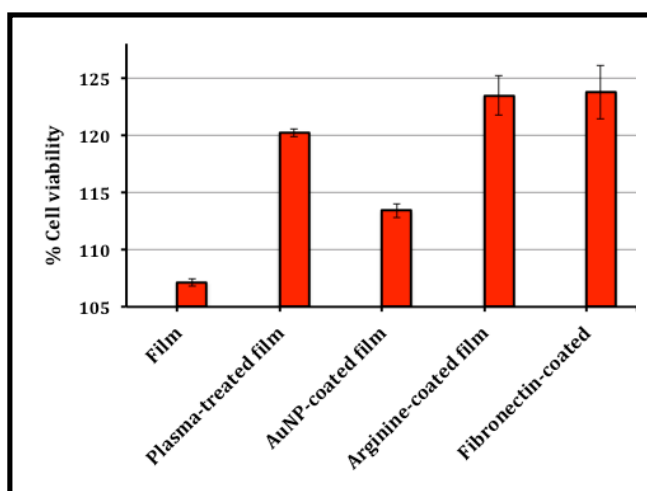


**Figure. 2.12.** Cell viability by mitochondrial activity using Resazurin indicator at 48 h. Data represented as  $\pm$ SD of  $n=3$

#### 2.4.3.2. Cell viability by live-dead imaging

For the detection of a dead and live cell, propidium iodide (PI), and acridine orange (AO) dye-based assays were performed, respectively. Here also, arginine-coated films showed an increased number of healthy cells population, but there were few dead cells [**Figure 2.13(a)**] as well. This may arise due to the dearth of space, and nutrients, which may impede the growth of cells and pushed the cells towards physiological death. On the other hand, fibronectin-coated films showed excellently adhered cells, and no dead cells were present according to PI staining. This may arise due to the presence of fewer cells in a smaller area (as the fibronectin-coated films are reasonably hydrophobic, contact angle  $68^\circ$ , **Figure 2.8**), while the amount of nutrition (volume of complete media) was the same in every other case (controls and arginine-coated films). So, the amount of media, was probably sufficient for the fewer cells present in the case of fibronectin-modified films to thrive. On the other hand in case of surface modification by arginine the amount of media was not adequate at providing nutrition for a larger number of cells that get adhered initially. We quantified the green (corresponding to live cells), and red (corresponding to dead cells) fluorescence intensities from several (>7) images. The emission intensity from the fields green (representing live cells stained by acridine orange), and red (representing dead cells stained by propidium iodide) as shown in the **Figure 2.13(b)** also supports this conclusion.

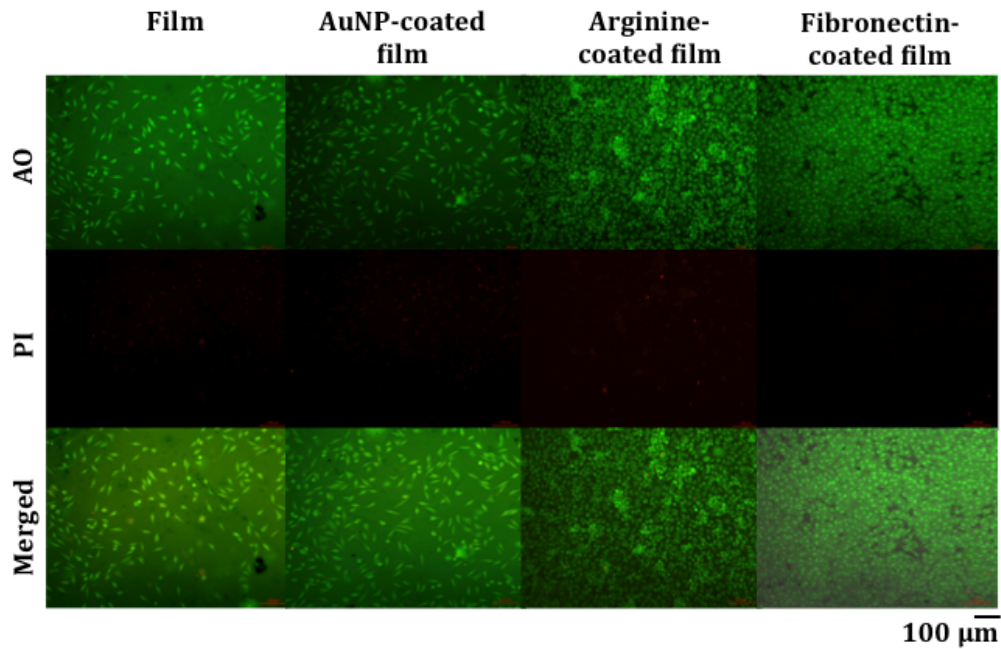


**Figure. 2.13(a):** Live-dead assay by live cells imaging. Live and dead cell stains are acridine orange (AO) and propidium iodide (PI). Scale bar 100  $\mu\text{m}$ .

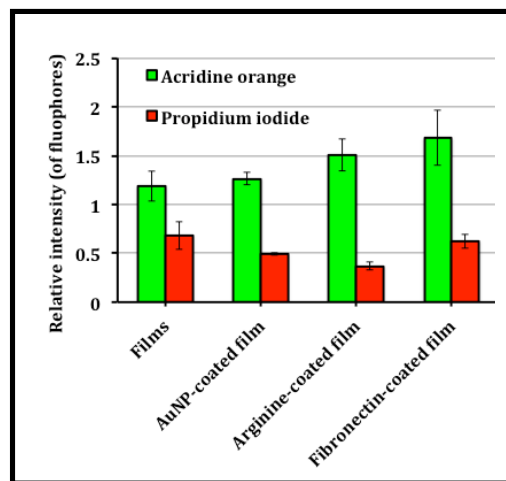


**Figure. 2.13(b):** Quantification of fluorescent tags from live-dead assay images. (A) Acridine orange (AO, green), and (B) Propidium iodide (PI, red) from figure 2.13(a). Data represented as a  $\pm$ SD of  $n=7$ .

### 2.4.4. Cellular proliferation analysis

#### 2.4.4.1. Cellular proliferation study by cell counting

To determine the extent of cellular proliferation, both cell counting, and imaging experiments were performed. Cell counting at different intervals (1 day and 2 days) shows that the approximate number of cells adhered to both arginine-, and fibronectin-coated surfaces were very similar (**Figure 2.14**) keeping in mind the reported doubling time<sup>22</sup> of L929 cells. In this experiment, at both one- (**Figure 2.14** blue columns), and two-days time points (**Figure 2.14** red columns) arginine-, and fibronectin-coated PEI films (after P-LbL) were found to produce almost equal number of live cells while gold-coated, and pristine films showed lower cell population. Similarly fresh plasma treated films, also indicated reasonably high number of cellular population.

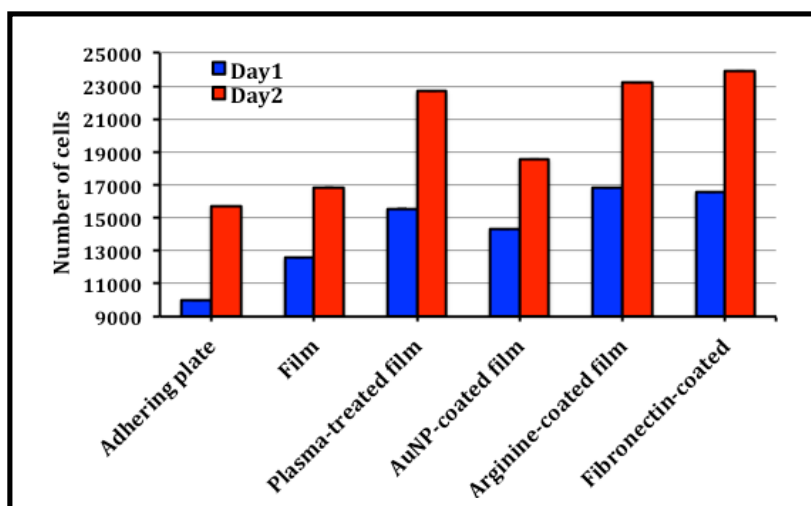


**Figure. 2.14:** Cell proliferation study by cell counting using Trypan blue exclusion test. Data represented as the mean  $\pm$ SD of  $n=3$ .

#### 2.4.4.2. Cellular population by fluorescence microscopy

Using this method, we visualized the cellular density of adhered cells on each surface modified, and control films. For pristine PEI films [**Figure 2.15(a)**, first row] the cellular density was low. For AuNP-coated surfaces [**Figure 2.15(a)**, third row], the cellular density was more than that of pristine films but definitely less than that

of the plasma-treated films. For both arginine-, and fibronectin-coated films, the cellular density was rather high, and uniform. However, fibronectin-coated films showed more sticky behaviour for fibroblast cells. Again, measurement of fluorescence intensity from green, and blue channels represented reasonably high cellular density, and their healthiness with both arginine-, and fibronectin- surface modifications [Figure 2.15(b)].

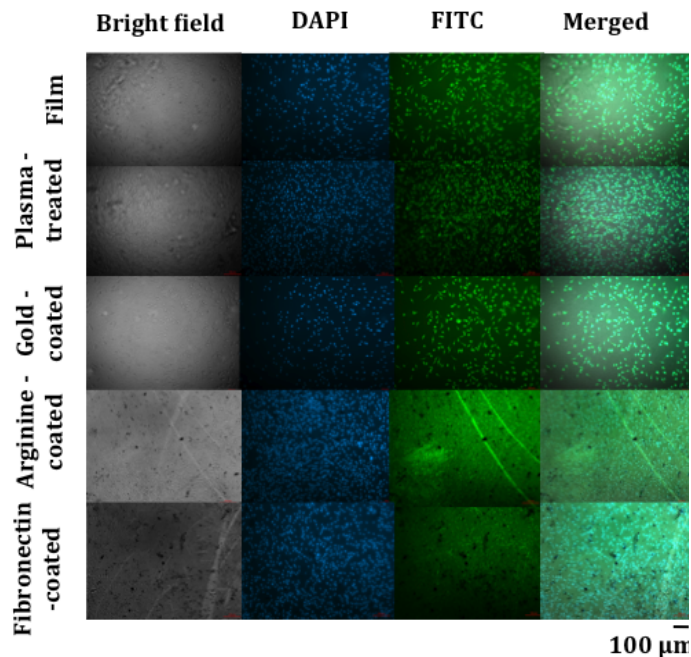


**Figure. 2.15(a):** Visualization of L929 fibroblast cells (using DAPI and CFSE) with the aid of a fluorescence microscope. Scale bar is 100  $\mu\text{m}$ .

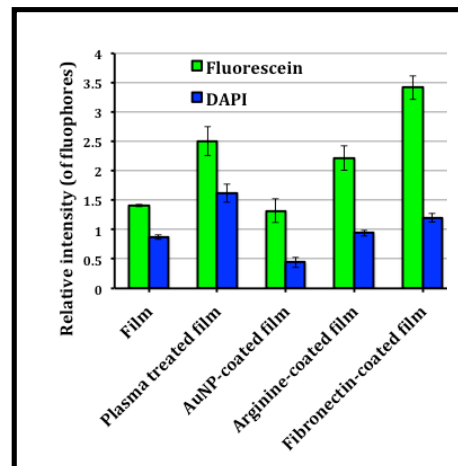


**Figure. 2.15(b):** Quantification of fluorescent tags from cells. CFSE and DAPI from figure 2.13(a). Data represented as a  $\pm$ SD of  $n=7$ .



Thus the results from several experiments clearly prove that arginine-, and fibronectin-coated films behave very similarly when it comes to viable cells accommodation. In the cellular proliferation study (**Figure 2.14**), using cell counting with Trypan blue, arginine-, and fibronectin-coated films showed very comparable cell counts that were significantly superior to control surfaces (pristine PEI surface, AuNP-coated surface). Cell viability (by mitochondrial activity) using resazurin as an indicator also showed that at the end of 2 days, both arginine-, and fibronectin-coated films showed remarkably higher viable cell population in comparison to control samples (**Figure 2.14**).

#### **2.4.5. Cellular morphology by actin cytoskeleton staining**

According to **Figure 2.16**, the arginine-coated films indicated the elongated disposition of actin filaments, which confirmed the healthy, and happy condition of cells. In fibronectin-coated films as well, the cells appeared elongated, and stretched which definitely arises due to the availability of the preferable RGD sequence. A closer look at the cellular adhesion (**Figure 2.16.A**) showed that L929 cells present on arginine-coated films are elongated. At the same time, they are a little folded at sides, which was absent in case of the fibronectin-coated films.

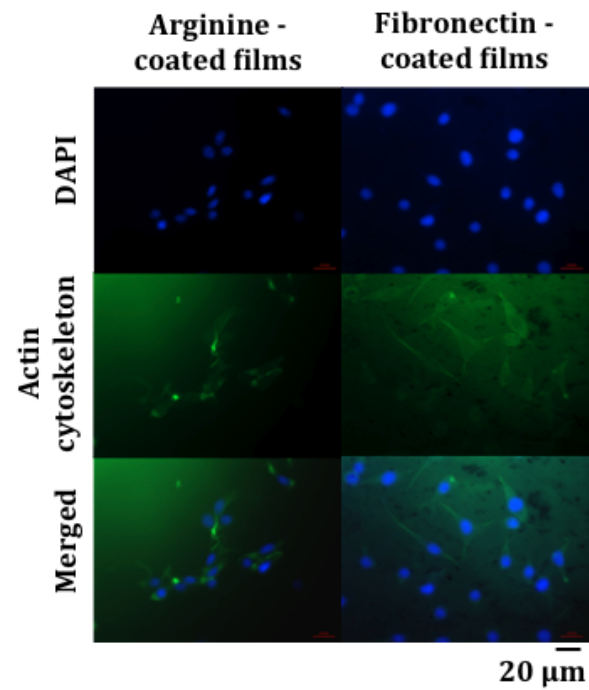


**Figure. 2.16:** Actin filament staining of L929 cells (using Alexafluor Phalloidin 488) and DAPI for nucleus counterstaining. Scale bar 20 μm.

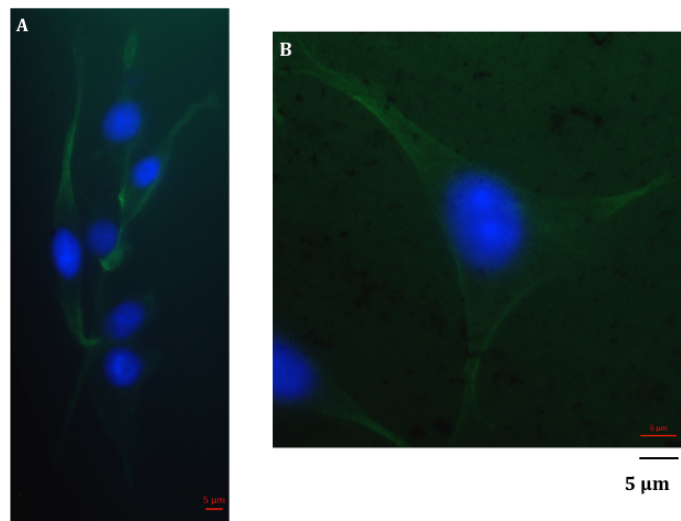


**Figure. 2.16.A:** and **2.16.B:** Actin cytoskeleton staining of arginine-coated (A), and fibronectin-coated (B) films. Scale bar 5 μm.

### 2.4.6. Production of collagen

In this experiment, we measured the amount of collagen expressed both from the cellular layer, and the spent media. The collagen estimation kit works on the principle of oxidation of both proline, and hydroxyproline present in the ECM, which is directly proportional to the amount of collagen produced by the healthy cells. Results indicate that in arginine-coated films the amount of collagen measured by the kit was significantly higher in comparison to plasma treated, and AuNP-coated films (**Figure 2.17.A**). This signifies, more number of collagen production, leading to the presence of healthy, and viable fibroblasts cells on the surface modified films. According to **Figure 2.17.B** collagen present in the spent media, i.e., collagen present in the soluble form is also high with arginine-coated films, which means the fibroblasts present on the arginine-coated films are healthy. But the amount of collagen with fibronectin-coated films are even higher; the RDG sequence present in fibronectin which is capable of recognizing the cell membrane could be responsible for this observation.

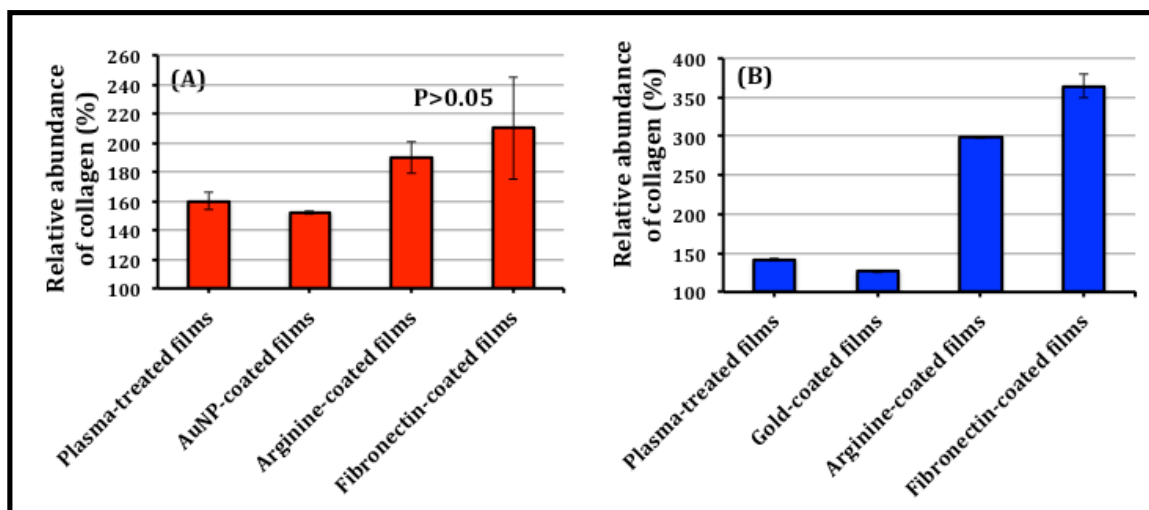


**Figure. 2.17:** Expression of collagen on the surface of differently surface-modified films (A), in corresponding well's spent media (B). Data represented as  $\pm$ SD of  $n=3$ .

The reason behind the considerably excessive density of cells in arginine-coated films in comparison to untreated controls can be supported by the hydrophilicity generated by the arginine coating. But being as good as the fibronectin-coated film is

really unanticipated. We speculate a three-fold reason behind this phenomenon. Arginine-coated films are blessed with two special properties: (i) increased surface roughness (**Figure 2.8**), hence hydrophilicity (contact angle data from **Figure 2.5**), and (ii) surface charge. These are supportive of cellular spreading on the surface-coated films.<sup>23, 24</sup> Several literature reports stress upon the fact that surface polarization, and roughness are crucial for cellular adhesion.<sup>25</sup> Numerous reports compared the cellular entry of positive, and negatively charged nanoparticles and found that the increasingly rough surface also encourages a 'foothold' of a cell-seeded on a material surface.<sup>26, 27</sup> Moreover, very fast spreading of water or media containing cells provides enough space in between cells for healthy development in future and/or cellular migration.<sup>28</sup> This effectively is a 'low seeding density experiment', which in one way should help the proliferation of adhering cells like fibroblast. Instead, fibronectin-coated films have the integrin-binding RGD sequence, which strongly encourages cells to bind to it, but at the same time these films being hydrophobic, do not allow the cells to spread over a larger surface area. As a result, during incubation, only a few cells adhere to fibronectin-coated films because of space constraints. Thus while fibronectin carries the RGD sequence and hence is friendly towards the cells, the arginine-coated films have the material advantages from surface roughness, low contact angle, and positive charge so much, that we believe they behave very similarly to the positive effects of the RGD sequence and ultimately become almost equally effective when it comes to viable cell accommodation. The equivalent efficacy of both the films is also reflected in collagen production (**Figure 2.17**) where both arginine-, and fibronectin-coated films produce a comparable amount of collagen. Also worth mentioning is the fact that at the event of cell-seeding, 2 h incubation, and aspiration of cells on films is considered to be a mimic of a dynamic system like polymeric implant installation in the body, where live cells are supposed to adhere in a flowing system rather than adherence aided by gravity (a general *in vitro* practice).

## 2.5. Conclusion

In this chapter, we described the modification of a surface hydrophobic nature of polyetherimide film to a hydrophilic one by simple procedures involving the layer-by-layer assembly approach. Traditionally expensive sticky proteins separated from animal tissue (fibronectin, vitronectin, laminin, *etc.*) are used for improved effects on cell adherence. Conversely, we demonstrated here that a small molecule like arginine is capable of serving the same purpose in terms of total viable cells. Medical translation of this simple concept could help lower down the costs related to polymeric implant installation and avoid complications arising out of hydrophobic scaffold implantation.

## 2.6. Bibliography

---

<sup>1</sup>Dhandayuthapani, B.; Yoshida, Y.; Maekawa, T.; Sakthi Kumar, D. Polymeric Scaffolds in Tissue Engineering Application: A Review. *International Journal of Polymer Science* **2011**, Article ID 290602, 19 pages, doi:10.1155/2011/290602.

<sup>2</sup>Can, Z. Z; Ercocen, A. R.; Apaydin, I.; Demirseren, E.; Sabuncuoglu, B. Tissue Engineering of high density porous polyethylene implant for three dimensional reconstruction: An experimental study. *J. Plast. Reconstr. Hand Surg.*, **2000**, *34*, 9–14.

<sup>3</sup>James, S. P.; Oldinski, R. (Kurkowski); Zhang, M.; Schwartz, H. *UHMWPE Biomaterials Handbook*. **2009**, 259-276.

<sup>4</sup>Deshpande, S.; Munoli, A. Long-term results of high-density porous polyethylene implants in facial skeletal augmentation: An Indian perspective. *Indian J. Plast. Surg.* **2010**, *43*, 34–39.

<sup>5</sup>Kim, Y. H.; Jang, T. Y. Porous high-density polyethylene in functional rhinoplasty: Excellent long-term aesthetic results and safety. *Plast. Surg. (Oakv)*, **2014**, *22*, 14–17.

<sup>6</sup>Fernandez-Bueno, I.; Di Lauro, S.; Alvarez, I.; Lopez, J. C.; Garcia-Gutierrez, M. T.; Fernandez, I.; Larra, E.; Pastor, J. C. Safety and Biocompatibility of a New High-Density Polyethylene-Based Spherical Integrated Porous Orbital Implant: An Experimental Study in Rabbits. *Journal of Ophthalmology*, **2015**, *2015*, Article ID 904096. 1-7. <http://dx.doi.org/10.1155/2015/904096>.

<sup>7</sup>Khalili, A. A.; Ahmad, M. R. A Review of Cell Adhesion Studies for Biomedical and Biological Applications. *Int. J. Mol. Sci.* **2015**, *16*, 18149-18184.

---

<sup>8</sup>Pignatello (Ed.) R.; Lotfi, M.; Nejb, M.; Naceur, M. Cell Adhesion to Biomaterials: Concept of Biocompatibility, *Advances in Biomaterials Science and Biomedical Applications*. **2013**, Chapter 8 DOI: 10.5772/53542.

<sup>9</sup>Montaño-Machado, V.; Chevallier, P.; Mantovani, D.; Pauthe E. On the potential for fibronectin/phosphorylcholine coatings on PTFE substrates to jointly modulate endothelial cell adhesion and hemocompatibility properties. *Biomatter*. **2015**, *5*, e979679.

<sup>10</sup>Agarwal, R.; González-García, C.; Torstrick, B.; Guldberg, R. E.; Salmerón-Sánchez, M.; García, A. J. Simple coating with fibronectin fragment enhances stainless steel screw osseointegration in healthy and osteoporotic rats. *Biomaterials*. **2015**, *63*, 137-45.

<sup>11</sup>He, L.; Tang, S.; Prabhakaran, M. P.; Liao, S.; Tian, L.; Zhang, Y.; Xue, W.; Ramakrishna, S. Surface modification of PLLA nano-scaffolds with laminin multilayer by LbL assembly for enhancing neurite outgrowth. *Macromol. Biosci*. **2013**, *13*, 1601-1609.

<sup>12</sup>Mehr, N. G.; Hoemann, C. D.; Favis, B. D. Chitosan surface modification of fully interconnected 3D porous poly( $\epsilon$ -caprolactone) by the LbL approach. *Polymer*, **2015**, *64*, 112-121.

<sup>13</sup>Shi, Q.; Qian, Z.; Liu, D.; Liu, H. Surface Modification of Dental Titanium Implant by Layer-by-Layer Electrostatic Self-Assembly. *Front. Physiol.*, **2017**, *8*, Article 574.

<sup>14</sup> <https://forschung-sachsen-anhalt.de/project/biomimetic-surface-modification-tissue-11863>. Accessed January 2019

<sup>15</sup>D'Britto, V.; Tiwari, S.; Purohit, V.; Wadgaonkar, P. P.; Bhoraskar, S. V.; Bhonde, R. R.; Prasad, B. L. V. Composites of plasma treated poly(etherimide) films with gold nanoparticles and lysine through layer by layer assembly: a "friendly-rough" surface for cell adhesion and proliferation for tissue engineering applications. *J. Mater. Chem.*, **2009**, *19*, 544-550.

<sup>16</sup> Sengupta, P.; Surwase, S. S.; Prasad, B. L. V. Modification of porous polyethylene scaffolds for cell attachment and proliferation. *International Journal of Nanomedicine*, **2018**, *13*, (T-NANO 2014 abstracts), 87-90.

<sup>17</sup> Sengupta, P.; Prasad, B. L. V. Surface Modification of Polymeric Scaffolds for Tissue Engineering Applications. *Regenerative Engineering and Translational Medicine*. **2018**, *4*, 75-91.

---

<sup>18</sup>Hong, J.; Prawer, S.; Murphy, A. B. Plasma Catalysis as an Alternative Route for Ammonia Production: Status, Mechanisms, and Prospects for Progress. *ACS Sustainable Chemistry and Engineering*, **2017**, *6*, 15-31.

<sup>19</sup>Jiao, Y.; Xu, J.; Zhou, C. Effect of ammonia plasma treatment on the properties and cytocompatibility of a poly(L-lactic acid) film surface. *J. Biomater. Sci. Polym. Ed.* **2012**, *23*, 763-777.

<sup>20</sup>Kleinhans, C.; Barz, J.; Wurster, S.; Willig, M.; Oehr, C.; Müller, M.; Walles, H.; Hirth, T.; Kluger, P. J. Ammonia plasma treatment of polystyrene surfaces enhances proliferation of primary human mesenchymal stem cells and human endothelial cells. *Biotechnol. J.* **2013**, *8*, 327-337.

<sup>21</sup>Turkevich, J.; Stevenson, P.C.; Hillier, J. A study of the nucleation and growth processes in the synthesis of colloidal gold. *Discussions of the Faraday Society*, **1951**, *11*, 55-75.

<sup>22</sup>Theerakittayakorn, K.; Bunprasert, T. Differentiation Capacity of Mouse L929 Fibroblastic Cell Line Compare With Human Dermal Fibroblast. *World Academy of Science, Engineering and Technology International Journal of Medical and Health Sciences.* **2011**, *5*(2), 51.

<sup>23</sup>Finkea, B.; Luethenb, F.; Schroedera, K.; Muellerb, PD.; Bergemannb, C.; Frantc, M.; Ohla, A.; Nebe, B. J. The effect of positively charged plasma polymerization on initial osteoblastic focal adhesion on titanium surfaces. *Biomaterials*, **2007**, *28*, 4521-4534.

<sup>24</sup>Khang, D.; Kim, S.Y.; Liu-Snyder, P.; Tayhas, R. G.; Stephen, P.; Durbinc, M.; Webster, T. J. Enhanced fibronectin adsorption on carbon nanotube/poly(carbonate) urethane: Independent role of surface nano-roughness and associated surface energy. *Biomaterials*, **2007**, *28*, 4756-4768.

<sup>25</sup>Miller, D.C.; Thapa, A.; Haberstroh, K. M.; Webster, T. J. Endothelial and vascular smooth muscle cell function on poly(lactic-co-glycolic acid) with nano-structured surface features. *Biomaterials*, **2004**, *25*, 53-61.

<sup>26</sup>Kim, D -H.; Paolo P.; Provenzano, Chris L.; Smith, A. L. Matrix nanotopography as a regulator of cell function. *Journal of Cell Biology*, **2012**, *197*, 351-360.

<sup>27</sup>Ranella, A.; Barberoglou, M.; Bakogianni, S.; Fotakis, C.; Stratakis, E. Tuning cell adhesion by controlling the roughness and wettability of 3D micro/nano silicon structures. *Acta Biomaterialia*, **2010**, *6*, 2711-2720.

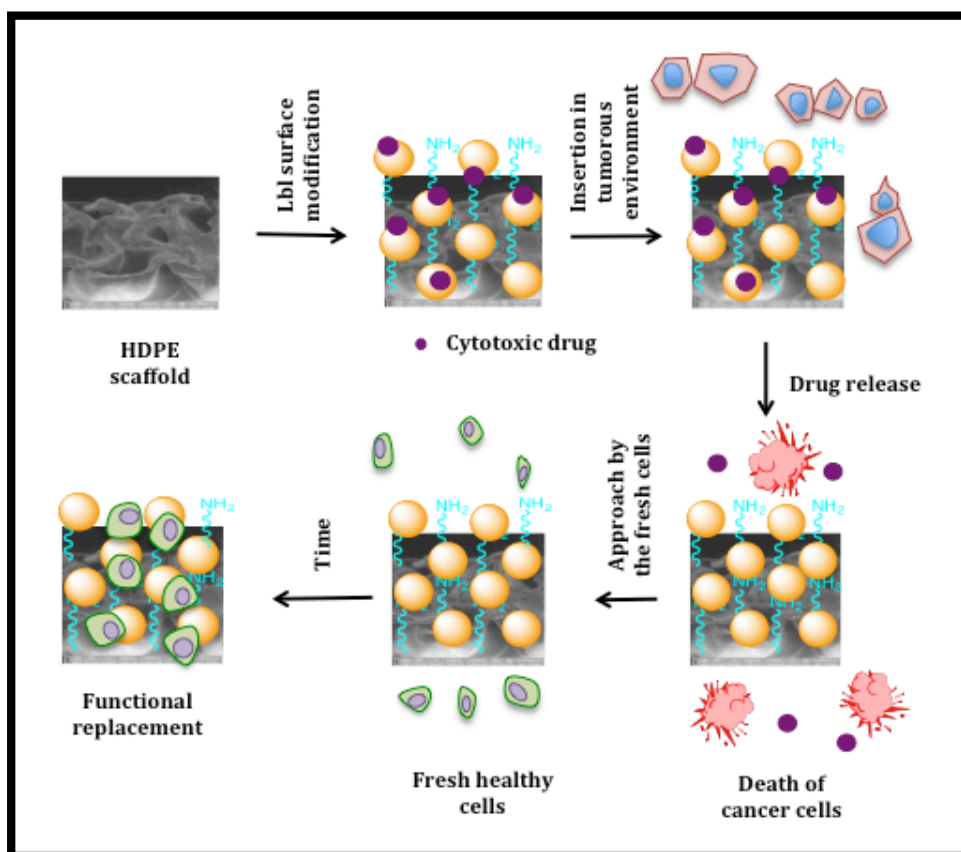
---

<sup>28</sup>Selhuber-Unkel, C.; Erdmann, T.; Lopez-Garcia, M.; Kessler, H.; Schwarz, U. S.; Spatz, J. P. Cell adhesion strength is controlled by intermolecular spacing of adhesion receptors. *Biophysical Journal*, **2010**, *98*, 543–551.



# Chapter 3

## Design and Fabrication of a Dual Purpose Scaffold by a Logical Combination of Drug-release and Tissue engineering



Part of the written chapter is under review in Chemistry Select journal:

*Development of a smart scaffold for sequential cancer chemotherapy and tissue engineering.* Poulomi Sengupta, Vinay Agrawal, Bhagavatula L. V. Prasad

### **Abstract**

Management of tumour (solid) has always been a challenge due to the multi-step treatment involved including surgery followed by systemic administration of chemotherapeutic drugs. In this chapter, using the P-LbL technique, we have designed, and fabricated a dual functional drug containing porous polymeric scaffolds. Herein, an HDPE scaffold has been the first surface modified using the established P-LbL technique, which was then chemically conjugated to cytotoxic drug cisplatin. These scaffolds were designed in such a way that they are capable of releasing cisplatin continuously in a slow and sustained manner over a minimum two days. Most importantly, subsequent to the drug-release, the scaffolds become hydrophilic, which can act as a cell-friendly surface thus allowing the non-cancerous cells to adhere, and proliferate leading to a potential material for effective drug carrier and volume filling applications. In this way, the scaffolds can serve a dual purpose (drug-delivery, and volume-filler), and can bypass the possibility of multiple surgical interventions needed for tumour surgery, and cosmetic corrections.

### 3.1. Introduction

P-LbL has established itself as a trustworthy, and reproducible procedure for the surface modification of hydrophobic scaffolds to make them friendly for cell adherence, and proliferation. In the previous chapter, we have shown its applicability for fast volume filling application. This convinced us of the fact that P-LbL strategy is dependable, and can be exploited for solving more complex problems. Our current chapter involves the use of P-LbL technique to develop a dual-purpose scaffold that could be used for the treatment of solid tumours that require multistep treatment. Treatment of cancer involving solid tumours (especially oral cavity cancer) entails three major steps: <sup>1</sup> 1) removal of the tumour by surgery, 2) chemotherapy/radiotherapy or combination and 3) reconstructive surgery. Here, the surgical intervention (removal of the tumour), the first line of therapy,<sup>2</sup> is generally followed by a planned exposure to chemotherapy, radiation therapy, targeted chemotherapy (for the treatment of the leftover cancerous tissue/cells) or combination of the above over a certain period of time. Finally a corrective surgery (also known as the 'limb salvage surgery') may be carried out to offset the deformities caused by the first surgery.<sup>3</sup> Depending upon the size, and stage of the tumour, this (corrective surgery) may be performed immediately after the removal of the tumour or after the chemotherapy regime is completed.<sup>4</sup>

Amongst the three steps listed above, while the surgical intervention has been established, the other two are fraught with few issues that need to be tackled. For example, depending on the severity of the cancerous growth, the chemotherapy/radiation therapy routine is implemented at predetermined time intervals for a given period of time. In this regime, highly toxic chemotherapeutic drugs (dosage, frequency, intervals are pre-decided by a group of oncologists) are systemically administered to the patients. In addition to the inconveniences caused because of repetitive hospital visits, the systemic administration of the highly toxic drugs leads to many side effects (rapid deterioration of health, weight, hair loss, vomiting, frequent hospitalization) due to the non-selective absorption of drugs into healthy tissues. This is the first, and major problem that needs to be addressed. Subsequent to this, the patient may need/want to undergo the corrective surgery as

mentioned above. This (corrective) surgery is generally performed using polymeric scaffolds, which act as an extracellular matrix that interacts with the cells leading to the formation of new tissues. For implant materials, polymer scaffolds are the best choice as they possess the proper architecture, mechanical properties in addition to supporting cell adhesion, proliferation, and differentiation. As discussed in Chapter 1, high-density polyethylene (HDPE) are the most preferred ones due to many advantages.<sup>5, 6</sup> Unfortunately, because of inherent hydrophobicity HDPE type polymers have a slower rate of integration<sup>7,8,9,10</sup> which may lead to dislocation followed by repetitive surgery. This is the second problem that needs to be dealt with by carrying out appropriate surface modifications on the HDPE scaffolds.

One way of addressing the above mentioned two problems is to design, and fabricate drug loaded scaffolds using HDPE like polymers that can provide 'local chemotherapy'<sup>11</sup> for a given period of time and subsequently become cell friendly to turn into the usual tissue engineering scaffolds. The drug-loaded scaffolds can be inserted at the region of surgery and the slow and sustained local release of cytotoxic drugs from the implanted scaffolds over a long period of time would be able to replace the repetitive chemotherapeutic treatment program. Most importantly, unlike systemic administration, in local chemotherapy, the drugs are exposed to a restricted area (tumourous region only). Furthermore, once the drug gets released the scaffolds present a proper surface architecture (hydrophilicity, surface chemistry) that will support cell adhesion, and proliferation.

In this chapter, we describe a modification of HDPE scaffolds by the P-LbL technique and further their decoration with the chemotherapeutic drug cisplatin. Cisplatin is an affordable chemotherapy medication that is widely used in treating most solid tumours including head and neck cancer.<sup>12</sup> At the same time, cisplatin is very toxic to healthy tissue, which invariably leads to terrible side effects.<sup>13,14</sup> To overcome these disadvantages, we have chemically conjugated aquated cisplatin to the HDPE surface *via* the acid-base chemistry involving carboxylic acid groups present on citric acids caps of AuNPs. We hypothesized that under *in vivo* condition, at tumourous pH, hydrated cisplatin molecules get released (from the scaffold) in a slow and sustained manner only at the tumourous region. After the drug release, the surface of the

biocompatible, non-biodegradable HDPE scaffold retains the hydrophilic character due to the presence of citrate-capped AuNPs promoting the adhesion and proliferation of non-cancerous cells, leading to a healthy tissue formation. Our results clearly indicate that cisplatin was highly effective when tested against human mouth carcinoma cell line KB under *in vitro* conditions. To validate that post drug release the same scaffold can promote the adherence and proliferation of non-cancerous cells, they were exposed to murine fibroblast cells (L929). Healthy growth of cells over a long period of time was observed proving the efficacy of the dual-purpose scaffold. We thus propose that a surface modified, drug attached HDPE scaffold can serve both the purposes; as a drug delivery system, and as attachment support for tissue regeneration (as a part of the post-surgical care of the limb salvage procedure). If translated, this strategy can bring down the level of trauma, and tension associated due to a series of surgeries performed on the solid tumour bearing patients.

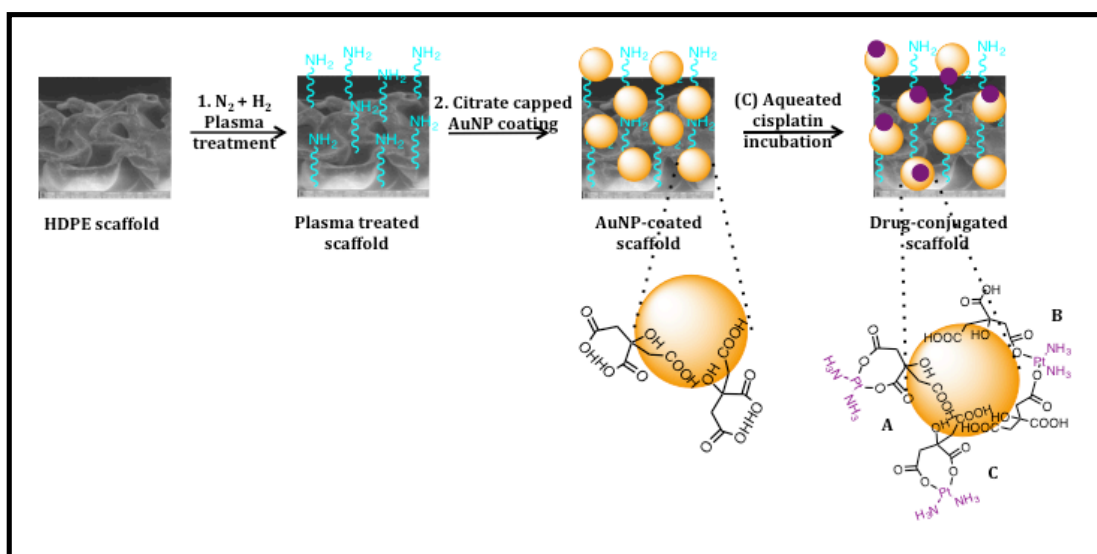
### 3.2. Materials

Dr. Vinay Agrawal from Clear Vision, Mumbai, kindly donated the HDPE scaffolds. Cisplatin, silver nitrate, *o*-phenylenediamine, propidium iodide (PI), acridine orange (AO), carboxyfluoresceinsuccinimidyl ester (CFSE), 4', 6-diamidino-2-phenylindole (DAPI), resazurin, phosphate-buffered saline (PBS) powder, HEPES powder were purchased from Sigma Aldrich. Annexin-V FITC conjugate was purchased from Life Technologies. RNase was from Thermo Fischer Scientific. Human oral carcinoma originated KB cell line, and murine fibroblast L929 cell line were procured from the animal cell repository maintained by NCCS, Pune, India. DMEM (low pyruvate) media, and FBS (fetal bovine serum) were purchased from Invitrogen.

### 3.3. Experimental section

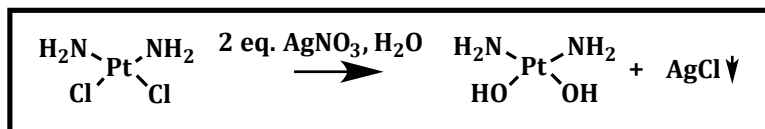
#### 3.3.1. Preparation of scaffolds

Porous HDPE scaffolds (with 1 mm height) were cut into 4 mm diameter circular discs. Those were plasma treated using  $N_2 + H_2$  plasma at 80 watts power for 20 minutes using Emitech Plasma Asher K1050X (**Scheme 3.1** step1). The scaffolds were immediately dipped, and stirred in citrate stabilized gold sol (AuNP) prepared following the Turkevich method [**Scheme 3.1** 2 to 3].<sup>15</sup> After overnight stirring on a magnetic stirrer, AuNP deposited on HDPE scaffolds.

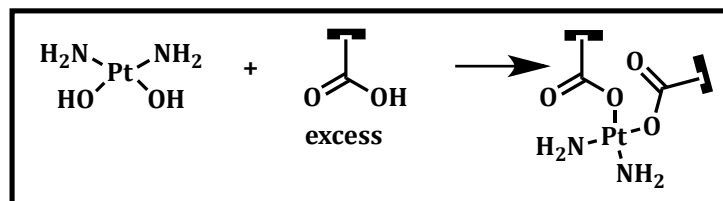


**Scheme 3.1:** Schematic representation of surface modification for HDPE scaffolds. 1. Plasma treatment polyethylene scaffolds using 3: 2 hydrogen, and nitrogen mixture. 2. Stirring of freshly plasma treated scaffolds with citrate stabilized gold nanoparticles (AuNPs). 3. Chemical conjugation between the scaffolds and aqueated cisplatin.

Cisplatin powder (10 mg, 0.033 mmoles) was taken in 10 mL Milli-q water (**Scheme 3.2**). 11.22 mg (2 equivalents, 0.066 mmole) of silver nitrate was added to the suspension, which immediately formed a white precipitate (of AgCl). It was allowed to stir overnight. The reaction mixture was mini-centrifuged for 10 minutes (at 12,500 rpm speed) and the supernatant was collected. It was filtered using a 0.22  $\mu\text{m}$  syringe filter, which restricted the leftover AgCl to come into the filtrate. The concentration of cisplatin was assumed to be 1 mg/mL.



**Scheme. 3.2:** Substitution of chloride with hydroxyl groups (in cisplatin) through precipitation of AgCl



**Scheme. 3.3:** Chemical conjugation of hydrated cisplatin to the HDPE scaffold via an ester bond formation

The water solution of aquated cisplatin was stirred with AuNP-coated HDPE scaffolds at room temperature (**Scheme 3.1** step 3). After 12 h of continuous agitation, the scaffolds were separated, washed with water and dried in air and vacuum. Scaffolds thus got ready for characterization followed by planned experiments.

### 3.3.1.1. Determination of cisplatin present on each scaffold

The cisplatin present on each scaffold was measured by the standard reaction with *o*-phenylenediamine<sup>16</sup> using a calibration curve. The procedure is written below. In this method, 1.2 mg *o*-phenylenediamine was weighed and taken into a 1.5 mL Eppendorf tube. To it 1.0 mL DMF, and a known amount of (say 2.0 mg) cisplatin were added. It was sealed with Teflon tape and heated at 100 °C for a total 2 h. The colour changed to a shade of blue. The amount of cisplatin was varied (say 1.0, 0.5, 0.25, 0.125 mg) in same amount of ligand (1.2 mg *o*-phenylenediamine), and solvent (1 mL DMF). The resultant colours were blue of different intensity depending on the concentration of cisplatin. In UV-Vis spectrophotometry, the solution showed a peak at 706 nm. With decrease or increase with the amount of cisplatin, the absorbance changed in a linear fashion. When the concentration versus absorbance (at 706 nm) was plotted it produced a straight line. This is the calibration curve (**Figure 3.1**), which will be used for the determination of unknown cisplatin concentration.

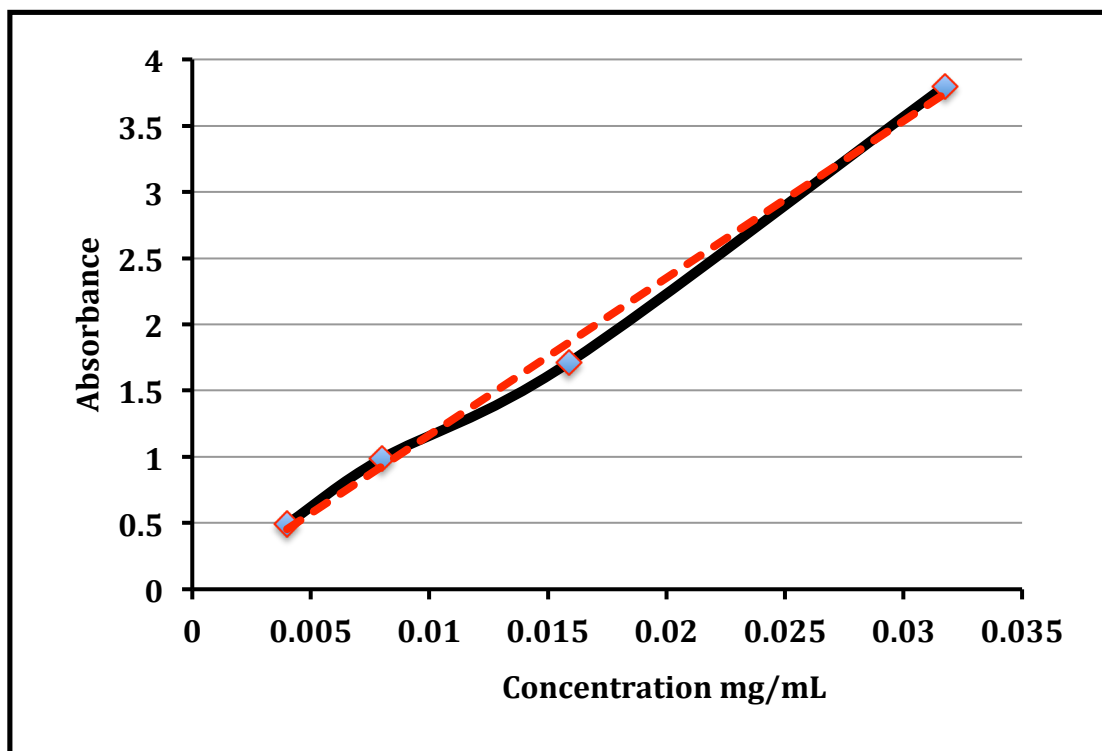


**Figure. 3.1:** Determination of cisplatin concentration by colourimetric assay: Plot of the absorbance of cisplatin *o*-phenylenediamine complex (Y-axis) with the amount of cisplatin (X-axis)

For knowing the amount of cisplatin present on a scaffold, or for release kinetics data points the same method as above was applied. A cisplatin-conjugated scaffold was dipped in 1.2 mg/mL of *o*-phenylenediamine in 1.0 mL DMF. It was sealed, and heated at 100 °C for 2 h. The absorbance was determined using the UV-Vis spectrophotometry. The concentration (hence the amount) of cisplatin present was back-calculated using the calibration curve drawn above (**Figure 3.1**). Similarly, the amount of cisplatin present in each fraction of the release kinetics experiment was also calculated using the same protocol.



### 3.3.2. Characterization

#### 3.3.2.1. UV-Vis spectrophotometry

Solid state UV-Visible data was collected using Shimadzu UV/Vis/IR/3600 spectrophotometer in the reflectance mode. Barium sulfate standard was used for the background corrections. The polymer samples were frozen, and powdered using a ball-miller (Retch Cryomill) before acquiring the data.

#### 3.3.2.2. Surface microstructure by SEM

SEM imaging was performed using FESEM NNS450. For the pristine scaffold, a gold sputtering was performed before exposure to the electron beam. Other samples (which are already gold-coated) were used as it is.

#### 3.3.2.3. Presence of platinum by XPS

The cisplatin-conjugated scaffolds were analyzed for the presence of platinum using the X-Ray, and UltraViolet Photoelectron Spectroscopy (XPS, and UPS). The instrument is Thermo Scientific-K-alpha +. The oxidation states of platinum atoms present on the scaffold surface were determined by de-convolution of the peaks.

#### 3.3.2.4. Release kinetics experiment

In the release experiment, 3 porous HDPE scaffolds (each 4 mm diameter and 1 mm thickness, N<sub>2</sub> + H<sub>2</sub> plasma treated, coated with AuNPs, and conjugated with cisplatin) were incubated in 10 mL of neutral PBS, as well as in the spent media (acidic) collected from the overgrown KB (human mouth carcinoma) cells. 37 °C temperature (human body temperature) was maintained by using a water bath, and the entire experiment was performed in triplicates. At definite time points 100 µL PBS or media (from the incubation mixture) was drawn out, and evaporated to dryness using a speed vac concentrator/evaporator. After the sample withdrawal, 100 µL of PBS or media was also added to the original incubation chamber to avoid error due to a reduction in volume. Amount of cisplatin was colourimetrically determined by reacting with *o*-phenylenediamine as per the protocol (described in section 3.3.1.1) utilizing the already established calibration curve (**Figure 3.1**). The total amount of

drug released at each time point was calculated by multiplying the amount of cisplatin ( $\mu\text{g}$ ) with proper dilution factor. The per cent release was calculated by normalizing with the average loading of cisplatin on each scaffold. Each experiment was carried out in triplicates, and the standard error was incorporated while plotting.

$$\% \text{ release} = \frac{\mu\text{g of Pt present at each time point} \times 100}{\text{Average loading of Pt (in } \mu\text{g) on one scaffold} \times 3}$$

### 3.3.3. Efficacy of drug conjugated scaffolds on KB cells

#### 3.3.3.1. Cell viability (KB cells)

Human mouth cancer cell-line KB was maintained in 10% FBS/MEM complete media. In each well of a treated 12 well tissue culture plate 50,000 healthy KB cells were seeded in 500  $\mu\text{L}$  complete MEM media. It was allowed to incubate for 24 h in 5%  $\text{CO}_2$  atmosphere at 37  $^\circ\text{C}$ . 3 wells were kept as control. Untreated HDPE scaffolds, AuNP-coated scaffolds, cisplatin-coated scaffold and the equivalent amount of aquated cisplatin were added in each well in triplicates. At 48 h the cells were incubated (6 h, 5%  $\text{CO}_2$  atmosphere, 37  $^\circ\text{C}$ ) with 100  $\mu\text{M}$  resazurin in complete MEM medium. The emission at 590 nm was obtained by exciting the resofurin containing media at 560 nm. While plotting, the emission from all the wells was normalized with the average emission of control cells (no treatment) and converted into a per cent. The per cent cell viability was plotted (**Figure 3.6**). The result from each experiment was plotted as a mean including  $\pm$  SE for  $n=3$ .

$$\% \text{ Cell viability} = \frac{\text{Average emission from the cells exposed to drug-loaded scaffolds} \times 100}{\text{Average emission from the control cells}}$$

#### 3.3.3.2. Estimation of cellular density by imaging

Cellular density was measured using fluorescently labelled cells. In this experiment, sterilized coverslips were aseptically placed in sterile 24 well plates. In each well 50,000 KB cells were seeded. It was incubated overnight. Next day drug containing scaffolds, and citrate gold containing scaffolds (as controls) were added (one in each well). Three wells were kept as control (without any scaffold). After overnight

incubation, scaffolds were aseptically picked up using sterilized forceps. Coverslips (along with cells) were washed with sterile PBS, fixed with 4% PFA, followed by incubation in 5% BSA, and 0.1% Triton X-100 in PBS (0.5 mL each well) for 1h, washed with PBS. Cells on coverslips were incubated in 300 nM DAPI for 4 minutes in the dark followed by washing twice with PBS. Cells were again exposed to 5  $\mu$ M CFSE in PBS followed by incubation at room temperature in the dark for 15 minutes. Coverslips (containing cells) were washed with PBS, wicked off on tissue paper, and mounted on glass slides with mounting media, and sealed. Cells were observed using the Axio Observer Z1 Carl Zeiss microscopes through green, and cyan filters. Compiled data is reported as **Figure 3.7(a)**, zoomed in **Figure 3.7(b)**. Emission of fluorescein, and DAPI from the cells were quantified, normalized with respect to area, and plotted [**Figure 3.7(c)**].

#### *3.3.3.3. Live-dead imaging assay*

In this assay, 50,000 healthy KB cells were seeded on the sterilized coverslips placed in each well of a 24 well plate. After overnight incubation, UV-sterilized citrate-capped AuNP-coated scaffolds, and cisplatin-AuNP-HDPE scaffolds (3 of each type) were placed (1 scaffold in each well). It was allowed to incubate overnight under cell culture condition. Cells were washed with sterile PBS, incubated in 0.1% TritonX-100, and 5% BSA in PBS for 5, 5 minutes in the dark. 10  $\mu$ L 7.5 mM propidium iodide, 1  $\mu$ L 0.67 mM acridine orange in 1.0 mL complete MEM media (for each well) was added and the cells were incubated under cell culture conditions for 1 h. The coverslips were washed with PBS, placed on clean slides upside-down, and visualized under Axio Observer Z1 Carl Zeiss microscope using green, and red channels. Images are compiled in **Figure 3.9(a)**. Fluorescence emission was quantified using ZEN 2012 software, quantified and reported in **Figure 3.8(b)**.

#### *3.3.3.4. Flow cytometry analysis*

In this assay,  $10^6$  human oral carcinoma KB cells were seeded in each well of a 6 well plate with 3 mL complete media. After overnight incubation drug(cisplatin)-loaded scaffolds, and simple untreated scaffolds were added one in each well. Control wells

were left blank. Again after overnight incubation, cells were washed with sterile PBS, trypsinized with 1 mL trypsin EDTA mixture (for each well). Content from each well was diluted using 2 mL of PBS. Cells were collected in labelled falcon tubes (15 mL). Tubes were centrifuged at 1500 rpm for 3 minutes, aspirated. 2.0 mL of PBS was added into each tube, the cell pellet was loosened (for washing), and centrifuged, PBS was aspirated. To 6 tubes (one set of 3 tubes with control scaffold, another set of 3 tubes with cisplatin-containing scaffold) a cocktail of 5  $\mu$ L of Annexin V FITC, and 95  $\mu$ L Annexin-binding buffer was added. Another set of three tubes (control cells, without any scaffold) was kept as it is. The tubes were allowed to incubate in ice for 15 minutes in the dark. After the incubation 2.0 mL Annexin-binding buffer was added to each tube, centrifuged, and aspirated. To each of these 6 tubes, 50  $\mu$ L PI reagent was added, and incubated for 10 minutes in the dark. They were dispersed, and filtered using a sterile strainer. Cells were directly analyzed for apoptosis using Accuri C6 flow cytometry instrument. Data was compiled using the Accuri C6 software and reported in **Figure 3.9(a)** Quantitative plotting is incorporated in **Figure 3.9(b)**.

Annexin binding buffer preparation: Annexin binding buffer was prepared by mixing the following ingredients: 50 mL dd-water, 0.4 gm NaCl, 14 mg CaCl<sub>2</sub>, 0.12 gm HEPES.

PI reagent preparation: PI reagent was prepared by mixing the following aliquots: 260  $\mu$ L 1 mg/mL PI stock, 600  $\mu$ L RNase (6  $\mu$ L RNase from the stock), and 3 mL Annexin binding buffer.

#### *3.3.3.5. Expression of phosphatidylserine by Annexin V imaging*

In this experiment, 50,000 healthy KB cells were seeded on coverslips placed inside each well of a 24 well plate. Drug-loaded scaffolds were placed inside wells. They were incubated for one, and two days. At each time point, cells were washed with PBS, incubated in 5% BSA, and 0.1% Triton X-100 in PBS (0.5 mL each well) for 1 h. 5  $\mu$ L Annexin V FITC mixed with 195  $\mu$ L Annexin-binding buffer and added in the wells. After incubating the plate for 15 minutes in the dark at 0 °C, the cells were washed. Coverslips were placed upside down on clean glass slides. Live cells were observed using Axio Observer Z1 Carl Zeiss microscopes green filter (**Figure 3.10**).

### 3.3.4. Regrowth experiment

#### 3.3.4.1. Effect of fibroblasts on drug-released scaffolds

After the release experiment (48 h time point) scaffolds were taken out, washed multiple times with PBS and sterilized using UV light inside a biosafety cabinet. Each of the scaffolds was placed in each well of a sterile 96 well plate. L929 (murine fibroblast) cells were maintained using 10% FBS/DMEM media. To each well, 5,000 number of L929 cells were added. As a control, the same number of cells was seeded on each well of an adherent 96 well plate. On each alternating day, media was changed. The experiment was followed by the resazurin assay performed on each alternative day on the cells with scaffolds, and control wells. The data from the scaffolds were normalized with the control adhering wells data on the corresponding days, converted into a percent, and plotted (**Figure 3.11**).

#### 3.3.4.2. Imaging of re-grown cells

Another experiment exactly like the regrowth experiment was performed with the same number of L929 cells. The growth on scaffolds was monitored by microscopy using CFSE, and DAPI as stains. The experimental procedure was similar like the regrowth experiment; only instead of the cell viability assay, at each time point, one scaffold was picked up using sterilized tweezers, fixed, permeabilized (using 5% BSA, and 0.1% Triton X-100 in PBS), and stained with DAPI, and CFSE. Scaffolds were imaged using Axio Observer Z1 Carl Zeiss microscopes green, and blue filter. Fluorescence from cells was quantified, normalized (with respect to the area), and plotted using Z1 Carl Zeiss 2012 software (blue) (**Figure 3.12**).

## 3.4. Result and discussion

### 3.4.1. Preparation and characterization of surface modified films

According to the surface modification procedure (**Scheme 3.1**, step 1) the scaffolds were first exposed to the  $N_2 + H_2$  plasma. Immediately after the plasma treatment (**Scheme 3.1**, step 2) the scaffolds were immersed in a sol containing citrate-capped AuNPs, which lead to the anchoring of AuNPs onto the scaffolds. Meanwhile, cisplatin was aquated with the help of silver chloride (**Scheme 3.2**). After the scaffolds were coated with AuNPs (**Scheme 3.1**, step 3), the hydrated cisplatin units were chemically

conjugated with the carboxylic acid units (arising from citric acid capping) present on the scaffold's surface using the facile acid-base coupling chemistry (**Scheme 3.1**, **Scheme 3.3**). The surface change due to the above treatments was first probed by UV-Visible spectrophotometry (**Figure 3.2**). In both the samples (AuNP-coated, and drug-loaded), typical Localized Surface Plasmon Resonance (LSPR) peak for AuNP was observed, which suggests the anchoring of AuNPs on the HDPE surface, and the retention of these AuNPs without falling off due to the chemical treatment it was subjected to during cisplatin conjugation.

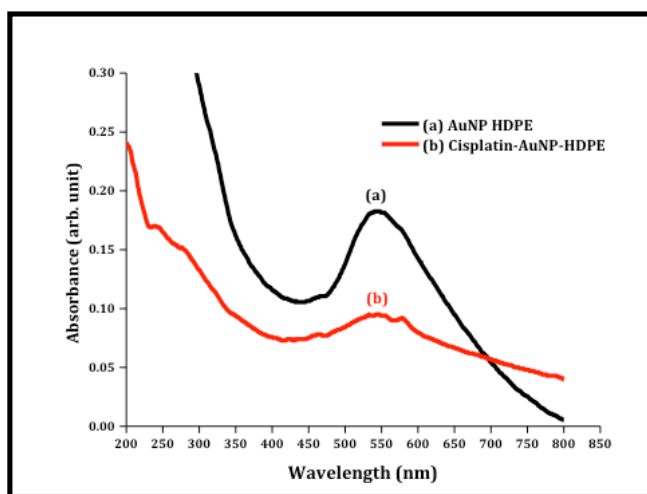


**Figure 3.2:** UV-Vis profile of AuNP-coated HDPE, and cisplatin coated HDPE.

In the case of AuNP coated HDPE [**Figure 3.2**, curve (a), black line], it is seen that the LSPR peak of AuNP appears around 543 nm.<sup>17</sup> This shift (typically AuNP's display LSPR peak at 520 nm) is ascribed to the aggregation of particles after deposition on the solid HDPE surface. After incubation with 1.0 mg/mL aquated cisplatin solution, the LSPR peak was again seen at 544 nm. Apart from that, a small hump at 580 nm was also observed [**Figure 3.2**, curve (b), red line] which we attribute to the interaction of AuNPs with the platinum atoms conjugated through citric acid linker [as shown in **Scheme 3.1**, (D1)]. The FWHM of the peak [curve (a), **Figure 3.2**] before drug loading was 48.5 nm, while the same for the drug-loaded scaffold turned out to be 63.8 nm. This broadening of gold SPR is another indication of a significant change in the environment surroundings of the AuNPs on the scaffold.<sup>22</sup> Thus, UV-Visible

experiments clearly prove the presence of AuNPs on scaffolds, and gave us a hint about the presence of cisplatin along with AuNPs on the scaffold surface. To confirm the presence of platinum on the HDPE surface the scaffolds after cisplatin conjugation were analyzed by XPS spectroscopy (**Figure 3.3**).

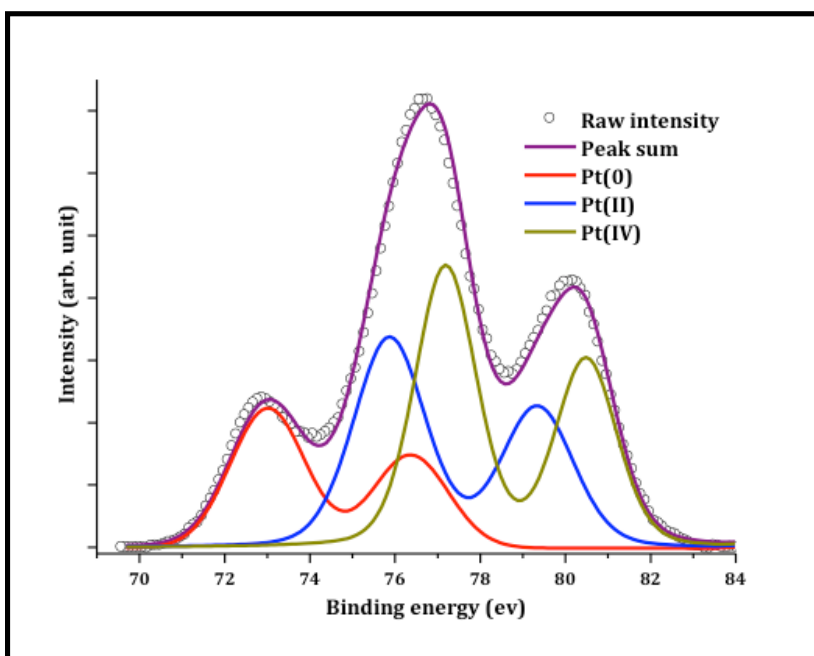


**Figure. 3.3:** Characterization of cisplatin-coated HDPE scaffolds by XPS.

The peaks in the XPS spectra in the 60-140 eV region could be fitted to three sets of curves. Amongst these, the first set of peaks at 65 and 98 eV are attributed to Pt(IV) species, while the ones at 76, and 110 eV, and 111 and 139 eV could be ascribed to Pt(II), and Pt(0) species respectively. Thus the XPS data indicated that platinum is predominantly present as Pt(IV), and Pt(II) species with a minor component corresponding to Pt(0). In aquated cisplatin, platinum exists as Pt(II). Pt(II) can attach to the citric acid present on the AuNP surface either by forming two covalent bonds intra or intermolecular, (**Scheme 3.1 A**, and **B** respectively), or one coordinate, and one covalent bond (**Scheme 3.1 C**). In all of those cases, Pt(II) is retained on the surface. Amongst these different Pt species, the amount of Pt(II), and Pt(IV) were found to be significant as determined by the area under the curves [ $23.8 \times 10^5$ , and  $23.2 \times 10^5$  square units for Pt(IV), and Pt(II) respectively]. The presence of Pt(IV) on

the scaffold may come from the disproportionation reaction of Pt(II) to Pt(0), and Pt(IV). Fortunately, Pt(IV) is also a pro-drug<sup>18, 19</sup> which *in vivo* gets converted to Pt(II) before it acts on nuclear DNA. Pt(IV) also is being widely researched for its ability to work in spite of acquired cisplatin resistance of cancer patients.<sup>20</sup> So having Pt(IV) will be an advantage, as both Pt(II), and Pt(IV) can act at different time points on cancerous cells having different growth phases, and lead to apoptosis. Finally to determine the amount of total Pt present on HDPE surface we carried out the *o*-phenylenediamine assay (please see section 3.3.1.1 for details) which revealed the loading of active platinum (by absorbance at 706 nm) on each scaffold to be 0.0771 mg. Cisplatin being very potent drug has very low IC<sub>50</sub> value for almost all cell lines (other than cisplatin resistant ones). For the cell line under study (human oral carcinoma cell line KB), the IC<sub>50</sub> value is 0.11 μM,<sup>21</sup> which indicates in chemotherapy as tiny as 1/700<sup>th</sup> of a scaffold can supply the required IC<sub>50</sub> dose. Of course, the chemotherapy planned by the oncologists depend on the affected area and stage of cancer, but with such high loading of drug, the scaffolds synthesized can meet any demand and have a good chance of being translated.

One of the concerns with the surface modification process is the possibility of loss of the porous interconnected structure of the scaffolds. To show the retention of the scaffold's morphology despite the scaffold's exposure to various chemicals, we analyzed them by SEM after each treatment. The SEM image in **Figure 3.4.A** at 4 μm resolution indicates 70-100 μm size interconnected pores present in the HDPE scaffolds. After N<sub>2</sub> + H<sub>2</sub> plasma treatment, and citrate gold coating, there was practically no change in the scaffold structure (**Figure 3.4.B**), which proves there is not much deformation associated with the surface modification technique. From **Figure 3.4.C** it is evident that cisplatin-coated HDPE scaffolds surface morphology is also not much different from the AuNP-coated ones. EDAX of cisplatin-coated HDPE scaffolds sample proved the presence of the cytotoxic drug cisplatin in 1.09 weight per cent (**Figure 3.4.D**).



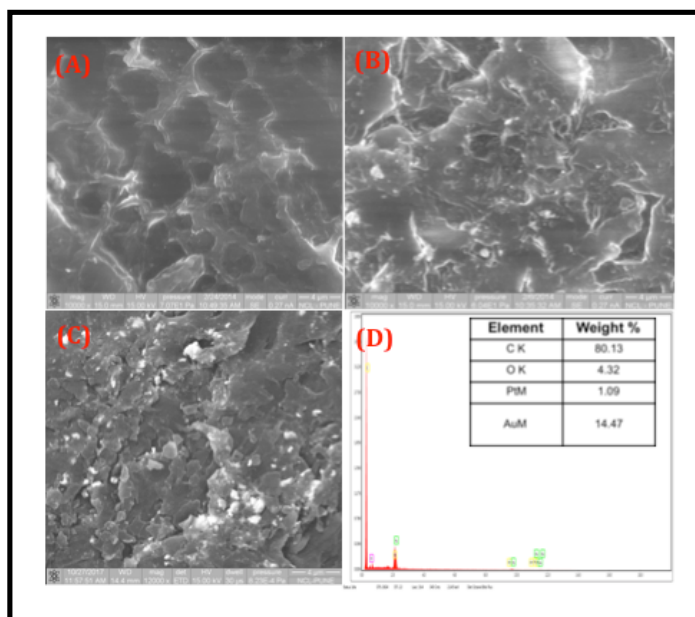


**Figure. 3.4:** Characterization using SEM: (A) HDPE scaffold, (B) AuNP-coated HDPE scaffold, (C) Cisplatin-conjugated HDPE scaffold, and (D) EDX of cisplatin-conjugated HDPE scaffold.

### 3.4.2. Cell viability and apoptotic assay

After establishing that the cisplatin is clearly anchored onto the AuNP decorated HDPE scaffolds and that there was no significant structural alteration in the scaffolds, we focused our attention on the release kinetics of the drug. For this, an *in vitro* release experiment was performed involving PBS (pH 7.4), and spent media (from overgrown KB cells) where % drug released was plotted against time. In this release kinetics experiment (see section 3.3.2.4. for details of the procedure used) amount of cisplatin released was calculated by reacting with *o*-phenylenediamine, and amount of cisplatin was calculated using the calibration curve (**Figure 3.1**). From the release kinetics experiment (**Figure 3.5**) it is observed that in the spent medium (acidic, pH 5.5), comparatively higher amount of cisplatin gets released with respect to that released in neutral PBS buffer. This may arise due to the faster hydrolysis of the ester-like group present in between Pt(II), and citric acid at these lower pH values.<sup>22</sup>

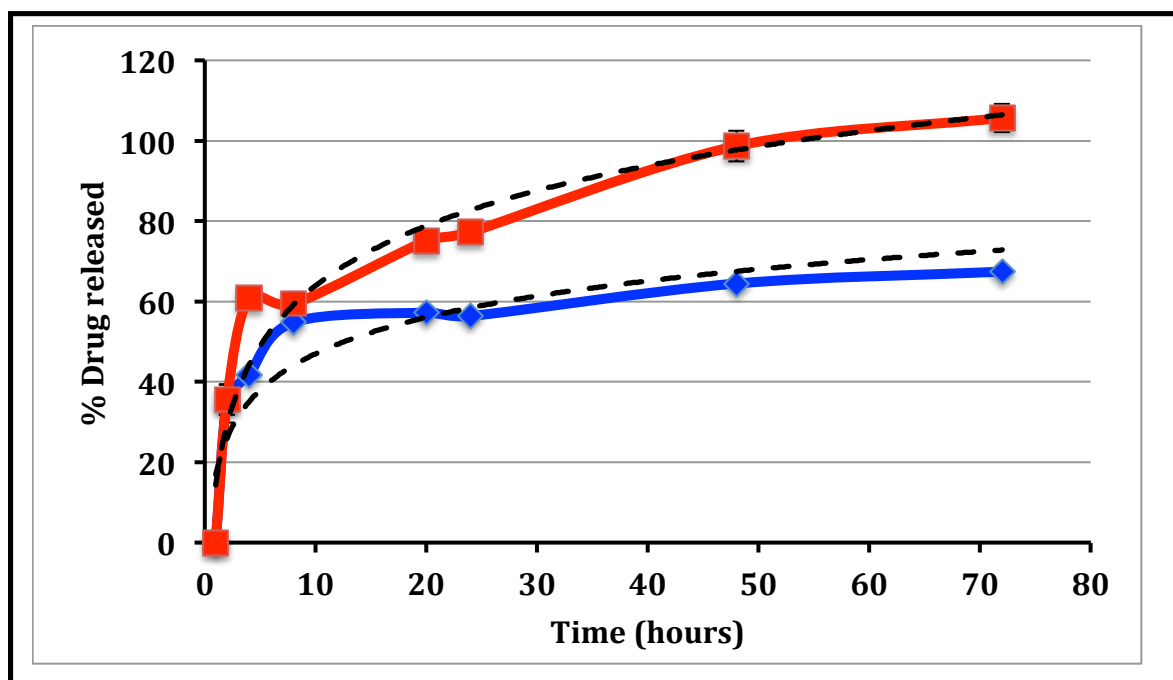


**Figure. 3.5:** Release profile of cisplatin in different environments. Optimal time for complete drug release: 48 h.

Under acidic condition, the carboxylic bond between the acid group, and hydrated cisplatin unit gets hydrolyzed easily. We anticipate that *in vivo*, this property will help to expedite the drug release in the affected (tumourous) region (acidic microenvironment) and be relatively dormant at the vicinity of healthy tissues, thus reducing side effects of chemotherapy. The trend of cisplatin released at specific time points for both acidic (red), and neutral (PBS, blue) solvent indicates the release profile is slow, and sustained, not a burst one. This may only result from a chemically conjugated drug, not an adsorbed or encapsulated formulation. From the plot, it is also evident that at 48 h (2 days) almost all the loaded cisplatin got released from the scaffolds in acidic media. This slow release will also help in managing the negative side effects arising from cytotoxic drugs, in addition to the advantages of local chemotherapy mentioned above.

The extent of the drug's effect on cells can be determined by a cell viability assay. We chose human mouth carcinoma KB cell line which was maintained in 10% FBS/MEM. In the experiment, we did control experiment using an unmodified scaffold, AuNP-

coated scaffold, and compared the results with cisplatin-containing scaffolds, along with aquated cisplatin (we used the same amount of cisplatin as was present on the scaffold). The release kinetics experiment presented showed that at 24 h at least 70% of the drug got released. Based on this, the time point for cell viability was decided to be 48 h.

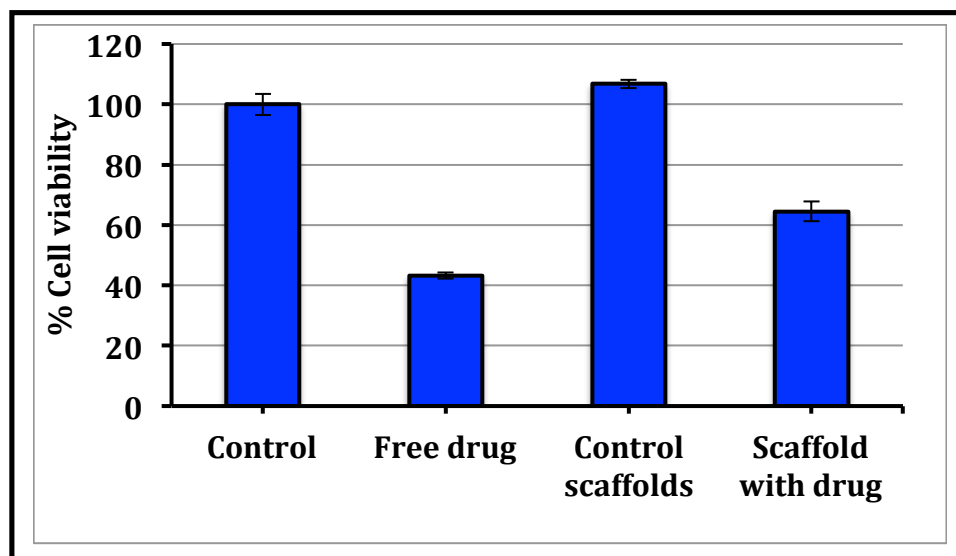


**Figure. 3.6:** Cell viability assay by mitochondrial activity (using resazurin indicator) with KB (human mouth cancer) cells at 48 h. Data represented as the mean  $\pm$ SD of  $n=3$ .

With the resazurin microtiter assay, it has been observed that when the cells were incubated with cisplatin loaded scaffolds only 60% of cells were viable (**Figure 3.6**) by the end of 48 h. In comparison, when exposed to a free drug of equal quantity only 40% of cells were found viable. This can arise from the easy internalization of free drugs into live cells, in comparison to polymer bound drug (via citric acid capped AuNP), which has to overcome a release step through ester hydrolysis. Quite gratifyingly, AuNP-coated scaffolds were found to be non-toxic (showing more than 100% cell viability in **Figure 3.6**), which is important, because according to our proposal the scaffolds after drug release should be accepting new cells, hence it should not portray any cytotoxicity.

With the help of CFSE (cytoplasm), and DAPI (nucleus) stains, cellular morphology analysis was performed. According to this [Figure 3.7(a)], the number of healthy cells was significantly low in the wells containing cisplatin-decorated scaffolds. The bright field image shows several cell debris, which can come from dead cells. Images collected using the 40x lenses elaborately show diffused nuclei [Figure 3.7(b)] indicating the presence of fragmented nuclei, which is an obvious result of cisplatin exposure. The cells in the control wells had more healthy spread. The number of cells was even more in just AuNP-coated scaffold containing wells. We tried to quantify the green, and blue fluorescence from different slides. Cells incubated with cisplatin decorated scaffolds or pure cisplatin showed a lower green fluorescence because of lowered cell number. Expectedly, the blue emission corresponding to DAPI (the nucleus stain) increased. This is due to the fragmentation, and spreading of nuclei since cisplatin mainly interacts with nuclear DNA.

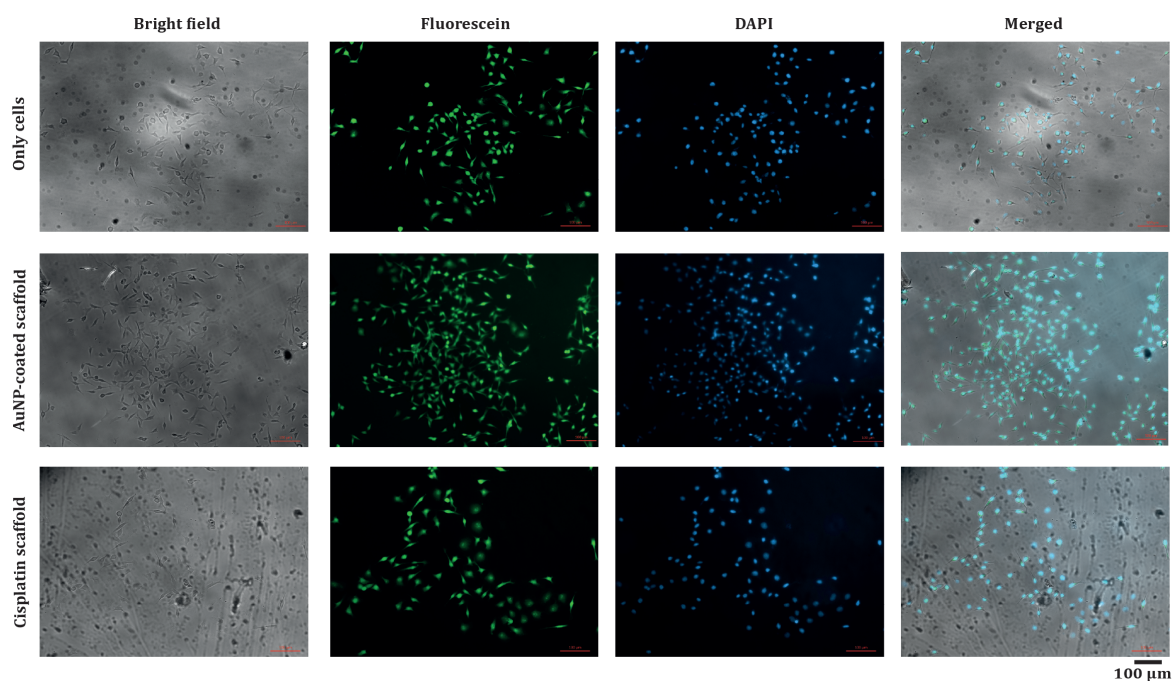


**Figure. 3.7(a):** Cellular morphology analysis in cisplatin-treated cells (using DAPI, and CFSE). Scale bar is 100  $\mu\text{m}$ .

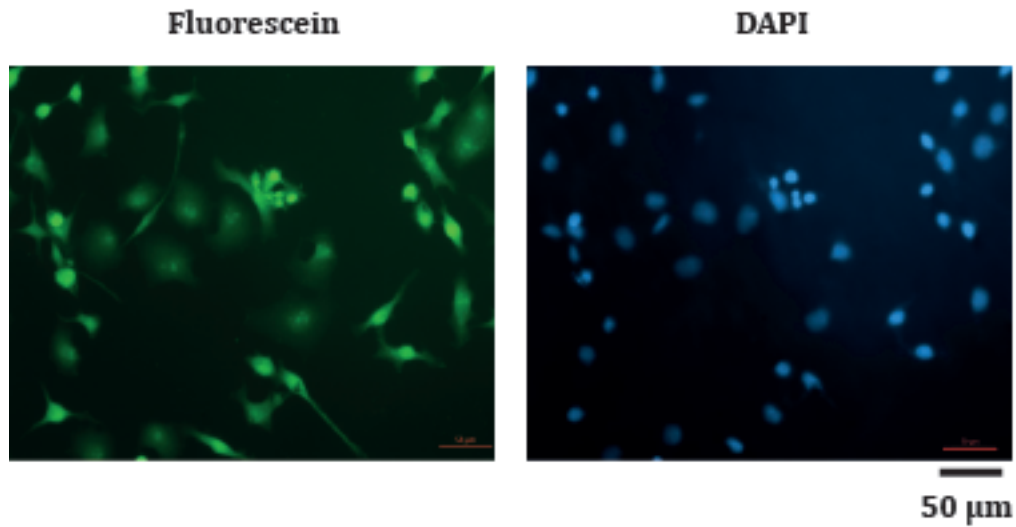


**Figure. 3.7(b):** High-resolution images of cisplatin affected KB cells, and controls. Scale bar is 50 μm.

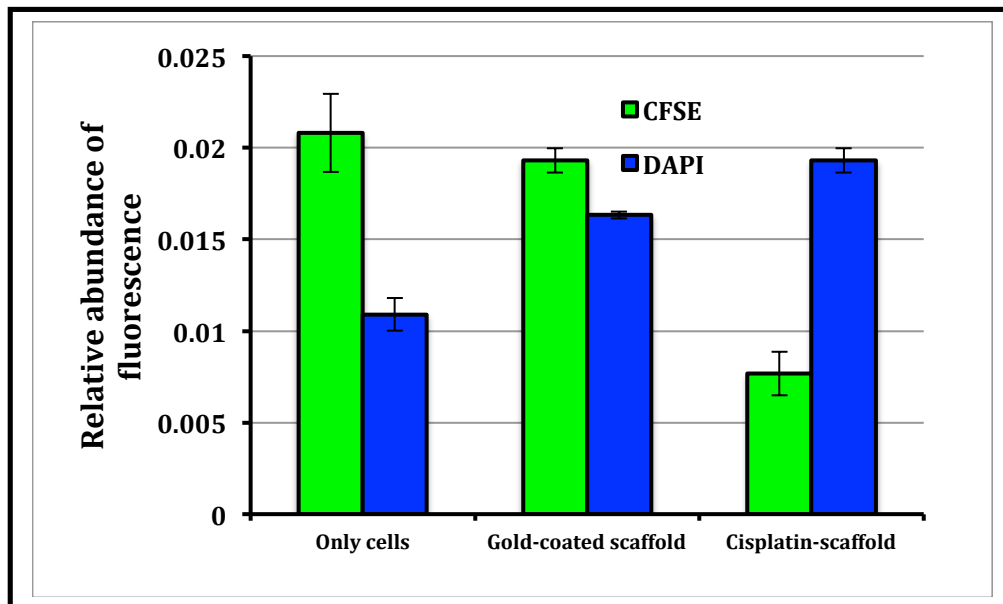


**Figure. 3.7(c):** Quantification of fluorescence emission from microscopy images from Figure 3.7(a) DAPI (blue), and CFSE (green). Data represented as a  $\pm$ SD of  $n=7$ .

To validate the presence, and quantity of dead, and live cells *in situ* a live-dead experiment was carried out. The control coverslips containing only cells showed a beautiful array of live cells; not a single dead cell was visible [Figure 3.8(a) upper panel]. For AuNP-coated scaffold containing coverslip, most of the cells were live although few dead cells were also seen [same Figure 3.8(a), middle panel]. For the cisplatin-carrying scaffold, mostly dead cells populated the coverslips. The fluorescence coming off the different channels also predict a similar trend [Figure 3.8(b)]. It is worth mentioning here that the ratio between live cells, and dead cells is quite similar to that obtained from the cytotoxicity study. Briefly, the amount (number) of cells for both control, and AuNP-coated scaffold containing wells are high, so it is relatively easier to get a trend.

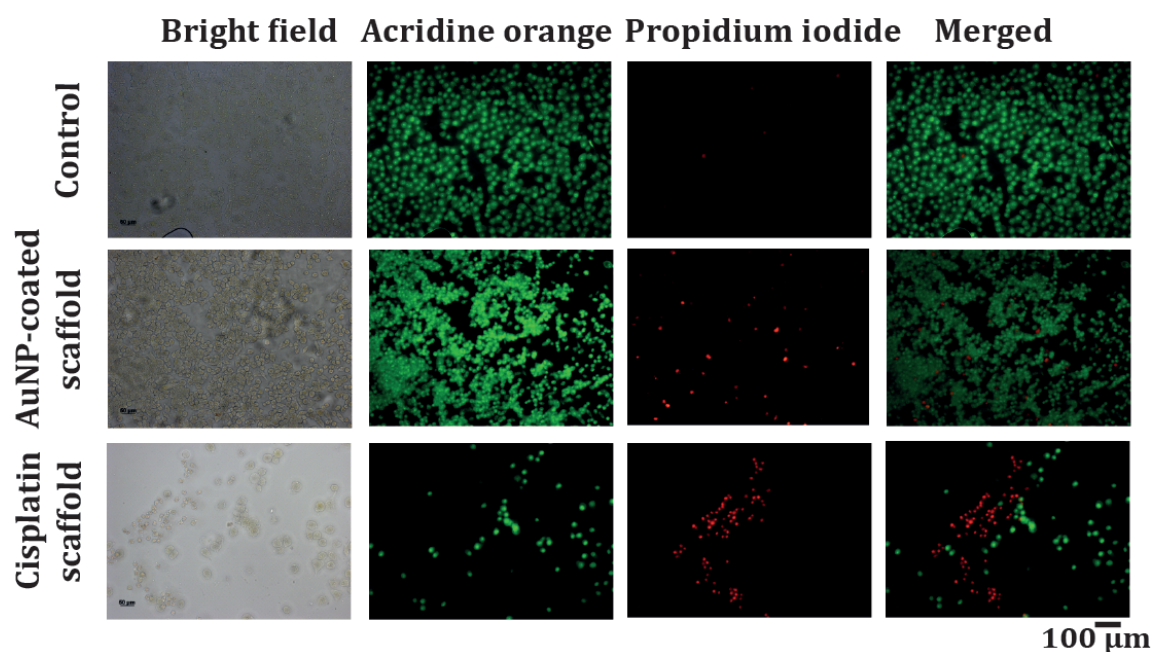


**Figure. 3.8(a):** Live-dead assay by live cells imaging. Live, and dead cell stains are acridine orange (AO), and propidium iodide (PI). Scale bar 100  $\mu\text{m}$ .

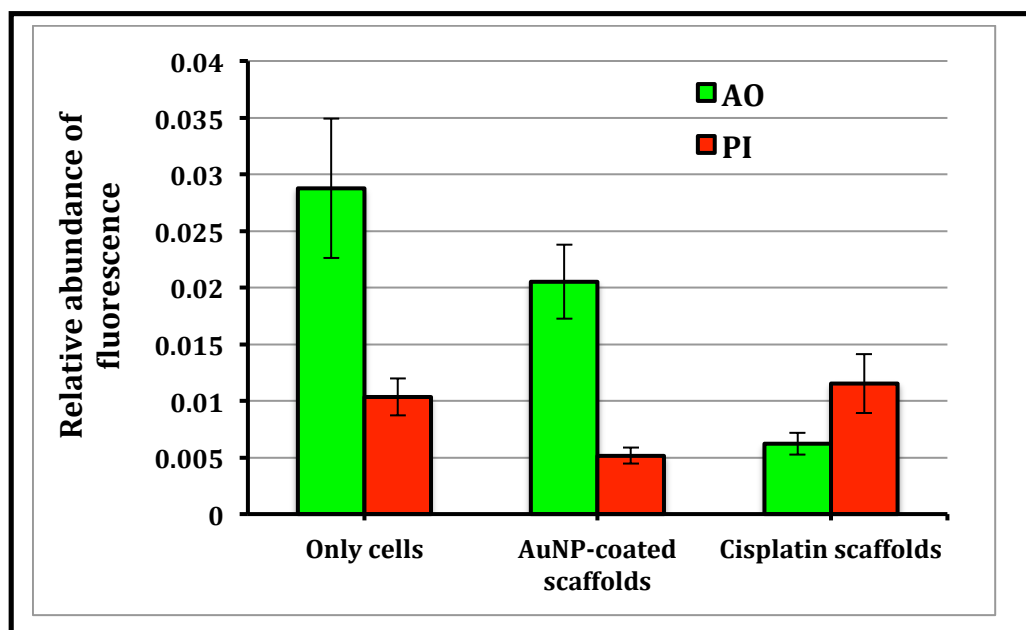


**Figure. 3.8(b):** Quantification of fluorescent tags from live-dead assay images. (A) Acridine orange(AO, green), and (B) Propidium iodide (PI, red) from figure 2.13.A. Data represented as a  $\pm$ SD of  $n=7$ .

But for drug-loaded scaffold containing wells, because of cisplatin's cytotoxicity, the cells die, and get washed away during PBS wash. So the majority of cells that get washed away are dead cells.

A cytotoxic drug like cisplatin initiates intercalation in the DNA of the nucleus of a live cell, and forces the cell to undergo apoptosis. With the help of flow cytometry, we planned to detect the extent of cell death initialized by cisplatin using Annexin-V FITC (apoptosis marker), and PI (dead cell marker) dyes. In this experiment cells exposed to cisplatin were stained with Annexin-V, and PI. In the cytometer, the cells residing in live, early apoptotic, late apoptotic, and necrotic phases can be tracked by following the fluorescence intensity. In the data plot [Figure 3.9(a)] The X-axis indicates green fluorescence, and Y-axis red fluorescence.



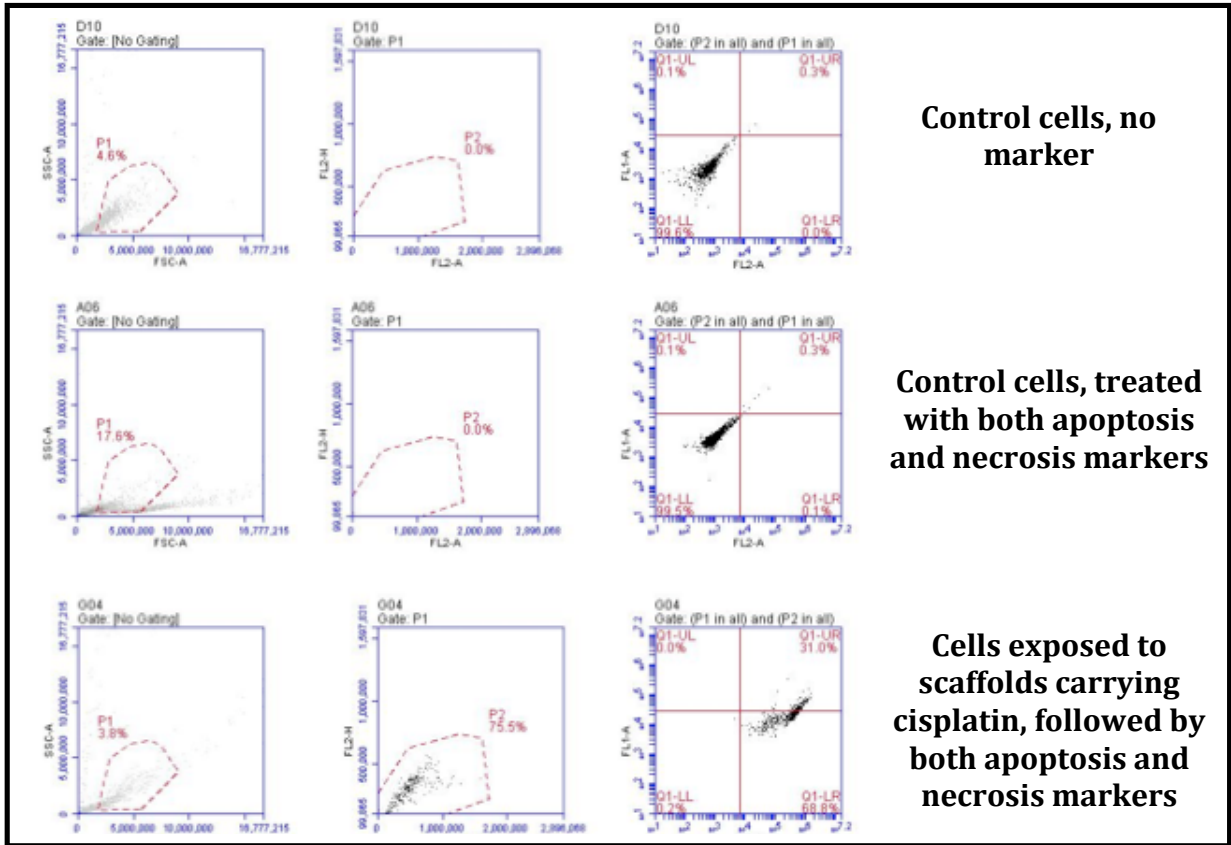


**Figure. 3.9(a):** Analysis of cell-death mechanism (extent of apoptosis) on KB cells with the help of a flow cytometer. Annexin V-FITC: apoptosis marker, PI: dead cell marker.



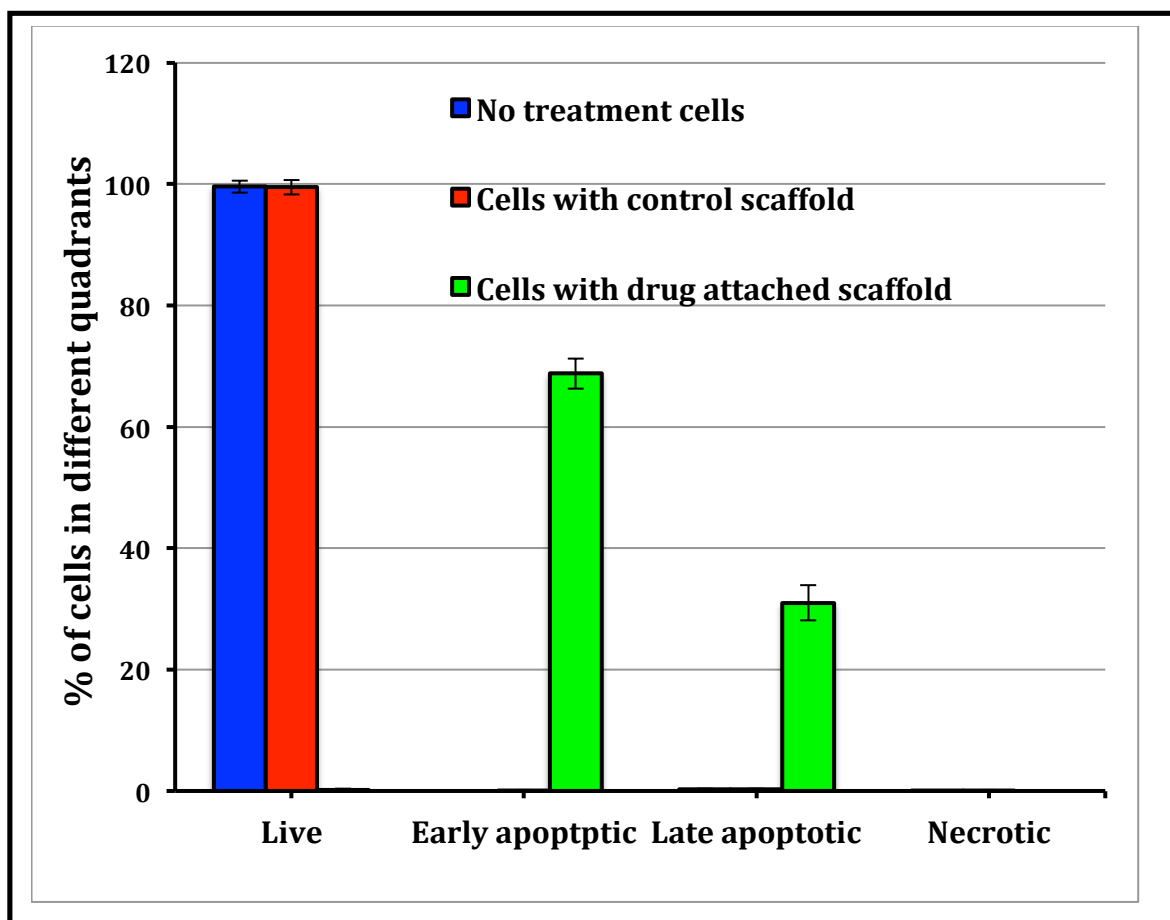


**Figure. 3.9(b):** Apoptosis assay plot [from Figure 3.9(a)]: *Cells present in different quadrant for different treatments.*

As a result, the first quadrant (bottom left) represents live cells, bottom right early apoptotic (no dead cells yet but some are green), top right represents late apoptotic cells (many cells are green), and finally, the top left quadrant represents dead cells. We first had to confirm whether cells were auto-fluorescent. For that control cells without any marker were allowed to pass through the analyzer but no signal for red or green fluorescence was observed [Figure 3.9(a) top panel]. For control cells (without any cisplatin exposure) where both markers were added no apoptosis or necrosis was in progress, so the cells were completely healthy and did not show any signal for red/green fluorescence [Figure 3.9(a) middle panel]. Cells, which have got exposed to cisplatin environment for 24 h showed a significant signal for early apoptotic, and late apoptotic stages. While plotting the data we figured out that the

cells, which were exposed to drug-loaded scaffolds, show 65% early apoptotic, and almost 30% late apoptotic cells [Figure 3.9(b)]. This proves the cells are being affected by the drug cisplatin (which encourage the apoptosis pathway of cell death) and not by any other means. It may also be noted that we chose 1 day time point for this analysis as the major amount of cells were found dead after 2 or later day time points in case of drug-carrying scaffolds. The remaining number of cells could not produce good data points in flow cytometry. AnnexinV- FITC conjugate was also used for imaging purpose, where the extent of phosphatidylserine expression can be visualized, and quantified. Figure 3.10 indicates that control cells (without any exposure to cisplatin scaffold) did not display any green fluorescence. With cisplatin-exposed cells on day 1, several cells showed green fluorescence around the cellular membrane region, which arose from the FITC attached to phosphatidylserine present in the cellular membrane. On day 2 (lower panel) almost all live cells had well-expressed phosphatidylserine along the cellular membrane.

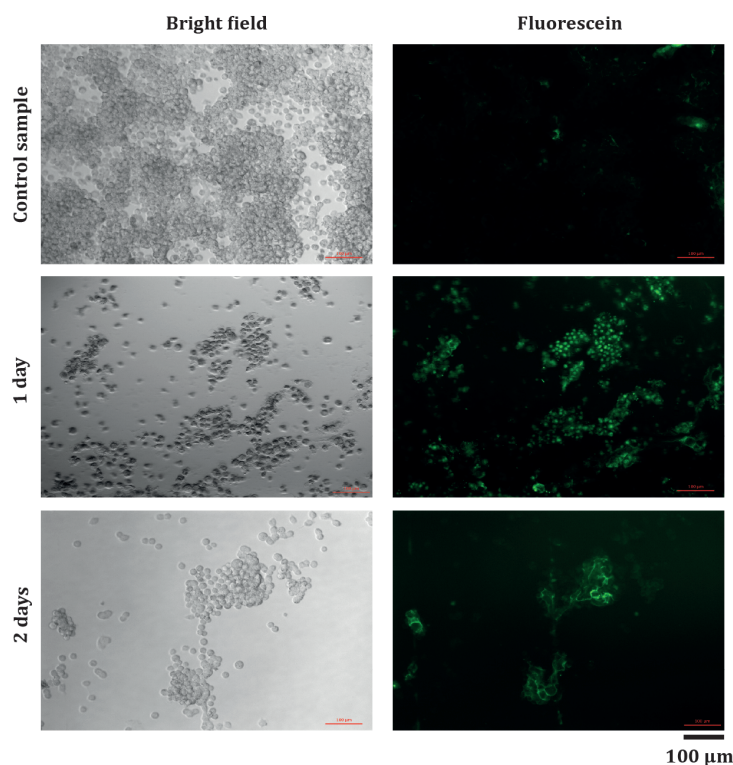


**Figure. 3.10:** Expression of phosphatidyl serine in KB cells by imaging. Scale bar is 100  $\mu\text{m}$ .

### 3.4.3. Cellular regrowth experiment

Until this point, we have shown that drug-loaded scaffolds could release the drug in a slow, sustained manner and can cause cell death by cellular apoptosis. But the uniqueness about the scaffolds that we prepared is their dual purpose. So post drug release they are supposed to become friendly to non-cancerous new cells so that the intended volume filling can be accomplished. To probe this property, we conducted the following experiment using L929 (murine fibroblast) cell line. 5,000 of these cells (L929) were seeded on the scaffolds from which the maximum amount of cisplatin was already released. The cell growth was followed by the resazurin assay. From the plot (**Figure 3.11**), it is evident that with time, the cellular population on scaffolds

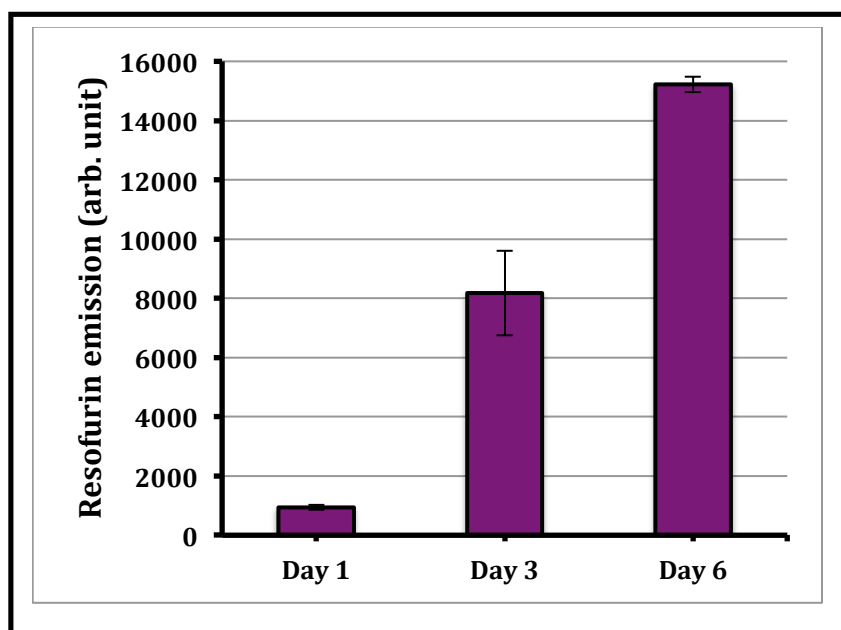


**Figure. 3.11:** L929 regrowth on cisplatin scaffolds after drug release. Data represented as the mean  $\pm$ SD of  $n=3$ .

increased indicating the non-toxicity of the scaffolds after 2 days of cisplatin release. With time, the cells proliferated considerably and came to a peak (day 6 data, later data points are not included). Nonetheless, there is a steady increase in viable cell population signifying the effectiveness of the drug-released scaffolds to maintain a healthy population. The increased population of fibroblast cells was evident from the images (**Figure 3.12**) of cellular population. Here, it can be clearly seen that at the beginning only a few cells were able to attach to the scaffold. It may also be possible that at this stage after adhesion cells died because of leftover cytotoxic drugs present.

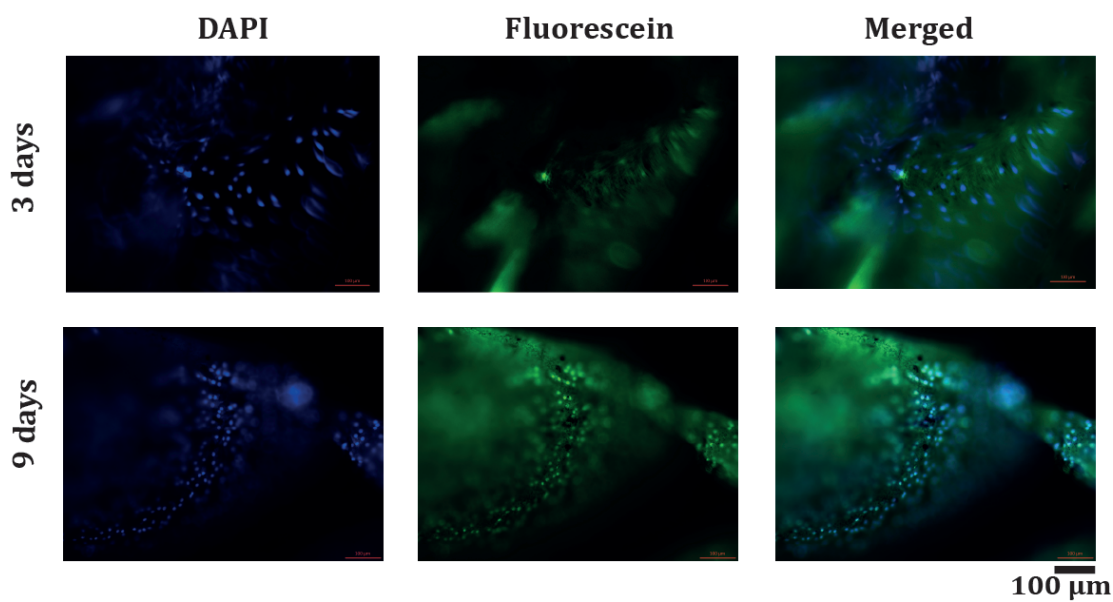


**Figure. 3.12:** Representative images on L929 regrowth on cisplatin scaffolds (stains: CFSE, and DAPI). Scale bar is 100 μm.

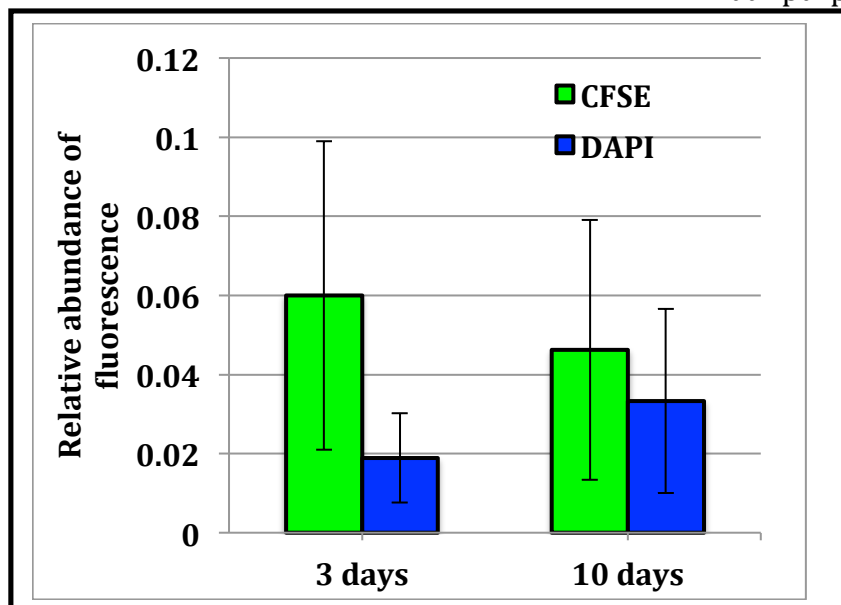


**Figure. 3.13:** *Quantification of fluorescence from each image in the fibroblast regrowth experiment.*

But on each alternate day as the media was changed, which can lead to two effects; 1) dead cells and released drug molecules get eliminated, 2) existing cells received nutrients necessary for growth, and proliferation. Ultimately on day 9, cells formed a big colony as shown in **Figure 3.12** (lower panel). The quantification experiments clearly support this contention suggesting a tremendous improvement in cell population over 9 days (**Figure 3.13**). Thus the presented cisplatin decorated scaffolds can release the cytotoxic drug during the first few days and hence can eliminate the remnant cancerous cells. Subsequent to the release of the drug, the cell friendly surface chemistry of the scaffolds helps in the cell proliferation and to maintain a healthy cellular colony. This proves that the scaffold would be able to fulfil the role of a functional replacement in the real case.

### 3.5. Conclusion

In this chapter, we described the chemical conjugation of cytotoxic drug cisplatin to porous solid scaffolds, which have been surface modified by citrate stabilized AuNPs. The scaffolds release drug in a slow and sustained manner, and then present a cell-friendly surface that can accept fresh cells happily in due course of time. The new cells

form a colony (as proven by cell viability assay, and cellular imaging), and thus the scaffolds can act as a functional replacement hugely needed for the treatment of solid cancer. Although there have been several reports<sup>23</sup> of solid scaffolds working as drug cargo (local chemotherapy), and as a tissue engineering base independently, the relevant overlap of both these phenomenon necessitates a surface modification strategy as described here where the scaffolds initially are highly cytotoxic before eventually becoming quite cell-friendly.

### 3.6. Bibliography

---

<sup>1</sup> <https://www.cancercenter.com/oral-cancer/types/tab/mouth-cancer/>

<sup>2</sup> Shah, J. P.; Gil, Z. Current concepts in management of oral cancer – Surgery, *Oral Oncology*, **2009**, 45(4-5), 394-401.

<sup>3</sup> Gupta, A.; Agrawal, G.; Tiwari, S.; Verma, K.; Agrawal, R.; Choudhary, V. Pectoralis major myocutaneous flap in head and neck reconstruction: an interesting experience from central India regional cancer center. *International Journal of Research in Medical Sciences*, **2015**, 3(11), 3065-3068.

<sup>4</sup> <https://www.cancer.org/cancer/oral-cavity-and-oropharyngeal-cancer/treating/surgery.html>

<sup>5</sup> Can, Z. Z.; Ercocen, A. R.; Apaydin, I.; Demirseren, E.; Sabuncuoglu, B. Tissue Engineering of high density porous polyethylene implant for three dimensional reconstruction: An experimental study. *J. Plast. Reconstr. Hand Surg.*, **2000**, 34, 9–14.

<sup>6</sup> James, S. P.; Oldinski, R. (Kurkowski); Zhang, M.; Schwartz, H. *UHMWPE Biomaterials Handbook*. **2009**, 259-276.

<sup>7</sup> E. Neovius, T.; Engstrand. Craniofacial reconstruction with bone and biomaterials: Review over the last 11 years, *Journal of Plastic, Reconstructive & Aesthetic Surgery*, **2010**, 63(10), 1615-1623.

<sup>8</sup> Deshpande, S.; Munoli, A. Long-term results of high-density porous polyethylene implants in facial skeletal augmentation: An Indian perspective. *Indian J. Plast. Surg.* **2010**, 43, 34–39.

<sup>9</sup> Kim, Y. H.; Jang, T. Y. Porous high-density polyethylene in functional rhinoplasty: Excellent long-term aesthetic results and safety. *Plast. Surg.* **2014**, 22, 14-17.

---

<sup>10</sup> Fernandez-Bueno, I.; Di Lauro, S.; Alvarez, I.; Lopez, J. C.; Garcia-Gutierrez, M. T.; Fernandez, I.; Larra, E.; Pastor, J. C. Safety and Biocompatibility of a New High-Density Polyethylene-Based Spherical Integrated Porous Orbital Implant: An Experimental Study in Rabbits. *J. Ophthalmol.* **2015**, No. 904096.

<sup>11</sup> Laquintana, V.; Trapani, A.; Denora, N.; Gallo, J. M.; Trapani, G. New strategies to deliver anticancer drugs to brain tumors. *Expert Opinion on Drug Delivery*, **2009**, 6(10), 1017-1032.V.

<sup>12</sup> Vermorken, J. B.; Remenar, E.; van Herpen, C.; Gorlia, T.; Mesia, R.; Degardin, M.; Stewart, J. S.; Jelic, S.; Betka, J.; Preiss, J. H. *et al. N. Engl. J. Med.* **2007**, 357, 1695-1704.

<sup>13</sup> <https://www.drugs.com/sfx/cisplatin-side-effects.html> Accessed February 2019

<sup>14</sup> Blanchard E. M. Cisplatin and solid tumours: still working, after all these years. *J Solid Tumors.* **2012**, 2, 26-33.

<sup>15</sup> Turkevich, J.; Stevenson, P.C.; Hillier, J. A study of the nucleation and growth processes in the synthesis of colloidal gold. *Discussions of the Faraday Society*, **1951**, 11, 55-75.

<sup>16</sup> Golla, E. D.; Ayres, G. H. Spectrophotometric determination of platinum with o-phenylenediamine. *Talanta.* **1973**, 20(2), 199-210.

<sup>17</sup> Mulvaney, P. Surface Plasmon Spectroscopy of Nanosized Metal Particles. *Langmuir* **1996**, 12, 788-800.

<sup>18</sup> Barnes, K. R.; Kutikov, A.; Lippard, S. Synthesis, characterization, and cytotoxicity of a series of estrogen-tethered platinum(IV) complexes. *J. Chem. Biol.* **2004**, 11, 557-564.

<sup>19</sup> Dhar, S.; Gub, F. X.; Langer, R.; Farokhzad, O. C. and Lippard, S. J. Targeted delivery of cisplatin to prostate cancer cells by aptamer functionalized Pt(IV) prodrug-PLGA-PEG nanoparticles *PNAS* **2008**, 105(45), 17356 -17361.

<sup>20</sup> Shen, D. W.; Pouliot, L. M.; Hall, M. D. and Gottesman, M. M. Cisplatin Resistance: A Cellular Self-Defense Mechanism Resulting from Multiple Epigenetic and Genetic Changes *Pharmacol Rev.* **2012**, 64(3), 706-721.

<sup>21</sup> Shen, D. W.; Akiyama, S. I.; Schoenlein, P.; Pastan, I.; and Gottesman, M. M. Characterisation of high-level cisplatin-resistant cell lines established from a human hepatoma cell line and human KB adenocarcinoma cells: cross-resistance and protein changes *British Journal of Cancer* **1995**, 71, 676-683.

<sup>22</sup> Paraskar, A. S.; Soni, S.; Chin, K. T.; Chaudhuri, P.; Muto, K. W.; Berkowitz, J.; Handlogten, M. W.; Alves, N. J.; Bilgicer, B.; Dinulescu D. M.; Mashelkar, R. A.; and Sengupta, S. Harnessing structure-activity relationship to engineer a cisplatin nanoparticle for enhanced antitumor efficacy *PNAS*, **2010**, 107(28), 12435-12440.

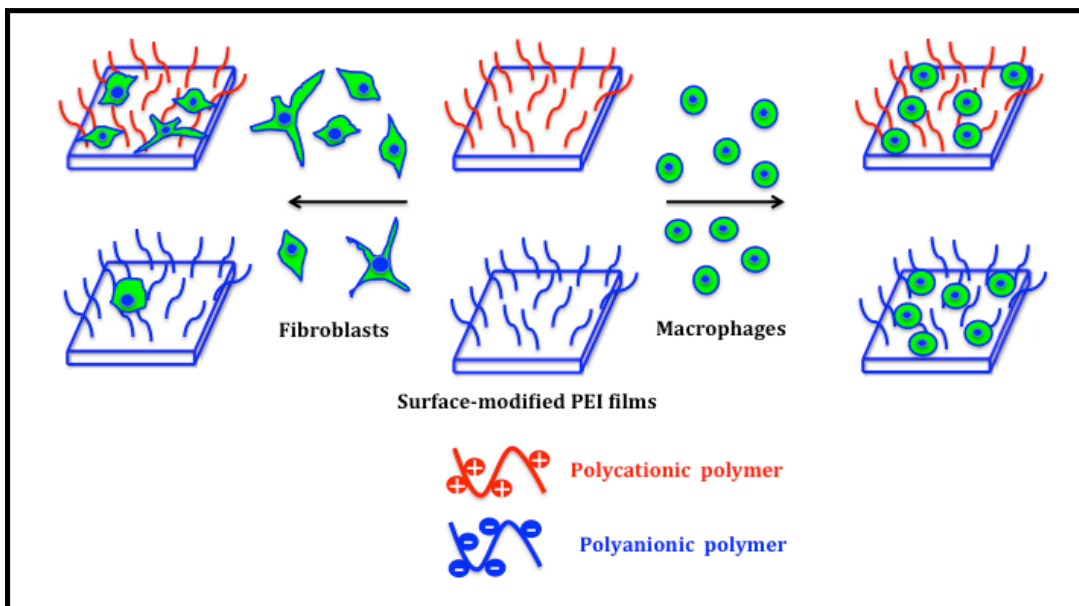
---

<sup>29</sup> Sharma, P. K. Taneja, S. Singh, Y. Hydrazone-Linkage-Based Self-Healing and Injectable Xanthan–Poly(ethylene glycol) Hydrogels for Controlled Drug Release and 3D Cell Culture. *ACS Appl. Mater. Interfaces* **2018**, *10*, 30936-30945.



# Chapter 4

## The response of macrophages with respect to surface charge alterations



### **Abstract**

The fate of a body implant is determined by its interaction with the immune cells inside the living system. Depending on the surface chemistry the cell-material interaction can be either productive or damaging. In this chapter, using the P-LbL method we have altered the material surface charge with the help of AuNPs, polycationic, and polyanionic polymers. The modified surfaces were characterized using contact angle measurement, FT-IR, Zeta potential measurement *etc.* These modified-surfaces were exposed to phagocytic immune cells (RAW264.7, murine monocyte macrophages), as well as non-phagocytic cells (HepG2, L929: human liver carcinoma cells, and murine fibroblasts). The affinity towards different kind of cells (immune, and non-immune) was examined by adhesion experiment. The finding was supported by live-dead experiment, and cell population experiments (fluorescent microscopy imaging).

## 4.1. Introduction

For decades synthetically derived materials are being used as implants inside live human tissue. Unfortunately, many time this leads to various side effects (of different seriousness), which were mostly disregarded until very recently.<sup>1</sup> With time we came to know that, each implant, irrespective of its shape, size, material properties, surface functionalities, has to confront the immune system as soon as it is put inside the body after a surgery. The immune system treats any implant as a foreign body, and this is termed as 'foreign body response' or FBR.<sup>2</sup> If the interaction is minimal and can be tackled by the living organism, the implant is considered biocompatible.<sup>3</sup> But often, the interaction between the immune system and the implant is not favourable and leads to issues like inflammation, fibrosis, thrombosis, and infection. In those cases, the implant is 'not biocompatible'. This may happen due to bacterial contamination, or adverse interaction between foreign materials and the immune system. This initial confrontation of the immune system and foreign body happens over several phases involving innate, and adaptive immunity and can span through approximately 20-25 days or more (**Figure 4.1**). Starting from the innate immunity (first exposure of implants to the living system), macrophages play critical roles.<sup>4</sup> In the case of microscopic foreign bodies, our immune system recruits macrophages and 'phagocytose' them. But in case of an implant, the size of the foreign body becomes significantly bigger to get digested by a macrophage. Under such circumstances, the macrophage converts itself into a multinuclear 'giant cell' and covers the material with the help of T cells, B cells, leucocytes, fibroblasts *etc.* Whichever be the case, depending on the macrophage's first interaction with the foreign material, the future of the material inside the human body is determined.<sup>5</sup> So, to manufacture a safe, modern, improved implant material, the interaction between macrophage and material (implant) surface should clearly be understood.

In this background, we reckoned that the material surface-macrophage interaction would be most crucial rather than the bulk of the material-macrophage interactions.

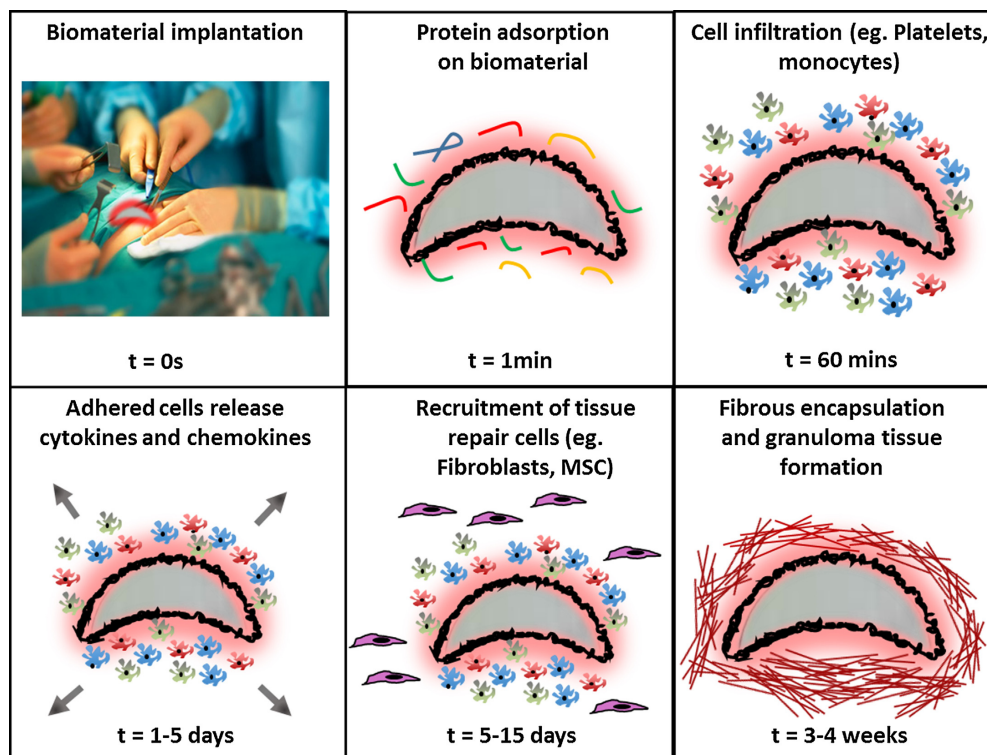


**Figure 4.1:** *Temporal sequence of events after biomaterial implantation.*<sup>18</sup> For license, please see page number 163

Because after the implant is inserted inside the body, the macrophage sees the surface of the material only and not the bulk. Hence, in this chapter we wanted to study how the surface chemistry of a material influences its interaction with the macrophages,<sup>6,7</sup> keeping every other parameter (material properties) constant. This, we surmised would lead to a better understanding of the macrophage-material interaction. In this context, it may be worth noting that there have been many recent reports concerning cell-material interaction, where cells were exposed to nanoparticles with different surface features to see how they get internalized into cells.<sup>8</sup> Among these, the effect of surface charge has mostly been researched using metallic/polymeric nanoparticles.<sup>9,10,11,12,13</sup> Hence, we envisaged that the P-LbL route would be the ideal one as we can modulate the surface characteristics through P-LbL by incubation of the plasma-treated gold nanoparticle coated films/scaffolds with molecules bearing different surface charges. The material's surface (bearing these different charges)-macrophage interaction was then probed using cellular-adhesion assay, and imaging. For adhesion assay, a flat, two-dimensional surface is

essential; hence we carried out the experiment on PEI films (surface modified by P-LbL method) instead of porous three-dimensional HDPE scaffolds. The surface-modified PEI films (AuNP-coated by P-LbL method) were further surface-coated with two different linear polymers: (i) poly cationic polymer poly diallyldimethylammonium chloride (PDADMAC), and (ii) anionic polymer polyacrylic acid (PAA). The reasons for selecting them were their simplicity in structure (linear polymer) and the different charge moieties that they possess (see **Scheme 4.1** for structures). Also, the syntheses of both PDADMAC,<sup>14</sup> and PAA-coated<sup>15</sup> AuNPs (citrate-stabilized) were reported, suggesting that the surface coating of AuNPs with these polyelectrolytes is achievable. Both PDADMAC, and PAA have positive, and negative charges respectively at each monomer unit in high frequency (the monomers being of low molecular weight, the charge repeats frequently), so the above charges are more likely to be found on modified surfaces. Most importantly, both PDADMAC, and PAA are FDA-approved up to a certain concentration, so there are good chances that a scaffold that is surface modified with them could find commercial acceptance if necessary. The surface-coated films were characterized using several spectroscopic, and light scattering techniques (for example, UV-Vis, contact angle, zeta potential, and FT-IR). We also quantified the number of polymers in each film. We carried out adhesion assay with three kinds of cells: (i) RAW264.7, (ii) L929 (murine fibroblast), (iii) HepG2 (human liver carcinoma). The main goal was to understand the interaction of macrophages with the modified surface, using the other two cell lines as a control. The extent of adhesion was monitored by resofurin assay, and imaging.

## 4.2. Materials

PEI (polyetherimide) sold under the trade name Ultem 1000®, was obtained from General Electrical Co., Schenectady, NY, USA. Chloroauric acid was obtained from the Seisco Research Laboratory, India. Carboxyfluoresceinsuccinimidyl ester (CFSE), 4', 6-diamidino-2-phenylindole (DAPI), phosphate-buffered saline (PBS) powder, resofurin, and propidium iodide (PI) were purchased from Sigma Aldrich. Murine

originated fibroblast cell line L929, murine monocyte-macrophage RAW264.7, and liver carcinoma cell HepG2 were procured from the cell line repository of NCCS Pune, India. DMEM, and FBS were purchased from Invitrogen. PAA (35% by weight in water, Mw 2,50,000 density 1.150gm/mL), and PDADMAC (20% by weight in water, Mw 1,00,000-2,00,000 density 1.04 gm/mL) were procured from Sigma Aldrich.

### 4.3. Experimental section

#### 4.3.1. Preparation of surface-modified films

##### *4.3.1.1. The casting of PEI film, plasma treatment, gold nanoparticle preparation, and surface coating*

For the methods of these steps the same protocols as discussed in sections 2.3.1., 2.3.2., 2.3.3., 2.3.4., and 2.3.5. were followed. For plasma treatment Toroidal Linear Plasma Devices were used.

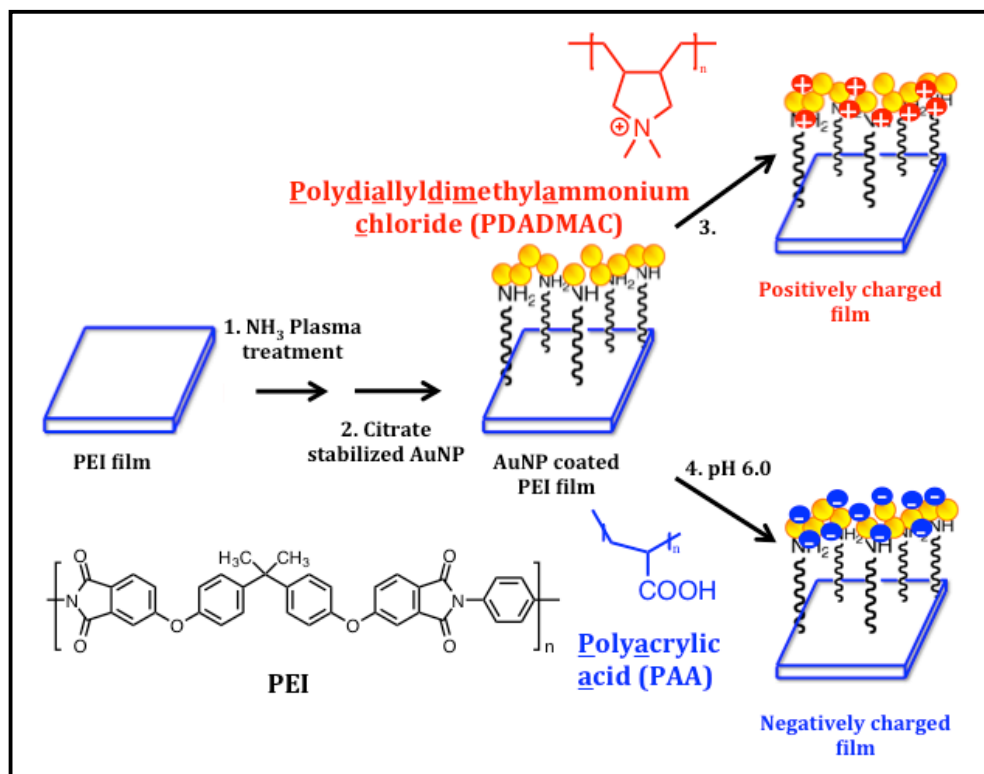
##### *4.3.1.2. PDADMAC-coating on PEI films*

The AuNP-coated PEI film (1 cm<sup>2</sup>, 1 no.) was allowed to incubate in a 5.0 mg/mL PDADMAC solution in milli-Q water.<sup>14</sup> After overnight incubation under mild shaking (50 rpm), the film was removed, washed with milli-Q water 3-times followed by aerial, and vacuum drying (**Scheme 4.1** step 3). Before taking to cell culture lab, the films were sterilized by UV-treatment for 30 minutes on each side.

##### *4.3.1.3. PAA-coating on PEI films*

PAA-coating on AuNP-coated PEI film was achieved in a stepwise manner. First, the AuNP-coated PEI films were incubated in 5.2 mM citric acid solution at 37 °C for two hours. The films were removed and washed with milli-Q water. One film was taken in 1.0 mL milli-Q water and pH was brought to 6.0 with the help of 0.5 (N) HCl. To this 7 µL, PAA was added. It was mildly shaken (50 rpm) at room temperature for 3 hours. The film was separated, incubated in milli-Q water for 1 hour and washed several times (step 4 in **Scheme 4.1**). It was dried in air followed by a vacuum

pump. Before taking to cell culture lab, the films were sterilized by UV-treatment for 30 minutes on each side.



**Scheme 4.1:** Schematic representation of the surface modification of polyetherimide films. 1. Plasma treatment using 3: 2 hydrogen, nitrogen mixture. 2. Incubation of plasma treated films in citrate stabilized AuNP sol. 3. Creation of positively charged surface using PDADMAC (overnight incubation) 4. Creation of negatively charged surface using PAA (3 h incubation)

### 4.3.2. Characterization

#### 4.3.2.1. UV-Vis spectrophotometry

Polymers after AuNP-coating were ground in the frozen state with the help of a cryomiller (Retch Cryomill). The powdered samples were incubated with different polymers following the same protocol as discussed in sections 4.3.2.1., and 4.3.2.1. Shimadzu UV/Vis/IR/3600 spectrophotometer was used in reflectance mode to collect data of the surface modified powdered samples. Barium sulfate was used as background correction.

#### 4.3.2.2. Zeta potential measurement

Zeta potential of polymer-coated (PDADMAC, and PAA) AuNPs (citrate-capped) was measured using PALS Zeta Potential Analyzer Ver. 5.76.

##### 4.3.2.2.1. Sample preparation for PDADMAC-coated citrate stabilized AuNPs

Citrate-stabilized AuNPs were prepared using Turkevich's method.<sup>16</sup> 5.0 mL of the resulting solution was centrifuged using Beckman Coulter Allegra 64R centrifuge at 14000 rpm for 40 minutes, and the supernatant was discarded. Pelleted AuNP was re-dispersed using milli-Q water. After 3 times washing the centrifuged AuNP pellet was re-suspended in 5.0 mg/mL PDADMAC solution in milli-Q water. It was allowed to shake at 50 rpm overnight. The resulting purple colored solution was centrifuged at 14500 rpm for 40 minutes, and the formed pellet was suspended in 1 mM NaCl solution. Zeta potential was measured using a flow cell. All experiments were performed in triplicates.

##### 4.3.2.2.2. Sample preparation for PAA-coated citrate stabilized AuNPs

In this method also citrate stabilized AuNPs were centrifuged to remove extra citric acid from the solution. The pelleted AuNPs were suspended in 1.0 mL pH 6.0 water and stirred mildly for overnight. The resulting solution was centrifuged again and dispersed in 7  $\mu$ L PAA in 1.0 mL milli-Q water. The final pH was adjusted to 7.0. Zeta potential was measured with the resulting solution.

#### 4.3.2.3. Contact angle measurement

The nature of the surface (hydrophobic or hydrophilic) was measured by using a contact angle meter (Kruss Drop Shape Analyser Version 1.41-02). 10  $\mu$ L of water droplets were placed at 5 different places on the modified surface at room temperature, and atmospheric pressure. Data represented  $\pm$ SD of n=5.

#### 4.3.2.4. FT-IR measurement (ATR mode)



Surface-modified films were subjected to FT-IR measurement using the Perkin Elmer Spectrum 2 spectrophotometer in ATR mode. For both the surface modified films, a background of only PEI was collected.

#### *4.3.2.5. Determination of the amount of polymer attached*

In this experiment, 8\*4 square centimetre PEI films (6 in no.) were surface treated with N<sub>2</sub> + H<sub>2</sub> plasma, and incubated in citrate stabilized AuNP sol. After dark purple coating of AuNPs on the PEI film, each film was dried in vacuum and individually weighed in the electronic balance, and marked. The weights were recorded. By following the protocols described in sections 4.3.1.2. and 4.3.1.3., surface modifications using electrolytes (3 for each polymer) were performed. After drying under vacuum, the films were again weighed. By subtracting the weight of the PEI films after and before the polymeric coating, the weight of the polymer adhered was determined.

#### *4.3.2.6. Cellular adhesion assay*

RAW264.7, and L929 cells were maintained in 10% FBS/DMEM media. HepG2 was maintained in 10% FBS/MEM media. The adhesion experiments were performed on 1 cm<sup>2</sup> surface-modified PEI films. The surface-modified films along with bare PEI films were UV exposed inside tissue culture hood for 30 minutes on each side. The experiments were performed in the sterile non-adhering 24 well plates. In the adhesion assay, 50,000 cells (of each type) were dispersed in 50 µL of their respective media and aseptically seeded onto the sterilized films. After 5, 30, 60, 120, 240 minutes the supernatant was aspirated. Each film was washed three times in sterile PBS (kept at 37 °C). The number of leftover cells on the films was determined by resazurin-based fluorescent assay where each film was incubated in 100 µL 100 µM resazurin solution in complete medium for 6 hours under cell culture condition. The resulting solution was excited at 560 nm, and emission at 590 nm was collected. The emission values were directly plotted using Microsoft Excel. Results from each experiment were plotted as a mean including ± SE for n=3.

#### 4.3.2.7. *Live-dead assay*

Like the adhesion assay, 50,000 cells (dispersed in 50  $\mu$ L of the respective complete media) were added on each film and incubated under the cell-culture condition for 1 h. At 1 h time point, each film was carefully washed by dipping in sterile PBS kept at 37  $^{\circ}$ C, followed by incubation in 1.0 mL of corresponding complete medium for 48 hours. After 48 hours the cells were washed several times with sterile PBS. Cells were incubated in 0.1% Triton X-100 in PBS for 5 minutes followed by washing (PBS). They were further incubated in 5% BSA for 20 minutes to avoid non-specific binding. Subsequently, they were incubated with the live-dead assay stain of 10  $\mu$ L 7.5 mM propidium iodide, 1  $\mu$ L 0.67 mM acridine orange in 1 mL complete media (for each well) under the cell culture conditions for 1 h. The films were washed with PBS and directly viewed under Axio Observer Z1 Carl Zeiss microscope using green, and red channels. Amount of fluorescence from both the colours representing live and dead cells was quantified (with blue Zen 2012 Carl Zeiss software), normalized with respect to area and plotted.

#### 4.3.2.8. *The population of cells on different surfaces*

Like the live-dead assay, 50,000 cells dispersed 50  $\mu$ L complete media were allowed to adhere to the modified film surfaces. After 1 hour, the media was aseptically aspirated. Films were washed in sterile PBS and incubated in complete media (1.0 mL for each well) for 48 h. At 48 h media was aspirated, followed by washing with sterile PBS for three times. Films were fixed using 4% PFA (0.5 mL for each well) for 15 minutes. After fixing PFA was aspirated, followed by washing with PBS at room temperature. Films were incubated in 0.1% Triton X-100 in PBS for 5 minutes followed by washing (PBS). They were further incubated in 5% BSA for 20 minutes followed by washing (PBS). They were treated with CFSE in PBS (5  $\mu$ M) for 15 minutes at room temperature in the dark followed by washing with PBS. The films were incubated with 300 nM DAPI at room temperature in the dark for 4 minutes followed by another brief PBS wash. Films were observed using Axio Observer Z1 Carl Zeiss microscope using green, and cyan filters. Emission of fluorescein, and

DAPI from adhered cells were quantified, normalized with respect to area, and plotted.

#### 4.4. Result and discussion

##### 4.4.1. Synthesis and characterization of surface modified films:

In order to carry out the intended study, we first proceeded to use the P-LbL technique to create a polymeric surface with different charges on it (**Scheme 4.1**). As per our protocol described in previous chapters, AuNP (citrate stabilized gold nanoparticle) coating on PEI film surface was achieved by sequential  $N_2 + H_2$  plasma treatment followed by stirring the plasma treated PEI films with an AuNP sol. Plasma treatment produced transient surface charges, which attracted citrate-stabilized AuNPs. As a result, the surface coating was facile, and the colour of the transparent PEI films changed into dark purple (due to AuNP deposition). Subsequently, the coating was achieved with overnight incubation of these AuNP coated films with the polymer solution under stirring conditions at low rpm (50). Low rpm was decided in order to avoid mechanical agitation, which may dislodge the AuNPs from PEI films. The polymer concentration was kept sufficiently high (5.0 mg/mL) so that there are enough polymers to coat the entire surface. PDADMAC being a polycationic polymer gets attracted to the oppositely charged (citrate capping on AuNPs) surface and spread on top of the AuNPs primarily because of electrostatic attraction. On the contrary, with PAA surface coating, this straightforward dip-coating technique did not work since citrate and acrylate group both being negatively charged would repel each other. Thus, to achieve surface covering of gold-coated PEI by PAA, the pH of the incubation solution was intentionally adjusted to 6.0 with 0.5(N) HCl. The pH 6.0 was decided from the pKa values of citric acid (pKa1, pKa2, and pKa3 respectively being 3.13, 4.76, and 6.40), which indicate that at pH 6.0 at least few carboxylic acid groups will be protonated. These can form constructive hydrogen bonding with the carboxylic acid groups present on PAA. To ensure that the gold nanoparticle coating on the PEI films was intact even after the surface coating by both the polymers, the UV-Vis spectra of the

films were acquired (**Figure 4.2**). The spectra clearly indicated, that the LSPR peak associated with the AuNPs appears around 595-600 nm, which is red-shifted compared to that observed for AuNP-coated PEI film (black line, the peak is at 569 nm). This red shift is ascribed to the aggregation of gold particles on PEI surface after PAA or PDADMAC coating. This may happen due to charge neutralization on the surface of AuNP. But the UV-Vis spectra clearly indicate, there is no loss/detachment of AuNPs because of polyelectrolyte treatment. Since there were no other UV-active groups present on either PAA or PDADMAC polymers UV-Vis spectroscopy of the polymer coated films did not display any additional peaks.

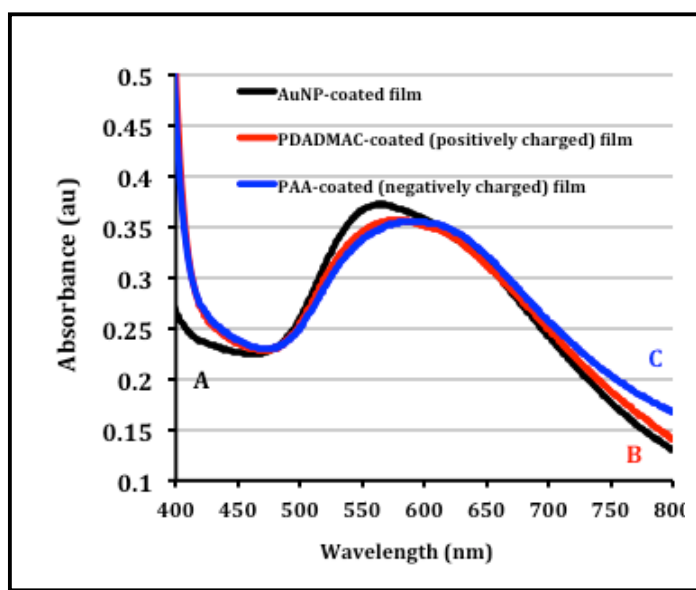


**Figure. 4.2:** Solid-state UV-Vis trace of A. AuNP-coated PEI film, B. PDADMAC-coated PEI film, C. PAA-coated PEI film.

After confirming the stability of AuNPs on PEI films we wanted to confirm the surface charge on the PAA or PDADMAC coated films. Since we are not equipped with solid-state zeta potential measurement tools, we followed a slightly indirect method to confirm the surface charge change after PAA or PDADMAC coating. For this, we incubated PDADMAC and PAA solutions separately with citrate stabilized gold nanoparticles in the absence of PEI films (methods are in sections 4.3.2.2.1, and 4.3.2.2.2). Before PDADMAC incubation, all extra citric acid present in the AuNP sol (prepared by Turkevich method) was intentionally removed through repeated

centrifugation. At this stage, it is safe to assume that the pelleted AuNPs carried only the capped citric acid molecules. Similarly, for the preparation of PAA-coated AuNPs also the extra citrate from sol was removed. Then, the zeta potential of the solution dispersed AuNPs was measured (-19.2 mV), and the zeta potential values were determined to be +33 mV for PDADMAC-coated AuNPs, and -48 mV for PAA-coated AuNPs (**Table 4.1**). This clearly indicated reverse surface charges from two types of nanoparticles. Since the AuNP-coated PEI films have the same surface chemistry (citrate-groups), logically we can extend our conclusion that the PEI films must be carrying the said charged as they were incubated with the same polymers (for example, positive charge for PDADMAC, and negative charge for PAA).

Citrate-capped AuNP	PDADMAC-coated AuNP	PAA-coated AuNP
-19.2 mV	33 mV	-48 mV

**Table. 4.1:** Zeta potential measured with citrate-capped AuNP, AuNP-coated with polyionic polymers PDADMAC, and PAA.

After confirming the surface charges, we wanted to understand the surface hydrophilicity/hydrophobicity of modified surfaces. With the help of a contact angle meter, the nature of the surface can be understood. In this machine, 10.0  $\mu\text{L}$  of water was slowly placed on the modified surface, and with a high-resolution camera, the image of polymer surface and water droplet contact place was captured. Contact angle measurement (**Figure 4.3**) revealed PAA-coated surfaces to be more polar in comparison to PDADMAC-coated ones. This can be ascribed to the possibility of hydrogen bonding between PAA carboxylic acid groups, and water molecules, which are absent in case of PDADMAC-coating.

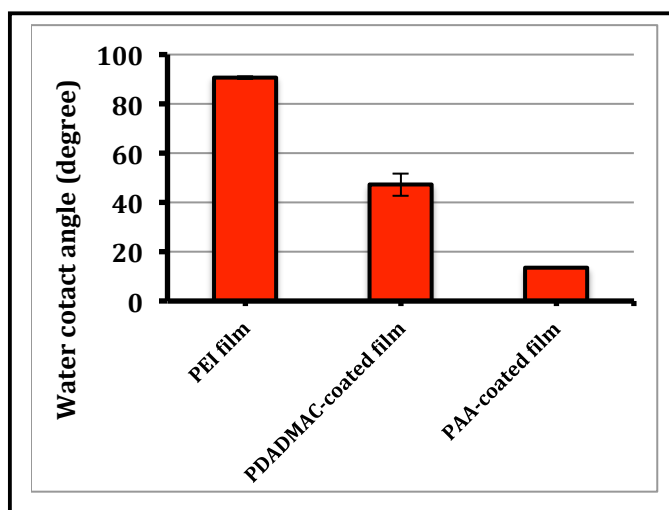


**Figure. 4.3:** Contact angle measurement using 10  $\mu\text{l}$  of a water droplet on the surface modified film. Data represented  $\pm$ SD of  $n=3$ .

For the spectroscopic signals of surface coating molecules (PDADMAC or PAA), the surfaces were probed with FT-IR (ATR mode) tool. As the amount of both the surface-coating polymers is very minimal compared to PEI, the signatures for the polymers were very less even after the spectra were baseline corrected with pure PEI. In **Figure 4.4(a)** the red curve corresponds to the PDADMAC-coated surface. The stretching frequency of quaternary ammonium to methyl group was evident from the peak (A) at around  $3400\text{ cm}^{-1}$ . Other peaks were buried inside pure PEI features [black line, **Figure 4.4(a)**] having similar stretching frequencies. For PAA-coating, the characteristic antisymmetric, and symmetric  $\text{CH}_2$  stretching modes (B,  $2900$ , and  $2850\text{ cm}^{-1}$ ) were observed for both PAA, and citrate. This reveals a higher amount of  $\text{CH}_2$  groups present in the backbone of a PAA chain compared to a citrate molecule. Furthermore, a shoulder at  $1750$  [part of C, **Figure 4.4(b)**] is attributed to the antisymmetric  $\text{C}=\text{O}$  stretching present in the carboxylic acid groups. The hydrogen bonded water, which is very difficult to remove even after high vacuum exposure, left its signature around  $1500\text{ cm}^{-1}$  (D).

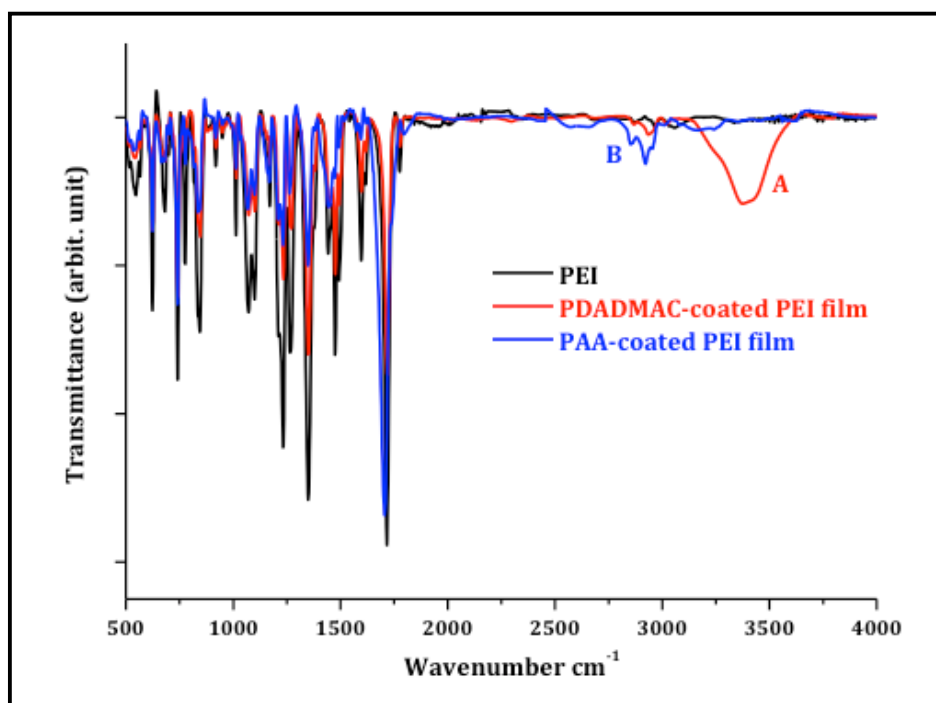


**Figure. 4.4(a):** Full-length FT-IR spectrum of PEI film (black), PDADMAC-coated PEI film (red), PAA-coated PEI film (blue).

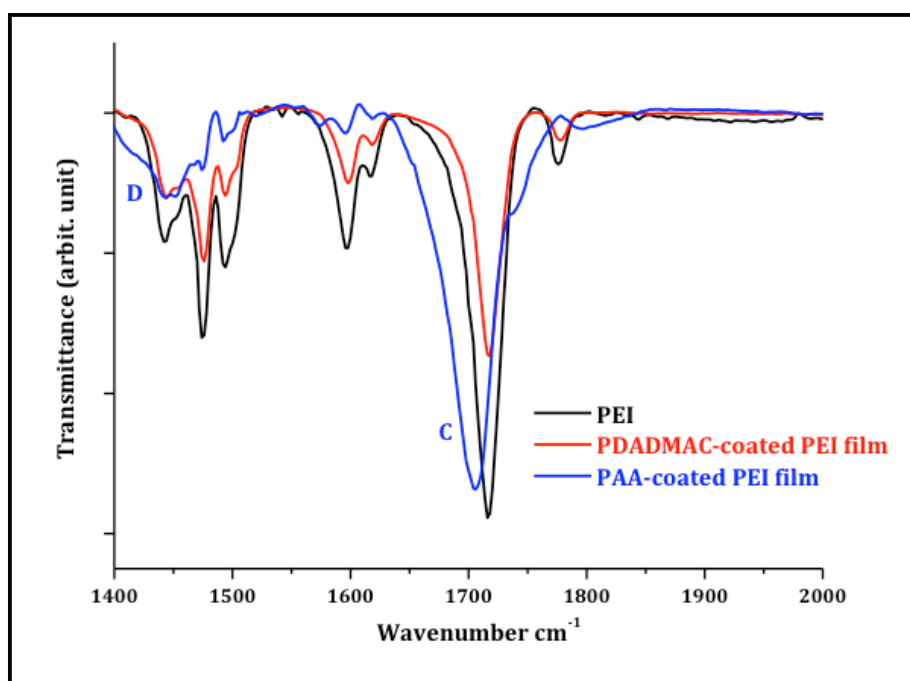


**Figure. 4.4(b):** Expanded 1400-2000  $\text{cm}^{-1}$  wavenumber range.

To find the quantity of the polymers (PDADMAC, and PAA) present on the PEI films after their modifications via P-LbL method, we incubated a big sheet of AuNP-coated PEI film with the respective polymers, and measured the increase in the weight of the films. From these measurements, it was determined that 0.02 mg/cm<sup>2</sup>, and 0.05 mg/cm<sup>2</sup> of PDADMAC, and PAA were coated on Au NP modified PEI films respectively (**Table 4.2**).

PDADMAC-coating	PAA-coating
0.02 mg/cm <sup>2</sup>	0.05 mg/cm <sup>2</sup>

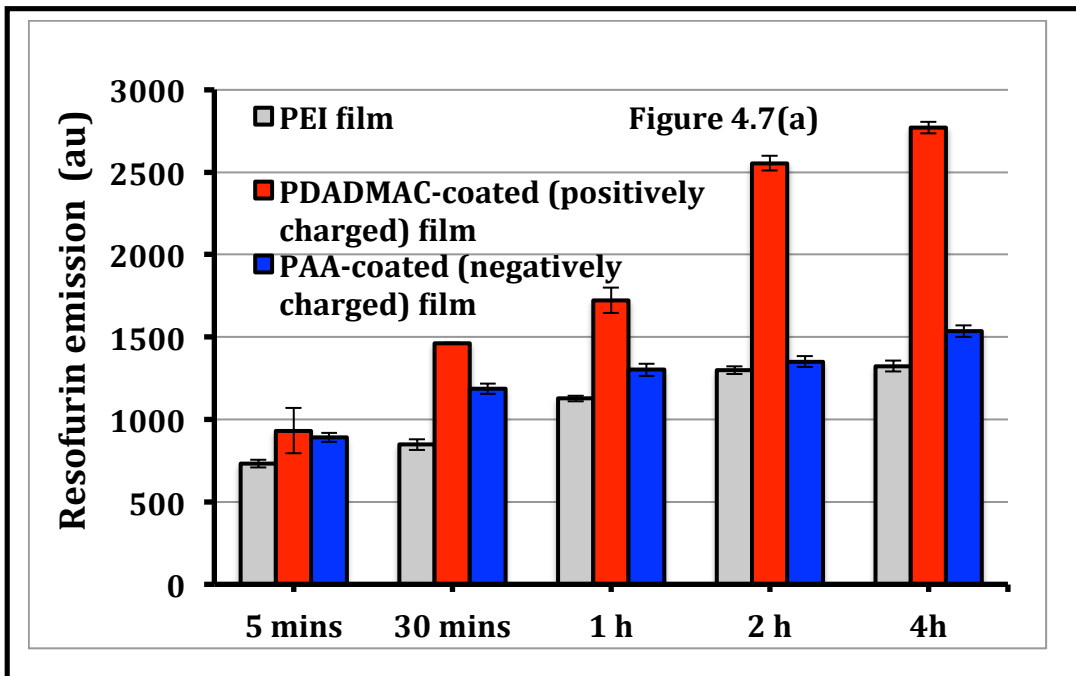
**Table. 4.2:** Amount of polymers attached to per cm<sup>2</sup> of AuNP-coated PEI films.

#### 4.4.2. Cellular adhesion assay

As mentioned earlier our main intention of the study incorporated in this chapter was to understand the immune cell's response on exposure to modified surfaces. For that purpose RAW264.7 (murine monocyte, macrophage) cells (which are easy to grow, and maintain) were chosen. As a control, two other well-studied cell lines - L929 (murine fibroblast), and HepG2 (human liver carcinoma) cells - were chosen. For understanding the interaction of cells with the polymer surface bearing different charges, our primary tool was cellular adhesion assay, where cells were exposed to different surfaces (under cell culture condition) for a predetermined time period ranging from 5 minutes to 4 hours. The extent of adhesion was evaluated by water-soluble resazurin microtiter assay. Here the relative amount of adhered healthy cells was indirectly determined with the help of mitochondrial reduction of resazurin to resofurin (emission at 590 nm). From **Figure 4.5(a)** it is evident that the macrophages (RAW264.7) did not differentiate between surface charge at lower time points, but at higher time points (1h, 2h, 4h) they preferentially adhered to PDADMAC-coated films (positively charged) in comparison to naked PEI films, or PAA-coated negatively charged films. It is worth noticing that the macrophages were adhering to naked PEI film almost as good as to PAA-coated films, which indicates the immune system was not especially repulsive to a negative charge, rather, it recognized both of those surfaces (neutral, and negatively charged)



similarly. In the case of HepG2, and L929 cells they had a distinct preference to PDADMAC-coated films in comparison to PAA-coated ones [Figure 4.5(b), Figure 4.7(c)]. This selectivity was spotted from their (cell's) very first interaction with the modified surfaces. The published literature indicates macrophages generally engulf (hence recognize the cellular membrane) both positive, and negatively charged particles in equal extent.<sup>17</sup> Surprisingly, our finding indicates, at the higher time point, the macrophages are more selective towards positively charged surfaces. But the interaction with macrophages mainly occurs in first one hour of placing an implant,<sup>18</sup> so we can conclude that according to adhesion assay, macrophages do not distinguish between positive, and negatively charged surfaces and that both types of surfaces will be prone to equal immunogenic response.



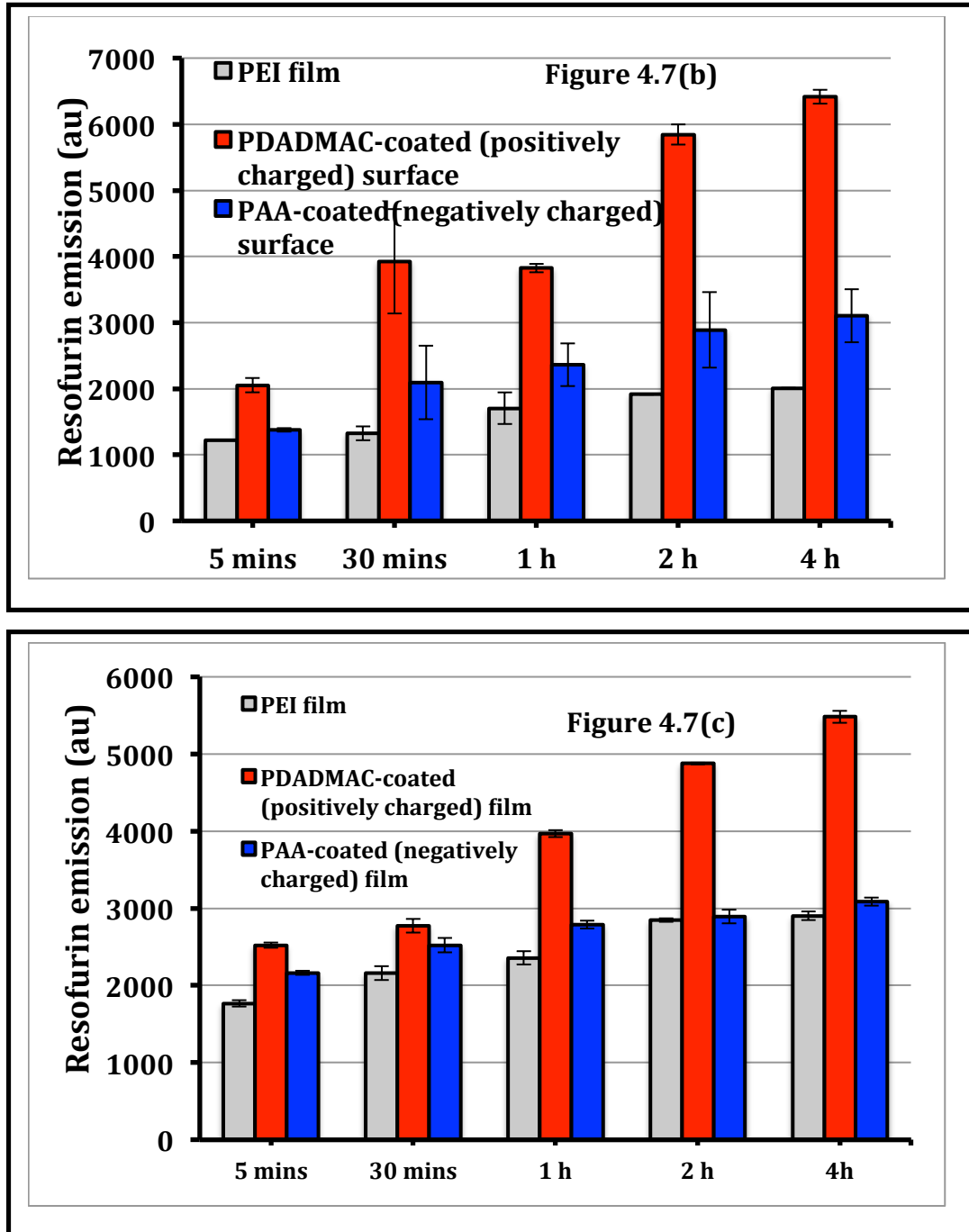


**Figure. 4.5:** Cellular adhesion experiment by resazurin assay: (a) RAW264.7, (b) HepG2, (c) L929 cells. Data represented as a  $\pm$ SD of  $n=3$ .

#### **4.4.3. Fluorescent microscopy images for live-dead assay, and healthy cell quantification:**

Live-dead assay was designed to visualize the approximate amount of live and dead cells on each surface. Dyes associated with live cells (acridine orange, green) and dead cells (propidium iodide, red) were used for this purpose. The adhesion assay (**Figure 4.7**) indicates that the first one-hour is very crucial for successful cellular adhesion. So after exposing the cells (all three kinds) to different surfaces for one hour (under cell-culture condition), we decided to withdraw the supernatant media. Subsequently, by repetitive washing of the PEI films in sterile PBS (37 °C), we ensured the removal of loosely bound cells from the PEI surface. At the same time, we believe the firmly attached ones remain on the surface despite this repetitive washing. After the films were incubated in complete DMEM for 48 hours, the remaining cells proliferated and created a healthy colony. **Figure 4.6(a)** top two panels show that for RAW264.7 cells both the surfaces were equally adherent, and these adherent cells were healthy, and proliferated well. Almost no dead cells were observed indicating macrophage's comfortable attachment towards both (PDADMAC, and PAA-coated) the surfaces. On the other hand, for HepG2 [second, and third panels of **Figure 4.8(a)**], and L929 cells [fourth, and fifth panels of **Figure 4.6(a)**], positively charged surface showed a clear preference for adhesion, and were capable of accommodating healthy cells. On the other hand, negatively charged surfaces showed a lower number of cells adhered, and even if they adhered, many could not maintain their healthiness leading to red dots in the presence of PI. At the same time, DAPI, and CFSE treated fixed cells on different surfaces [**Figure 4.7**] reiterated our findings from the live-dead assay. The cellular crowding was distinctly high in all positively charged (PDADMAC-coated) surfaces for all kinds of cells (macrophage, or non-macrophage). For macrophage (RAW264.7 cells) even the negatively charged surface was well populated. In contrast, for fibroblast, and liver carcinoma cells, the number of cells on negatively charged surfaces were scarce. This finding indicates the non-selectivity and aggression of immune cells towards surfaces carrying any charge.

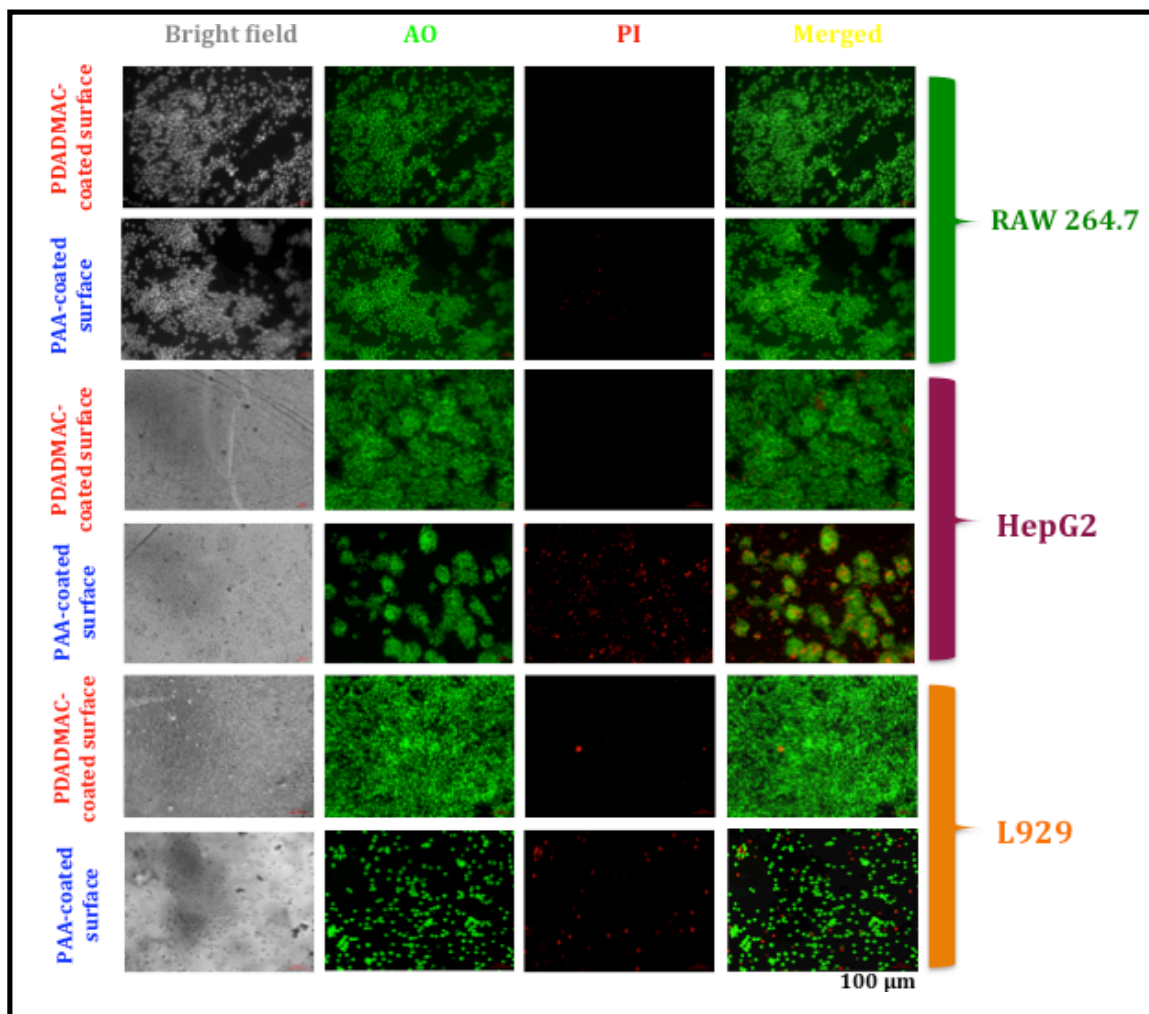


**Figure. 4.6(a):** Live-dead assay by live cells imaging. Live, and dead cell stains are acridine orange (AO), and propidium iodide (PI). Scale bar 100 μm.

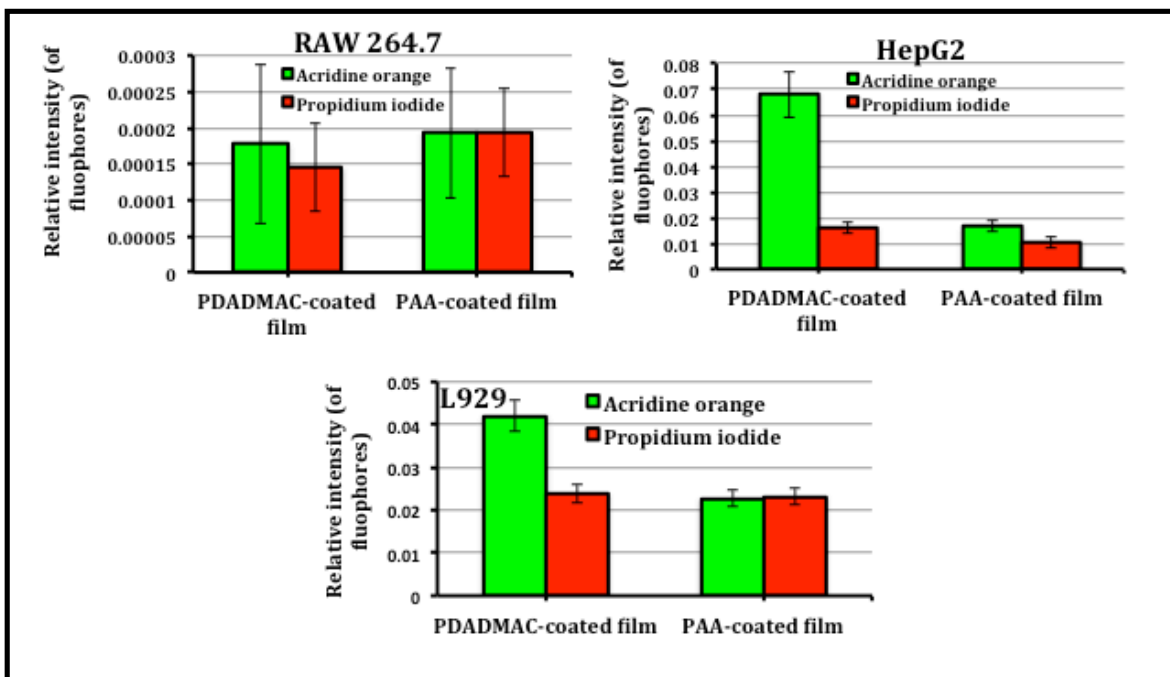


**Figure. 4.6(b):** Quantification of fluorescent tags from live-dead assay images. (A) Acridine orange (AO, green), and (B) Propidium iodide (PI, red) from figure 2.13.A. Data represented as a  $\pm$ SD of  $n=7$ .

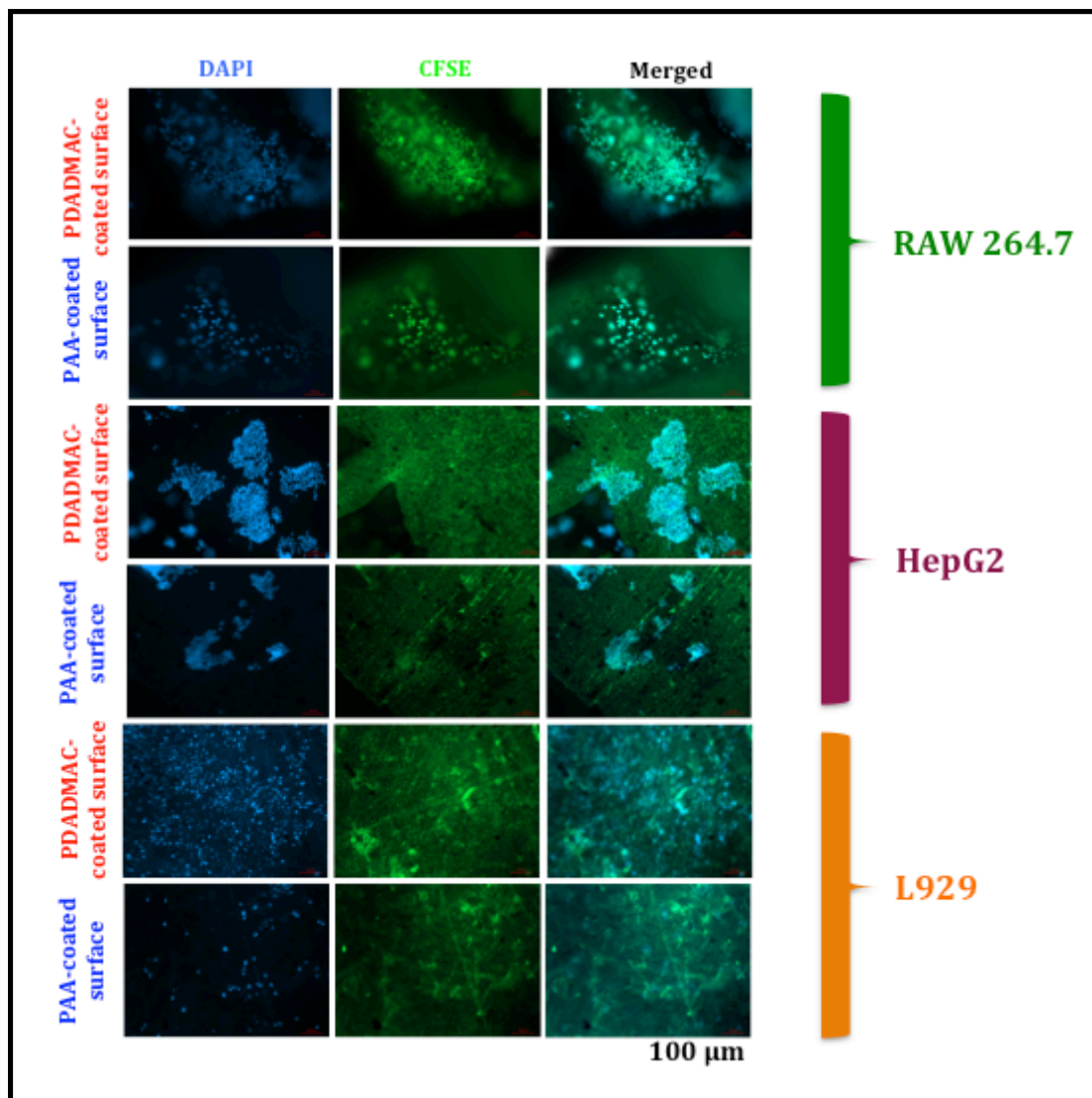


**Figure 4.7:** Visualization of different subtypes of cells (a) RAW264.7, (b) HepG2, (c) L929 on differently charged surfaces. Stains: CFSE, and DAPI. Scale bar 100  $\mu\text{m}$ .

#### 4.5. Conclusion

We have successfully modified the PEI films with two oppositely charged polyionic polymers. The modified surfaces were allowed to interact with immune cells as well as normal cells, which resulted in cellular adhesion on these surfaces to different extents. At lower time points (up to 1h) the immune cells were equally prone to adhere to both positive, and negatively charged surfaces. Image was taken at this time point also showed equally populated healthy cells. While at higher time

exposure cellular adhesion to positively charged films was more effective. For control cells (L929, and HepG2) at all the time points (5 mins to 4 h) positively charged surfaces showed greater preference towards adhesion, and hosted more healthy cells. Since immuno-response is very decisive at lower time points, we conclude that charge alteration cannot be a way out for the evasion of adverse immunological reaction. Changing the surface chemical constituent may help in designing a next-generation implant.

#### 4.6. Bibliography

---

<sup>1</sup> Sadtler, K.; Singh, A.; Wolf, M. T.; Wang, X.; Pardoll, D. M.; Elisseeff, H. Design, clinical translation and immunological response of biomaterials in regenerative medicine. *Nature Reviews Materials*, **2016**, *1*, Article number 16040.

<sup>2</sup> Rodriguez, A.; Chang, D. T.; Amnderson, J. M. Foreign body reaction to biomaterials. *Semin Immunol.* **2008**, *20*(2), 86–100.

<sup>3</sup> Lotfi, M.; Nejib, M.; Naceur, M. Cell Adhesion to Biomaterials: Concept of Biocompatibility <http://dx.doi.org/10.5772/53542>

<sup>4</sup> Chung, L.; Maestas, D. R.; Housseau, F.; Elisseeff, J. H. Key players in the immune response to biomaterial scaffolds for regenerative medicine, *Advanced Drug Delivery Reviews* **2017**, *114*, 184–192

<sup>5</sup> Nich, N.; Goodman, S. B. The role of macrophages in the biological reaction to wear debris from joint replacements. *J Long Term Eff Med Implants.* **2014**, *24*(4), 259–265.

<sup>6</sup> Thevenot, P.; Hu, W.; Tang, L. Surface chemistry influencing implant biocompatibility, *Curr Top Med Chem.* **2008**, *8*(4), 270–280.

<sup>7</sup> Blaszykowski, C.; Sheikh, S.; Thompson, M. Surface chemistry to minimize fouling from blood-based fluids. *Chem. Soc. Rev.*, **2012**, *41*, 5599–5612.

<sup>8</sup> Huang, L.; Zhang, T.; Liaw, P. K.; He, W. Macrophage responses to a Zr-based bulk metallic glass. *J Biomed Mater Res Part A*, **2014**, *102A*, 3369–3378.

<sup>9</sup> Fröhlich, E. The role of surface charge in cellular uptake and cytotoxicity of medical nanoparticles. *International Journal of Nanomedicine* **2012**, *7*, 5577–5591

<sup>10</sup> Sakulku, U.; Mahmoudi, M.; Maurizi, L.; Coullerez, G.; Amtenbrink, M. H.; Vries, M.; Motazacker, M.; Rezaee, F. and Hofmann, H. Significance of surface charge and shell material of superparamagnetic iron oxide nanoparticle (SPION) based

---

core/shell nanoparticles on the composition of the protein corona. *Biomater. Sci.*, **2015**, *3*, 265-278.

<sup>11</sup> Wang, J.; Chen, J.; Yang, J.; Wang, H.; Shen, X.; Guo, M.; Zhang, X. Effects of surface charges of gold nanoclusters on long-term in vivo biodistribution, toxicity, and cancer radiation therapy. *International Journal of Nanomedicine* **2016**, *11*, 3475–3485.

<sup>12</sup> Jiang, S.; Cao, Z. Ultralow-Fouling, Functionalizable, and Hydrolyzable Zwitterionic Materials and Their Derivatives for Biological Applications. *Adv. Mater.* **2010**, *22*, 920–932.

<sup>13</sup> Yue, Z.; Wei, W.; Lv, P.; Yue, H.; Wang, L.; Su, Z.; Ma, G. Surface Charge Affects Cellular Uptake and Intracellular Trafficking of Chitosan-Based Nanoparticles, *Biomacromolecules* **2011**, *12*, 2440–2446.

<sup>14</sup> Fuller, M.; Köper, I. Polyelectrolyte-Coated Gold Nanoparticles: The Effect of Salt and Polyelectrolyte Concentration on Colloidal Stability. *Polymers*, **2018**, *10*, 1336-1345.

<sup>15</sup> Jans, H.; Jans, K.; Lagae, L.; Borghs, G.; Maes G.; Huo Q. Poly(acrylic acid)-stabilized colloidal gold nanoparticles: synthesis and properties. *Nanotechnology*, **2010**, *21*, 455702

<sup>16</sup> Turkevich, J.; Stevenson, P.C.; Hillier, J. A study of the nucleation and growth processes in the synthesis of colloidal gold. *Discussions of the Faraday Society*, **1951**, *11*, 55-75.

<sup>17</sup> Liu, X.; Huan, N.; Li, H.; Jin, Q.; Jian, J. Surface and Size Effects on Cell Interaction of Gold Nanoparticles with Both Phagocytic and Nonphagocytic Cells. *Langmuir* **2013**, *29*, 9138–9148 .

<sup>18</sup> Sridharan, R.; Cameron, A. R.; Kelly, D. J.; Kearny, C. J.; O'Brien J. Biomaterial based modulation of macrophage polarization: a review and suggested design principles. *Materials Today*, **2015**, *18*(6), 313-325.



# **Chapter 5**

## **Conclusion**

## 5.1. Introduction

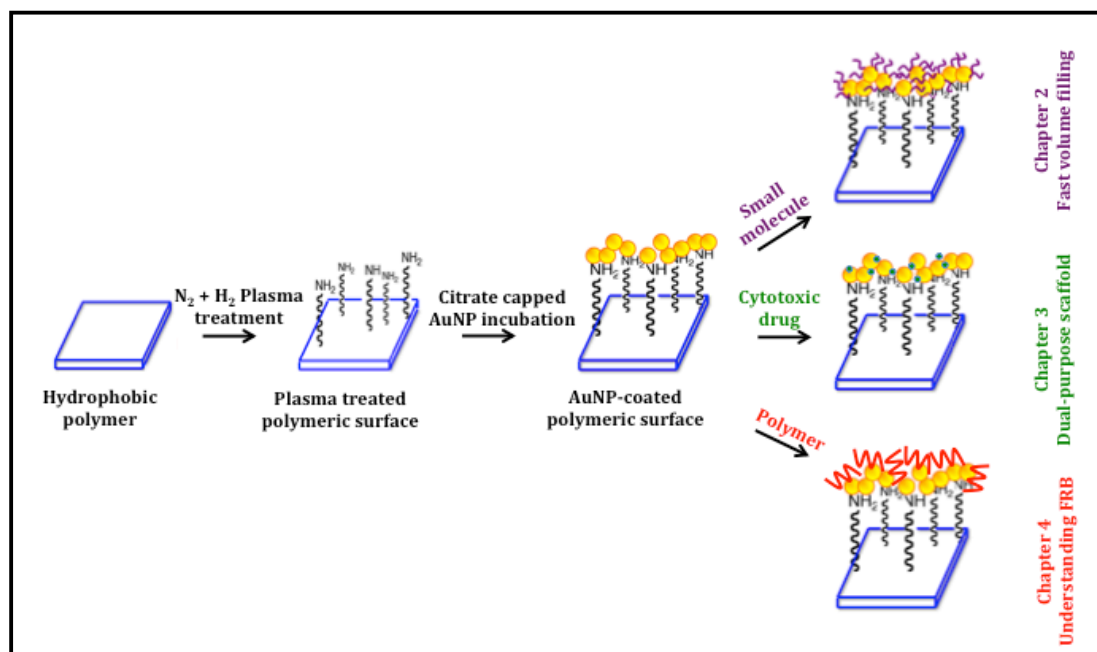
Usage of bio-implants to regularize or correct physiological functions, disorders or as supports for bone fractures *etc.* is a well-established field of medicine today. Cardiac stents, knee replacements, *etc.* have become very common.<sup>1</sup> At the same time, there are also many unanswered questions regarding the biocompatibility (problems of infection, fibrosis) of implants, their performance inside the human body, and complications during the patient's recovery. Most of these problems have their genesis in the 'tissue-material' interaction where the surface properties of the material play a crucial role. Though a plethora of interesting materials with desired mechanical, and structural properties have been made many of them fail because of their unsuitable surface characteristics, which could be addressed by carrying out appropriate surface modifications. In this thesis we have tried to address this issue of surface modification of tough hydrophobic polymers, which are routinely being used for implant application. The plasma treatment followed by layer-by-layer citrate stabilized AuNP coating (P-LbL) strategy followed by us turned out to be very convenient by which the bulk material properties were retained and only the surface characteristics were changed. Apart from turning the hydrophobic surfaces to hydrophilic ones, through P-LbL we could attach a wide variety of biological cues to the surface of the hydrophobic polymer (implant material). We exploited this easy, and convenient technique and explored the application of hydrophobic material for three distinct purposes (**Scheme 5.1**).

## 5.2. Conclusions drawn from different chapters

### 5.2(a) Fast volume filling application

Although hydrophobic polymers are excellent implant materials, they lack the cell-adhesive property, which may lead to post-surgical problems like slow tissue integration, hence long recovery time, organ dislocation or repetitive corrective surgery. We have a surface modified the hydrophobic scaffolds with hydrophilic amino acid arginine with P-LbL followed by dip-coating technique. The surface-modified polymers retained their hydrophilicity for a very long period (unlike plasma treated surface), to which murine fibroblast cells (L929) adhered in an

excellent manner. The modified surface was capable of hosting healthy cells, produced collagen and in every way was comparable to fibronectin (a well-known adherent protein) modified surfaces. Thus this simple surface modification technique turned out to be an adherent protein treatment equivalent, which could have implications in developing fast volume filling implantable materials.



**Scheme. 5.1:** Outline of thesis: Surface modification of hydrophobic polymeric surface, and different applications.

### 5.2(b) Dual-purpose scaffolds

In certain solid tumour (especially in oral cancer) treatment regime, surgical removal followed by chemotherapy, and corrective surgery is quite customary. This certainly increases trauma, trouble, weakness due to chemotherapy side effects, and chances of infection to the patients. One way to tackle this would be to create a dual purpose scaffold which can deliver cytotoxic drug (cisplatin) locally by pH-triggered (tumourous environment) release and (ii) after release can become hydrophilic and allow the adherence and proliferation of healthy cells. Accordingly, we fabricated a dual-purpose scaffold based on the P-LbL technique by chemically conjugating the cytotoxic drug aquated cisplatin to the AuNPs anchored on the HDPE scaffold by the P-LbL technique. Our results indicated that the released drug killed the human

mouth cancer KB cells and promoted the adherence of healthy fibroblast cells later. Based on this we could envisage the development of a scaffold, which releases the drug locally avoiding the systemic exposure of the drug, and reduce side effects to healthy tissues. The polymer after drug-release can stay *in vivo* (since non-biodegradable) and advent towards fresh non-cancerous cellular (L929) adhesion, which has the potential for volume filling application. Thus by one surgical intervention, it is possible to meet two goals: deliver drug without any side effect, as well perform cosmetic surgery.

### **5.2(c) Understanding the immune reactions**

Any foreign body inside live tissue has to face the immune system. This interaction may lead to adverse reactions like infection, thrombosis *etc.* To make a new generation implant we must understand the response of immune cells (macrophages) towards a foreign body. Alterations in surface charge towards recognition, and internalization in different types of cells including macrophages have been well researched in literature so far<sup>2</sup> but the same cannot be said about the understanding of the interaction between macrophages and the material surface bearing different charges. To address this, through P-LbL method we converted the hydrophobic polymers into positive charge, and negative charge carrying surfaces. We exposed the macrophage (RAW264.7) cells, and L929/HepG2 cells towards surfaces carrying these different charges. To our surprise, the macrophages were rather aggressive and attached to different types of surfaces at equal ease. But at higher time points positively charged surfaces were more preferred by macrophages. On the other hand, for normal cells showed a clear preference towards positively charged surfaces. Nevertheless, our results indicate that a simple charge based surface modification is not sufficient to ward off immunogenic response as the FBR mainly occurs in the first one hour of placing an implant.

Finally, we conclude that P-LbL is an easy, and convenient tool to modify the surfaces of polymer implants in a permanent way and using this we could develop a better understanding of the material surface-cell interaction. Such an understanding would be very useful to build a multi-functional improved implant. Our last chapter

findings also clearly establish that there are still innumerable issues that need to be addressed before an all-rounder, problem-free bioimplant could be developed.

### 5.3. Bibliography

---

<sup>1</sup> <https://biomaterials.materialsconferences.com/events-list/biomaterials-companies-and-market-analysis> Accessed February 2019

<sup>2</sup> Liu, X.; Huan, N.; Li, H.; Jin, Q.; Jian, J. Surface and Size Effects on Cell Interaction of Gold Nanoparticles with Both Phagocytic and Nonphagocytic Cells *Langmuir* **2013**, *29*, 9138–9148 .

## Copyright of Figures 1.3, 1.4

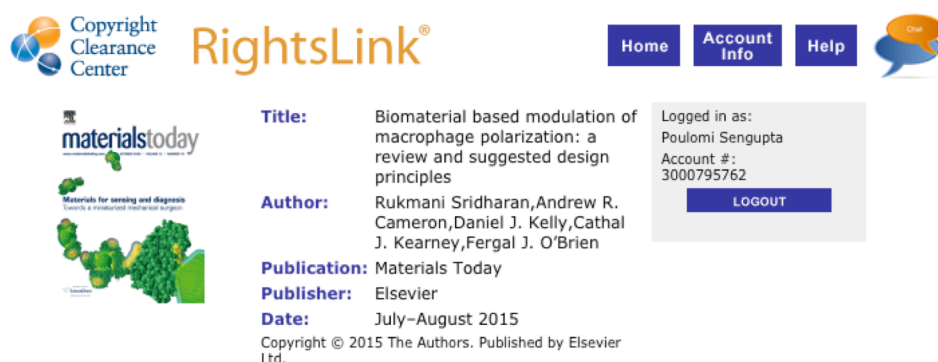
### SPRINGER NATURE LICENSE TERMS AND CONDITIONS

Feb 21, 2019

This Agreement between Poulomi Sengupta ("You") and Springer Nature ("Springer Nature") consists of your license details and the terms and conditions provided by Springer Nature and Copyright Clearance Center.

License Number	4533531165022
License date	Feb 21, 2019
Licensed Content Publisher	Springer Nature
Licensed Content Publication	Nature Nanotechnology
Licensed Content Title	Nanotechnological strategies for engineering complex tissues
Licensed Content Author	Tal Dvir, Brian P. Timko, Daniel S. Kohane, Robert Langer
Licensed Content Date	Dec 12, 2010
Licensed Content Volume	6
Licensed Content Issue	1
Type of Use	Thesis/Dissertation
Requestor type	academic/university or research institute
Format	print and electronic
Portion	figures/tables/illustrations
Number of figures/tables/illustrations	2
High-res required	no
Will you be translating?	no
Circulation/distribution	<501
Author of this Springer Nature content	no
Title	Poulomi Sengupta
Institution name	CSIR National Chemical Laboratory
Expected presentation date	Feb 2019
Portions	Figure 2
Requestor Location	Poulomi Sengupta Room no 293 CSIR-National Chemical Laboratory Dr. Homi Bhaba Road Pune, Maharashtra 411008 India Attn: Poulomi Sengupta
Billing Type	Invoice
Billing Address	Poulomi Sengupta Room no 293

## Copyright of Figure 4.1



The screenshot shows the RightsLink interface. At the top left is the Copyright Clearance Center logo. To its right is the RightsLink logo. Further right are navigation buttons for Home, Account Info, and Help, along with a chat icon. Below the logos is a thumbnail of the article cover from Materials Today, titled "Materials for sensing and diagnosis: Towards a miniaturized mechanical organ". The main content area displays the following details:

- Title:** Biomaterial based modulation of macrophage polarization: a review and suggested design principles
- Author:** Rukmani Sridharan, Andrew R. Cameron, Daniel J. Kelly, Cathal J. Kearney, Fergal J. O'Brien
- Publication:** Materials Today
- Publisher:** Elsevier
- Date:** July–August 2015

Below the article details, it states: "Copyright © 2015 The Authors. Published by Elsevier Ltd." On the right side, there is a user login box showing "Logged in as: Poulomi Sengupta" and "Account #: 3000795762", with a LOGOUT button.

**Creative Commons Attribution-NonCommercial-No Derivatives License (CC BY NC ND)**

This article is published under the terms of the [Creative Commons Attribution-NonCommercial-No Derivatives License \(CC BY NC ND\)](#).

For non-commercial purposes you may copy and distribute the article, use portions or extracts from the article in other works, and text or data mine the article, provided you do not alter or modify the article without permission from Elsevier. You may also create adaptations of the article for your own personal use only, but not distribute these to others. You must give appropriate credit to the original work, together with a link to the formal publication through the relevant DOI, and a link to the Creative Commons user license above. If changes are permitted, you must indicate if any changes are made but not in any way that suggests the licensor endorses you or your use of the work.

Permission is not required for this non-commercial use. For commercial use please continue to request permission via Rightslink.

[BACK](#)

[CLOSE WINDOW](#)

Copyright © 2019 [Copyright Clearance Center, Inc.](#) All Rights Reserved. [Privacy statement](#). [Terms and Conditions](#). Comments? We would like to hear from you. E-mail us at [customercare@copyright.com](mailto:customercare@copyright.com)

## Research publications

(Accepted or in review, related to this thesis):

1. **Poulomi Sengupta**, Bhagavatula L. V. Prasad. Surface modification of polymers for tissue engineering applications: Arginine acts as a sticky protein equivalent for viable cell accommodation. *ACS Omega*, **2018**, 3(4), 4242-4251.
2. **Poulomi Sengupta**, Sachin S. Surwase, Bhagabatula L. V. Prasad. Modification of porous polyethylene scaffolds for cell attachment and proliferation. *International Journal of Nanomedicine*. **2018**, 13, 87-90.
3. **Poulomi Sengupta**, Bhagavatula L. V. Prasad. Surface Modification of Polymeric Scaffolds for Tissue Engineering Applications. *Regen. Eng. Transl. Med.* (Springer Nature group) **2018**, 4, 75-91 <https://doi.org/10.1007/s40883-018-0050-6>
4. **Poulomi Sengupta**, Vinay Agrawal, Bhagavatula L. V. Prasad. Development of a smart scaffold for sequential cancer chemotherapy and tissue engineering. Under review in *Chemistry Select*.